Linearization of RF Power Amplifiers

by

Mark A. Briffa.

A thesis submitted for the degree of

Doctor of Philosophy

at

Victoria University of Technology

December, 1996.

Department of Electrical and Electronic Engineering

BOX 14428 MCMC

Melbourne VIC 8001

AUSTRALIA

ATTENTION

This thesis entitled, "Linearization of RF Power Amplifiers" was submitted in December, 1996, and has been converted into electronic form by the author in 2001.

This thesis has been made available to interested parties in good faith, such that no part of the thesis may be copied or printed for commercial gain without prior consent from the author. This copy however can be freely read and distributed.

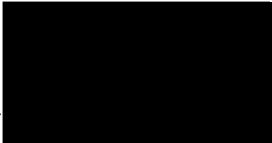Comments and queries regarding this work can be directed to the author:

markbriffa@yahoo.com
http://www.geocities.com/markbriffa/

Statement of Originality

I hereby certify that the work contained in this thesis is the result of original research (except where due reference is given) and has not been submitted for a higher degree to any other university or institution.

This thesis may be made available for consultation within the Victoria University Library and may be photocopied or lent to other libraries for the purposes of consultation.

(Signed) .... December, 1996.

Mark A. Briffa

ABSTRACT

Linearization of RF power amplifiers is surveyed, reviewed and analyzed. Cartesian feedback is specifically presented as an effective means of linearizing an efficient yet non-linear power amplifier. This reduces amplifier distortion to acceptable levels and enables the transmission of RF signals utilizing spectrally efficient linear modulation schemes with a lower consumption of DC power. Results from constructing experimental hardware shows an intermodulation distortion (IMD) reduction of 44dB (achieving a level of −62dBc) combined with an efficiency of 42% when transmitting π/4 QPSK. The careful amplifier characterization measurement method presented predicts performance to within 2dB (IMD) and 4% (efficiency) of practical measurements when used in simulations.

A comprehensive stability analysis is developed using piecewise amplifier models within a multiple-input, multiple-output block diagram representation of the cartesian feedback loop. The analysis shows how RF amplifier non-linearity, the RF phase adjuster setting, loop gain, bandwidth and delay affect stability. A graphical interpretation of the analysis is given that indicates how stable a given RF amplifier will be when setting up a practical cartesian feedback loop. Instability is shown to result when the amount of RF phase rotation introduced by AM/PM distortion, and by setting error in the RF phase adjuster within the loop, equals the open-loop phase margin. For one of the amplifiers investigated, the analysis predicts that instability results just after the transistor turn-on

region when the phase adjuster is adjusted above optimum, and instability also results at transistor saturation when adjusted lower than optimum. This is also demonstrated with experimental hardware.

From the analysis, the perturbated behaviour of the non-linear piecewise amplifier model is shown to display two forms of operation when placed in a feedback loop, namely: spiral mode and stationary mode. Spiralling tends to cause the noise floor of the output spectrum to rise on one side depending on the direction of the spiral. The direction is in turn dependent on the setting of the RF phase adjuster within the loop. When the phase adjuster is in the forward path, phase adjustments lower than optimum, will cause the noise to rise on the right side of the output spectrum (anti-clockwise spiralling) and vice-versa. With the phase adjuster in the feedback path the reverse is true.

Loops with low stability margins are demonstrated to exhibit closed-loop peaking which can affect the out of band noise performance of a cartesian feedback transmitter. In order to achieve a non-peaking condition for a first order loop with delay, the phase margin of the loop needs to be around 60°. It is also possible to approximately predict the degree of peaking from the gain and phase margins. Further investigation of noise performance suggests the loop compensation should be placed as far up the forward chain as possible (i.e. close to the power amplifier) in order to minimize the out-of-band noise floor. This too is demonstrated experimentally.

The concept of dynamic bias is also presented as a method to improve cartesian feedback efficiency. The method works by setting up optimum bias conditions for the power amplifier (derived from amplifier characterizations) and then having the cartesian feedback loop make fine adjustments to the RF drive to achieve the exact required output. This way the bias conditions do not have to be applied perfectly, implying simple (i.e low switching frequency) switched mode power supplies can be used to apply the desired collector voltage for example. The simple step-down switch mode power supply constructed achieved an efficiency of 95% at high output levels. Applying it to a cartesian

feedback loop markedly improved efficiency. At an output power of 20dBm average, the linearized amplifier efficiency lifted from 45% to 67%, an improvement of over 20% and a reduction in current consumption by 33%.

PREFACE

In this thesis I present my work in *Linearization of RF Power Amplifiers*. The work primarily examines cartesian feedback as the means by which efficient yet non-linear RF (radio frequency) power amplifiers can be linearized over a narrow bandwidth.

Linearization, or the reduction of distortion in electronic systems, has been a goal for electronic engineers for as long as electronics has existed. Feedback has had widespread and successful application to achieve this end. In recent times, the need for linear RF power amplifiers has been spurred on by the demands of cellular and wireless communications to carry more traffic over a given spectrum. As I present in chapter 1, this has led to the increased use of spectrally efficient modulation schemes. These schemes have modulation on the envelope and hence require linear RF power amplifiers in the transmitter. Other applications for linear RF power amplifiers are also discussed in this introductory chapter.

In chapter 2, I collated background material which surveys the field of RF power amplifier linearization as it applies to modern transmitter architectures. The non-linear aspects of the RF power amplifier are presented and the consequences of such non-linearities and distortions are shown. A number of linearization methods can reduce these distortions with varying degrees of success and these are reviewed with my comments.

The rest of the thesis represents a summary of the work I performed in the area of cartesian feedback. In chapter 3, I detail the methods used to carefully characterize two RF power amplifiers. These characterizations led to simulation results which were in close agreement with the constructed cartesian feedback loops. Very early in the research it was apparent that instability was an important issue. Stability analysis as it applies to cartesian feedback is my major contribution to the field. The analysis is presented in its most complete and mature form in chapter 4 and can predict potential instability with any (memoryless) non-linear RF power amplifier. The development of the analysis was the most personally rewarding aspect of this work, and the results obtained yielded some surprising facts regarding the nature of non-linear amplifiers and cartesian feedback stability. The extension of the analysis into noise performance provided the most practical benefit and showed how the placement of the loop filter could reduce out of band noise. Some aspects of the analysis were also presented in the following publications:

I   M. A. Briffa and M. Faulkner, "Stability Analysis of Cartesian Feedback Linearisation for Amplifiers with Weak Non-Linearities", *IEE Proc. Communications*, Vol. 143, No. 4, Aug. 1996.

II   M. A. Briffa and M. Faulkner, "Gain and Phase Margins of Cartesian Feedback RF Amplifier Linearisation", *Journal of Electrical and Electronics Engineering, Australia*, Dec. 1994, Vol. 14, No.4, pp 283-289.

III   M. A. Briffa and M. Faulkner, "Stability Considerations for Dynamically Biased Cartesian Feedback Linearization", in *Proceedings of the 44th IEEE Vehicular Technology Conference*, Stockholm, Sweden, VTC-94, June 1994, pp. 1321-1325
.

IV   M. A. Briffa, M. Faulkner and J. MacLeod, "RF Amplifier Linearisation using Cartesian Feedback", in *Proceedings of the 1st International Workshop on Mobile and Personal Communications, University of South Australia,* Adelaide, Australia, November 1992, pp. 343-348.

In chapter 5, I look at ways of improving the efficiency of cartesian feedback loops. This work is of particular significance in handheld portable wireless equipment. The work presented on dynamically biased cartesian feedback involved many challenges such as simulating the power amplifier and the dynamic effects of the switch mode power supply. Designing and constructing a discrete switch mode power supply was another significant challenge (every electronics engineer should build at least one switchmode power supply in his/her career!). This work is partly described in the following paper:

V   M. A. Briffa and M. Faulkner, "Dynamically Biased Cartesian Feedback Linearization", in *Proceedings of the 43rd IEEE Vehicular Technology Conference*, Secaucus, USA, VTC-93, May1993, pp. 672-675,

and after much learning about the patenting system, in:

VI   M. Faulkner and M. A. Briffa, "Linearized Power Amplifier", *U.S Patent No. 5 420 536*, May 30, 1995.

During the course of the research I have collaborated with others in the field and the following papers may be of interest:

VII   M. Faulkner and M. A. Briffa, "Amplifier Linearisation using RF Feedback and Feedforward Techniques", in *Proceedings of the 44th IEEE Vehicular Technology Conference*, Chicago, USA, VTC-95, June 1995, pp. 525-529.

VIII   M. Johansson, M. A. Briffa and L. Sundström, "Dynamic Range Optimization of the Cartesian Feedback Transmitter", *IEEE Transactions on Vehicular Technology,* accepted for publication.

ACKNOWLEDGEMENTS

CONTENTS

ATTACHED PAPERS

1 INTRODUCTION

Rudimentary communications systems such as telephones and radio have existed for much of the twentieth century. Advances in microelectronics and circuit miniaturization have dramatically transformed these innovations to a point whereby mobile telephony is now commonplace. Rapid developments in mobile and wireless communications will continue to have striking impacts in many areas including commerce, industry, Information Technology (IT), personal communications, and so on.

Extensive and growing use of mobile radio services has however, increased pressures on frequency spectrum allocation. Adopting the cellular architecture has to some extent released the pressure of limited spectrum. In theory, reducing cell sizes could increase capacity to any desired level. In practice however, various factors restrict the minimum cell size. The most prominent of these factors is the high cost of basestation infrastructure.

The push of IT requirements for mobile services to also carry data coupled with the demand for communications systems to interface with the digital system infrastructure, has driven the adoption of new digital modulation techniques in preference to existing analog technologies.

In portable wireless applications, the final Radio Frequency (RF) Power Amplifier (PA) is a high consumer of the battery power budget. Power consumption is of prime

importance since users now expect a compact and lightweight unit which can operate for several hours/days between recharges. The so called "talk-time" of a mobile terminal is often used to attract a larger market share in a highly competitive market. Another significant marketing feature is the improved security aspects of digital communication.

Many recently adopted modulation schemes reflect the constraint that most power efficient forms of RF power amplification are generally non-linear. Techniques based on Continuous Phase Modulation (CPM) which convey information only on the phase of an RF carrier, are generally seen as a good compromise between spectral efficiency and retaining a constant envelope - a necessity with non-linear yet efficient power amplification.

Introducing amplitude variations to the carrier can improve the spectral efficiency allowing higher information throughputs for a given channel. The transmission of these signals however, requires the use of a linear amplifier. This is a serious concern. A linear Class A amplifier operated at the appropriate level of back-off for example, has poor efficiency and would have an excessive deleterious effect on battery life. A non-linear amplifier cannot be used because the distortion of the signal envelope and phase produces intermodulation components in the adjacent channel that cannot be filtered out. Linearizing a non-linear yet efficient RF power amplifier satisfies both requirements of linearity and low power consumption. The aim of this research is to study possible linearization strategies that allow efficient RF power amplifiers (e.g class AB-C) to be used with modern modulation schemes that have a varying envelope.

Efficient linearized amplifiers can be applied in several areas. In mobile communications, applications for linearized power amplifiers can be found in both cellular systems and emerging PMR (Private Land Mobile Radio) systems. In the U.S, the cellular system AMPS (Advanced Mobile Phone Service) has been augmented with DAMPS (Digital AMPS). DAMPS makes use of linear modulation and hence requires linear amplifiers. The move to DAMPS has increased spectral efficiency by three times. Another linearly

modulated cellular system application currently in use in Japan is PDC (Pacific Digital Cellular).

Linear modulation has also been proposed for PMR. Systems such as APCO25 (Ambulance Police Communications Officers) and TETRA (Trans European Trunked Radio) were designed with the availability of linearized power amplifiers in mind. These systems have very tight linearity specifications. Capacity increases and benefits similar to those of digital cellular are expected for these PMR schemes.

Other applications for linearized power amplifiers include NTT Digital Cordless and satellite communication systems such as the Australian OPTUS digital satellite mobile network. It is also possible to apply such amplifiers in traditional systems such as Single Sideband (SSB) High Frequency (HF) radio, and even broadcast Amplitude Modulation (AM) transmitters.

A desirable by-product of linear amplification is the constant gain relationship between input and output of the amplifier. This obviates the needs for output levelling control circuits for transmitters with power control requirements. Power control allows close-by mobiles to transmit at lower powers to those further away (hence reducing the near-far dominated interference at the basestation). This is a major requirement in systems using Code Division Multiple Access (CDMA) such as Qualcomm's CDMA digital cellular system.

A linear power amplifier is also capable of amplifying signals with any combination of amplitude and phase modulation. This broadens the selection of modulation schemes and increases the versatility of the amplifier considerably. In situations where different modes co-exist on the same band the linearized amplifier is capable of fulfilling the requirements of both modes. The efficient linearized amplifier therefore delivers "a one size fits all" option to manufacturers of mobile equipment. It obviates the need to re-design for new modulation methods when the need arises. Selecting the modulation scheme is simpler

through software control without regard to the RF amplifier. Changing modulation schemes dynamically could have important military applications.

Developments in multicarrier basestations indicate that it is possible to neatly combine individual channels to be transmitted at baseband rather than at high power RF. The traditional RF combination of signals requires the use of several RF power amplifiers, isolators and cavity filters. When the channels are combined at low power, the entire RF band is amplified and fed to a single antenna. The advantages of this technique include reduction in power losses inherent in combiners, isolators and cavity filters, lower overall cost and size, and improved flexibility in terms of channel allocation. The amplifier required for such a design needs to be wideband, highly linear and is consequently a candidate for the application of a linearized RF power amplifier.

The linearization solutions were developed here by investigating feedback methods which are inherently narrowband. One method - Cartesian Feedback, is a technique of power amplifier linearization using negative feedback of the modulation components. The term *cartesian* refers to the manner by which the baseband modulation is expressed in its in-phase and quadrature components rather than the polar form of amplitude and phase. This linearization technique compares the input modulation signals to those demodulated at the transmitter output and drives the amplifier with the necessary pre-distorted signal such that the output closely matches the input and hence distortion is minimized.

This work extensively covers cartesian feedback and provides a detailed stability and noise analysis. The power efficiency of cartesian feedback was improved by varying the bias conditions of the RF amplifier. This was achieved by careful characterization of the RF amplifier to enable the selection of the best bias conditions for operation at peak efficiency.

Chapter 2 introduces the field of RF amplifier linearization. Much of the early work presented in this thesis concentrated on system characterization. This is dealt with in

chapter 3 where the system was characterized using instruments controlled by GPIB (General Purpose Instrument Bus). The resulting models from the measurements were utilized throughout most of this work. Simulations based on these models are presented in chapter 3 which also discusses the essential details of cartesian feedback linearization and gives results from a constructed system.

Chapter 4 presents an in-depth analysis of cartesian feedback linearization. Both a linear and non-linear piecewise stability analysis are presented along with an out-of-band noise analysis and is the major theoretical contribution to the work.

Chapter 5 describes Dynamically Biased Cartesian Feedback as a means of providing efficiency improvements to conventional cartesian feedback. Simulations are given along with hardware measurements.

The final chapter summarizes the major conclusions of the work presented in this thesis, and the possibility for future work is also discussed.

2 BACKGROUND

When communications systems are devised many factors contribute to the overall configuration of the system. One prominent factor is the choice of the modulation scheme. In determining what modulation method will be chosen for digital mobile communications, the system designers generally attempt to meet some specification based on the allowable Bit Error Rate (BER) for given spectrum restrictions. Research into this area has resulted in several techniques being proposed.

Constant envelope modulation schemes are usually adopted if transmitter power efficiency or channel non-linearity is of concern. This was a consideration when Gaussian Minimum Shift Keying (GMSK) was selected for the European and Australian digital cellular system GSM (Global System for Mobile communications). In the digital cordless area, the Digital European Cordless Telephone System (DECT), CT2 (Cordless Telephones), CT3 and the Personal Communications Network (PCN)/Personal Communications Systems (PCS) have adopted (or likely to adopt) constant envelope modulation.

Because of the increasing pressures for extra capacity, the advantages of retaining a constant envelope have given way to linear modulation. This form of modulation results

when Nyquist filtering is introduced to digital quadrature modulation. By filtering, the spectrum requirements are reduced at the expense of introducing envelope variations. Linear modulation is overviewed in section 2.1. It will be shown in section 2.2 and 2.3 that such signals when passed through non-linear amplifiers undergo distortion which results in a spreading of the spectrum and a degradation of BER.

Spectral spreading causes interference to other users in the adjacent channels. For this reason authorities specify a maximum adjacent channel interference (ACI) limit; examples are given in section 2.4. To solve the problem of ACI various linearization techniques have been proposed and these are reviewed in section 2.5. One of the more promising techniques is Cartesian Feedback and this is discussed in section 2.6.

2.1 LINEAR TRANSMITTER ARCHITECTURE

Emerging linear modulation schemes are typically transmitted using the direct conversion digital transmitter structure shown in figure 2.1. The Digital Signal Processor (DSP) converts the digital data stream to be transmitted into two baseband analog signals ($I_{in}(t)$ and $Q_{in}(t)$). The upconversion process quadrature modulates these baseband signals directly to an RF (Radio Frequency) carrier frequency (ω_c). Subsequent *linear* amplification brings the modulated RF signal ($S(t)$) up to a power level suitable for radio transmission.
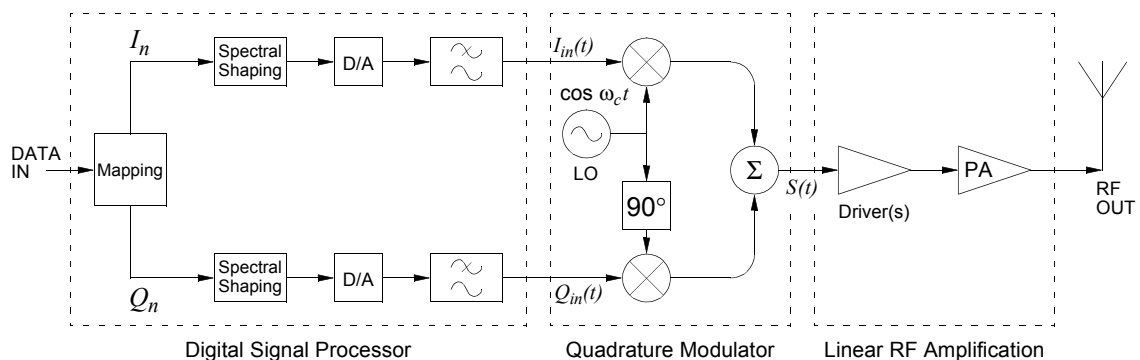
Figure 2.1: *Direct conversion digital linear transmitter.*
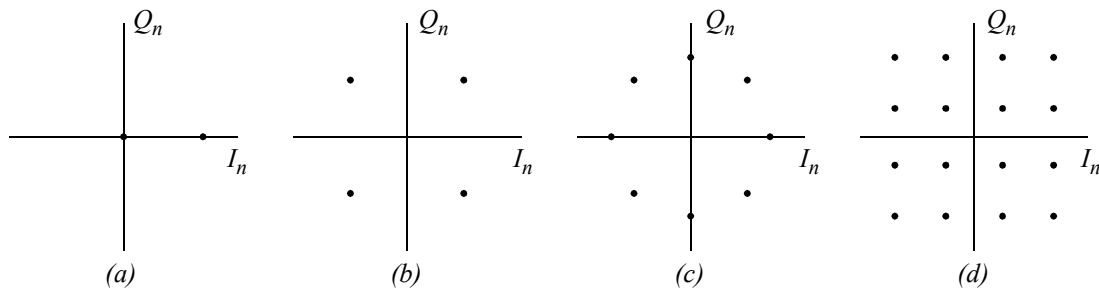
Figure 2.2: *Scatter diagrams for (a) OOK, (b) QPSK, (c) 8-PSK (or π/4 shift QPSK), (d) 16QAM.*

2.1.1 DSP Functions

The DSP circuit first maps the input data stream into two data streams I_n and Q_n where n denotes the nth signalling period or symbol period. The mapping employed will govern what possible discrete values I_n and Q_n adopt and how changes in these values will take place in the next symbol period. If M is used to denote the number of possible states there are generally three types of modulation formats possible: M-ASK (M-level Amplitude Shift Keying), M-PSK (M-level Phase Shift Keying) and M-QAM (M-level Quadrature Amplitude modulation).

Figure 2.2(a) gives and example of 2-ASK otherwise known as on-off keying (OOK). This modulation is generated if all Q_n's are set to zero and the I_n's can take a value of either zero or one.

If $I_n = \cos\Phi_n$ and $Q_n = \sin\Phi_n$, (where each Φ_n is taken from M evenly spaced values between $\pm\pi$) M-PSK results with each state uniformly distributed on the unit circle. Figure 2.2(b) shows 4-PSK or QPSK (Quadri-Phase Shift Keying), and figure 2.2(c) shows the case for $M = 8$.

Letting I_n and Q_n take the following possibilities ±1, ±3,..., $\pm(\sqrt{M} - 1)$, generates M-QAM. Figure 2.2(d) demonstrates 16-QAM with the states lying on a square lattice of 16 points. M-QAM can be thought of as a combination of both amplitude modulation (M-ASK) and phase modulation (M-PSK).
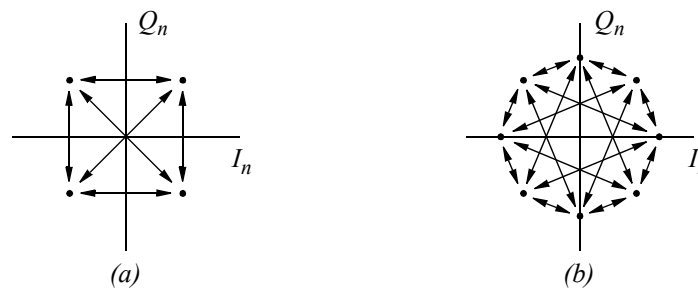
Figure 2.3: *Space diagrams for (a) QPSK, (b) π/4 shift QPSK.*

The scatter diagrams of figure 2.2 give no indication of the nature of movement between different states. Transition between states is governed by the spectral shaping filter and any constraints which the mapping imposes. Figure 2.3 shows the transitions which exist for filtered QPSK and a common mobile modulation scheme π/4 shifted QPSK. For QPSK some of these transitions travel through zero. This ultimately causes the amplitude of the modulated output signal (*S(t)*) to also cross zero. A zero crossing implies infinite dynamic range and forces operation in typically non-linear turn-on regions of RF PA's (Power Amplifiers). π/4 shift QPSK was proposed by Akaiwa[1] as a means of avoiding the zero crossing area for linearly modulated digital mobile communications systems[1]. The "π/4 shift" originates from the fact that the modulation scheme can be generated by rotating (or "shifting") a QPSK constellation by π/4 radians every alternate symbol. With each symbol (2 bits) a movement is made which is either ±π/4 radians or ±3π/4 radians giving a signal constellation which never passes through zero. The North American DAMPS (Digital-Advanced Mobile Phone Service) system has adopted a differentially encoded version of this modulation, π/4 DQPSK (Differential Encoded π/4 shift QPSK).

Nyquist filtering enables the transmitting of digital information in the smallest possible bandwidth without introducing ISI (Inter-Symbol Interference)[2]. The filtering is an important DSP function and is normally performed in the time domain. One particular form of filter which is currently used extensively and in the DAMPS system is derived from the raised cosine family. By separating the filtering function into two - one at the

1. Under power control however, the turn-on region can still present problems.

transmitter and one at the receiver, the filter utilized at each end is a square root raised cosine filter. The frequency response of such a filter is given by [3]

$$B(f) = 1 \qquad\qquad 0 < f < \frac{1+\alpha}{2T}$$

$$B(f) = \sqrt{\frac{1 - \sin\left(\left(\frac{\pi}{2\alpha}\right)(2fT-1)\right)}{2}} \qquad \frac{1-\alpha}{2T} < f < \frac{1+\alpha}{2T} \qquad (2.1)$$

$$B(f) = 0 \qquad\qquad f > \frac{1+\alpha}{2T}$$

where

f is the frequency,

α is the excess bandwidth,

T is the symbol period.

The nature of the filter shows three distinct parts - a flat pass band which continues up to a value determined by the excess bandwidth, a transition band which occupies twice the excess bandwidth, and a stopband which exists outside the excess bandwidth. The excess bandwidth refers to the percentage bandwidth the filter exceeds that of the minimum nyquist filter. The term *raised cosine* is derived from the transfer function produced when the excess bandwidth is 100% ($\alpha = 1$) giving a raised cosine function.

The equivalent time domain response is

$$b(t) = \frac{\pi\sin((1-\alpha)\Omega t) + 4\alpha\Omega t\cos((1+\alpha)\Omega t)}{t(\pi^2 - 16\alpha^2\Omega^2 t^2)} \qquad \text{where: } \Omega = \frac{2\pi}{2T} \qquad (2.2)$$

The impulse and frequency responses described above are shown in figure 2.4 for DAMPS. This figure was generated with the filter design software DFDP[2] and shows the

---

2. DFDP - Digital Filter Design Package, Atlanta Signal Processors Incorporated.
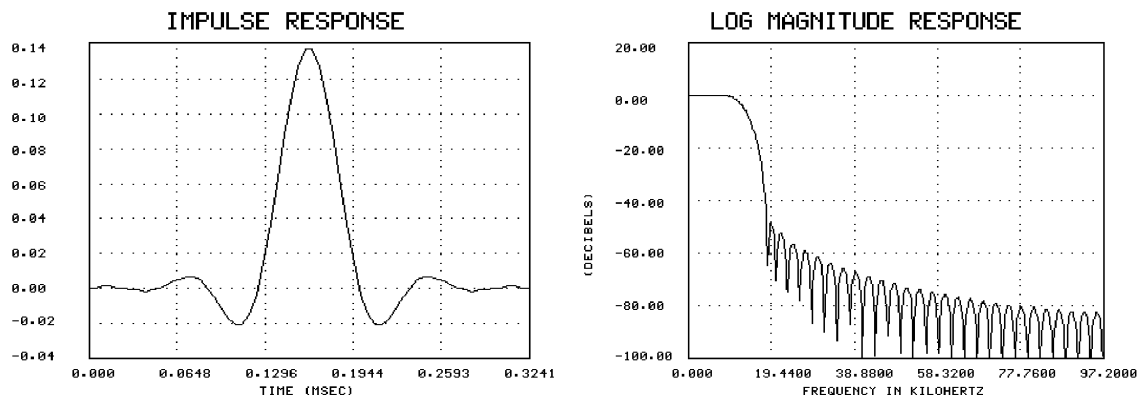
Figure 2.4: *Response of DAMPS filter.*

windowed impulse response along with the logarithmic magnitude response. With the DAMPS system $\alpha = 0.35$ and because the filter impulse response is truncated to a length of 8, a Kaiser window is applied to limit the effects of truncation on the spectral integrity in adjacent channels. The Kaiser co-efficient is 2.4. An oversampling rate of 16 allows the use of a 100kHz reconstruction filter with a data rate of 48.6kBits/s.

The remaining functions in the DSP are the DAC's (Digital to Analog Convertors) and subsequent reconstruction filters which convert the digitally generated signal to an analog signal ready for modulation.

2.1.2 Quadrature Modulation

The quadrature modulator block shown in figure 2.1 represents a well known technique of directly upconverting baseband analog signals $I_{in}(t)$ and $Q_{in}(t)$ to a carrier frequency (ω_c).

The frequency mixers multiply $I_{in}(t)$ and $Q_{in}(t)$ with an in-phase and quadrature $(+90°)$ component of a Local Oscillator (LO) respectively. The outputs from the mixers are combined to yield the modulated RF output signal $S(t)$. Since $I_{in}(t)$ and $Q_{in}(t)$ are modulated orthogonally they effectively occupy two independent I (in-phase) and Q (quadrature) channels.

The quadrature modulation process modulates both the amplitude and phase of a carrier in

a manner governed by a cartesian to polar conversion, with $I_{in}(t)$ and $Q_{in}(t)$ being the cartesian representations i.e

$$
\begin{aligned}
S(t) &= I_{in}(t)\cos\omega_c(t) + Q_{in}(t)\sin\omega_c(t) \\
&= A(t)[\cos(\omega_c(t) + \phi(t))]
\end{aligned}
\tag{2.3}
$$

It is convenient to consider *S(t)* as the real part of a complex signal

$$
\begin{aligned}
S(t) &= \text{Re}[A(t)e^{j(\omega_c(t) + \phi(t))}] \\
&= \text{Re}[A(t)e^{j\phi(t)}e^{j\omega_c(t)}] \\
&= \text{Re}[S_b(t)e^{j\omega_c(t)}]
\end{aligned}
\tag{2.4}
$$

The complex envelope $S_b(t)$ can therefore be used to describe the RF signal without reference to the carrier signal. *A(t)* is the amplitude of the signal and $\Phi(t)$ is the phase of the signal given by

$$
A(t) = \sqrt{I_{in}(t)^2 + Q_{in}(t)^2} \qquad \phi(t) = \text{atan}\frac{Q_{in}(t)}{I_{in}(t)}
\tag{2.5}
$$

And the complex envelope signal is given by

$$
\begin{aligned}
S_b(t) &= I_{in}(t) + j\,Q_{in}(t) \\
&= A(t)e^{j\phi(t)}
\end{aligned}
\tag{2.6}
$$

Complex baseband envelope representation was used in all of the simulations in this work. This is advantageous since the sample rate does not have to be so high as to accommodate the carrier frequency resulting in higher computational efficiency[4].

2.1.3 Linear RF Amplification

The modulated RF signal *S(t)* may contain amplitude variations. To amplify such a signal linear RF amplification is needed. Linear Class A RF amplifiers are typically used in driver stages of figure 2.1. This work looks at means by which non-linear (yet efficient) RF power amplifiers can be used in the final stages. The next sections discuss how non-

linear amplifiers distort linearly modulated signals and means by which these non-linear amplifiers can be linearized.

2.2 RF POWER AMPLIFIER NON-LINEARITIES

It is common to distinguish large signal amplifiers with class operation set by bias conditions. Most active devices have limited linear regions and bias conditions are normally chosen to give a desired amplifier linearity at the expense of efficiency.

BJT (Bipolar Junction Transistor) amplifiers can be biased to operate under different classes depending on the base-emitter bias voltage (figure 2.5)[5] and corresponding collector currents. Negative voltages push the transistor into operation with lower conduction angles and towards Class C operation. Although lowering the conduction angle improves the collector efficiency[3], drive levels must be increased to sustain reasonable output powers. Consequently, power added efficiency[4] falls. Finding the optimum bias conditions for maximizing power added efficiency is covered in more detail in chapters 3 and 5.
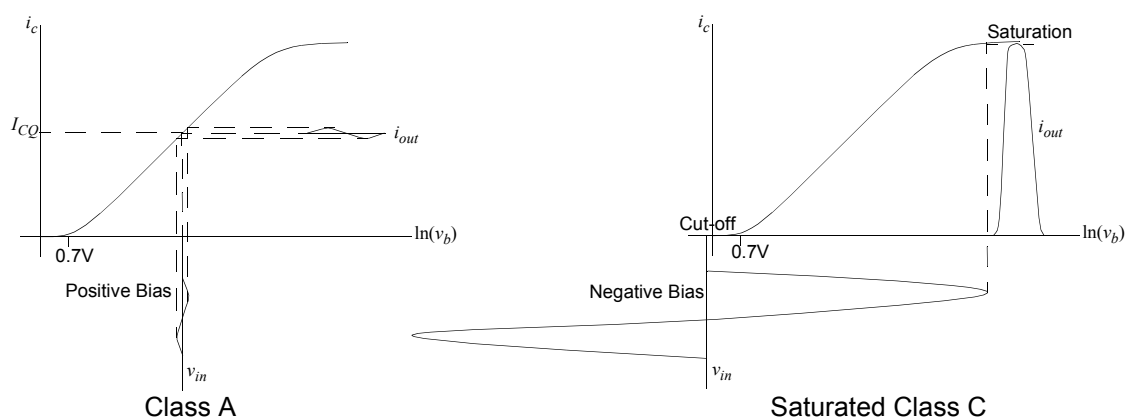
Figure 2.5: *Effect of bias and drive level on class of amplifier operation.*

---

3. Collector efficiency is defined as P_{out}/P_{DC}.
4. Power added efficiency is defined as $(P_{out} - P_{in})/P_{DC}$.

Higher (positive) bias voltages allow the device to operate over more of its linear region thus improving the amplifier linearity. Class A operation occurs when the transistor is biased to conduct for 360° i.e the transistor conducts all the time. This increase in conduction angle however results in lower collector efficiencies.

Increasing the RF drive level leads to a family of amplifiers operating under saturation (e.g saturated Class A, AB, B, C). The transistor begins to behave more like a switch (rather than a current source) giving some gains in power output and efficiency. Indeed, a whole range of switching type RF amplifiers exist (Classes D to F), some with efficiencies approaching 100%[6].

The non-linearities described above are termed AM/AM distortion (Amplitude Modulation to Amplitude Modulation). The deviation from a straight line input-output transfer function in the cut-off region and in the saturation region results in envelope amplitude distortion induced by the amplitude changes on the input. Largely because of voltage dependent collector capacitance (caused by a varying depletion layer width) another form of distortion is introduced, namely - AM/PM (Amplitude Modulation to Phase Modulation). The most disturbing aspect of the AM/PM distortion of the BJT amplifier is the distinct kink when the amplifier leaves cut-off and enters the linear region.

AM/AM and AM/PM distortion is present in most power amplifiers irrespective of the amplifying device. Although much of this research was developed around two BJT RF power amplifiers, TWT (Travelling Wave Tube) amplifiers are commonly used for digital radio and serve as an interesting comparison (figure 2.6). The TWT non-linearity is the analytical model found in SPW[5]. TWT's generally have longer delays than BJT's in addition to the differing characteristics.

This research is mainly concerned with linearization over a relatively narrow frequency

---

5. SPW Signal Processing Worksystem - The DSP Framework, COMDISCO Systems, Inc.
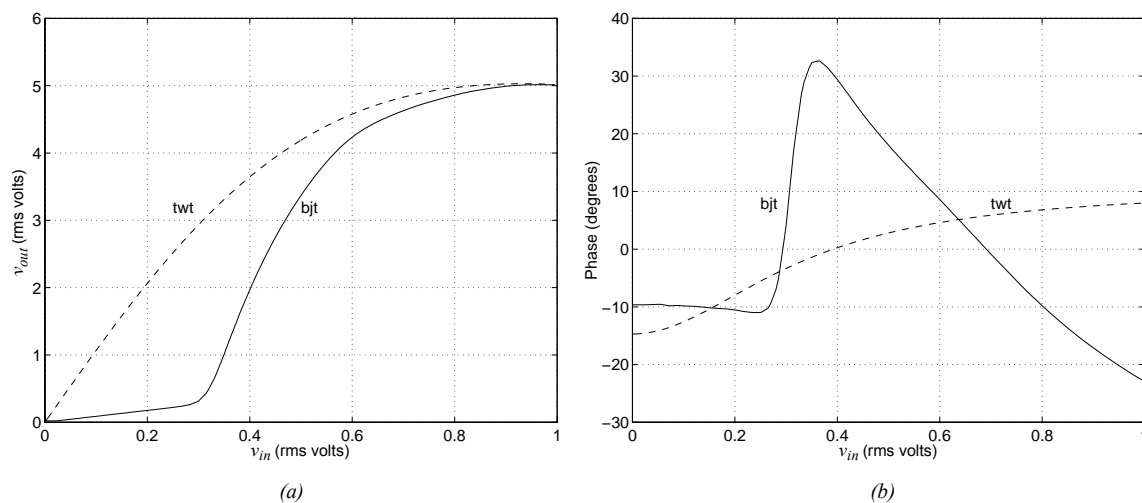
Figure 2.6: *Comparison of twt and bjt RF amplifier characteristics. (a) Amplitude response showing AM/ AM distortion. (b) Phase response showing AM/PM distortion.*

band. It is common to therefore assume for modelling purposes that the amplifier is wideband compared to the modulation and hence frequency induced variations of the RF amplifier parameters are neglected[7]. Some frequency restriction does however exist in the RF amplifier and this is modelled as an extra delay and discussed in chapter 3. Other frequency dependencies and memory effects can manifest themselves as hysteresis in the time domain. The hysteresis can cause the intermodulation products of a two-tone test to be asymmetrical in the time domain.

2.2.1 Environmental Factors affecting RF power Amplifiers

The characteristics of an amplifier do not remain static. The operating conditions, both internal and external to the amplifying device, will affect the amplifier characteristics. A linearization system must therefore be robust enough to cope with these changes. With feedback systems the control loop robustness is crucial in order to maintain stability.

Thermal time constants within the device and the ambient temperature alter the BJT threshold voltage and peak saturated power capability. Significant memory effects can also be introduced by bias circuitry[8] and power supply variations.

Another external influence which is especially important with hand portable mobiles is antenna load fluctuations. As the unit is moved towards and away from the head and other objects in close proximity, the changes in standing waves result in a variation of phase angle through the amplifier. Such phase changes will degrade loop stability in feedback systems and can be misinterpreted by some linearization systems as modulation information. Measures such as isolators or other supervisory circuitry are often necessary to overcome these problems. Changes in carrier frequency also result in a phase changes through the amplifier.

2.3 EFFECTS OF NON-LINEARITIES ON MODULATION

Amplifier non-linearities cause distortion of linear signals resulting in two detrimental effects. First, as witnessed by the phase plane diagrams of figure 2.7, the signal trajectories are distorted. Figure 2.7(a) shows the undistorted phase plane trajectory of $\pi/4$ shift DQPSK using a root raised cosine filter with a reduced impulse length of two (a reduced impulse length reduces the number of trajectories and makes the figure clearer). After amplification by a non-linear RF PA, the signal trajectories become distorted (figure 2.7(b)). Consequently the received signal will be harder to detect hence degrading the BER[9].

The second effect is that the distortion causes the spectrum to spread into adjacent channels (figure 2.9). Figure 2.8 gives a selection of three complex envelope signals in the time domain with each signal presented in magnitude (amplitude) and phase format. The unfiltered $\pi/4$ shift DQPSK modulation is given by figure 2.8(a). Without filtering the envelope will be constant as shown by the upper magnitude trace of figure 2.8(a), and the phase transitions will be instantaneous as shown by the lower trace.

Introducing the full length root raised cosine filter used in DAMPS introduces envelope variations and smooths the phase transitions as shown in figure 2.8(b). After non-linear

(a)   *(b)*
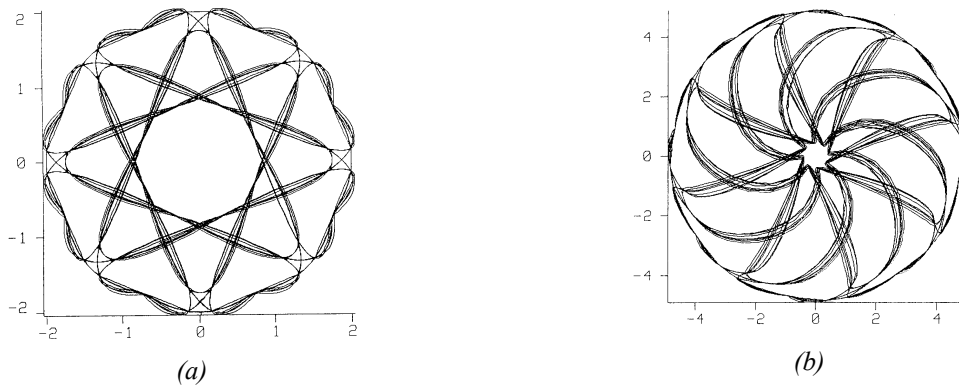
Figure 2.7: *(a) Undistorted phase plane trajectory of π/4 shift DQPSK using a root raised cosine filter with an impulse length of two. (b) Same signal after amplification by non-linear power amplifier.*
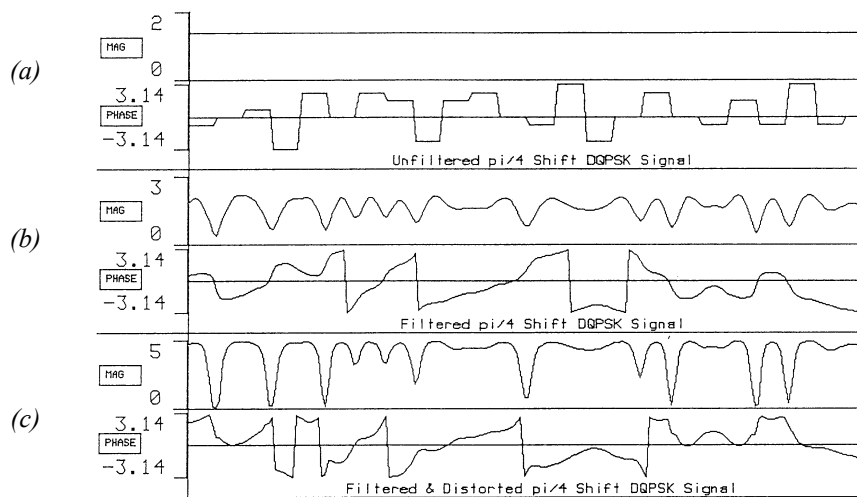
Figure 2.8: *Time domain representation in magnitude and phase format. From top to bottom: (a) Unfiltered π/4 Shift DQPSK; (b) Same signal after root raised cosine Nyquist filtering; and (c) Filtered signal after undergoing amplifier distortion.*

(a)   *(b)*   *(c)*
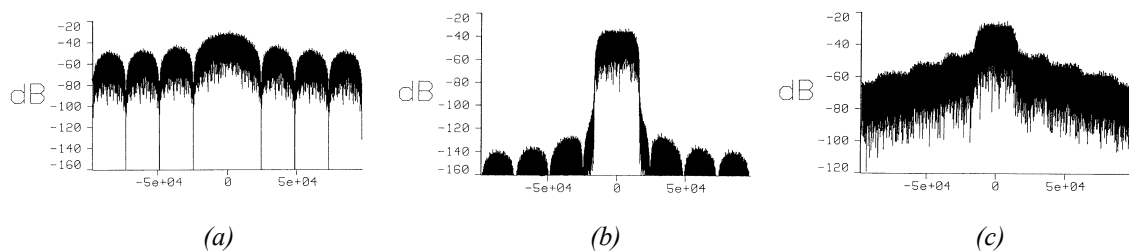
Figure 2.9: *(a) Unfiltered π/4 Shift DQPSK. (b) Same signal after root raised cosine Nyquist filtering. (c) Filtered signal after undergoing amplifier distortion.*

amplification the AM/AM distortion corrupts the envelope and the AM/PM distortion corrupts the phase (figure 2.8(c)).

Figure 2.9 shows the spectrum of the same three signals. Figure 2.9(a) is the original unfiltered π/4 shift DQPSK signal. After the application of the nyquist filter, the bandwidth required to transmit the data is substantially reduced (figure 2.9(b)). Non-linear amplification however degrades the spectrum, spreading it back into the adjacent channels and hence destroying the benefits of the nyquist filtering.

2.3.1 Intermodulation Distortion Measurement

Intermodulation distortion is generated by amplifier non-linearities. Linearization aims to remove these non-linearities and hence remove the intermodulation distortion artifacts which interfere with adjacent channels. The two-tone test is a common method used to quantify the degree of non-linearity in an amplifier (or other non-linear devices such as mixers).

The test involves generating two tones at the carrier frequency as shown by the solid lines of figure 2.10. This is easily achieved where quadrature inputs are available since applying a single tone (with frequency f_m) at either the In-phase or Quadrature input will yield two tones at RF. With RF inputs, two RF signal generators can be combined. After passing through the non-linearity the two tones intermodulate resulting in the undesired products as shown by the dashed lines in figure 2.10 ($f_c \pm 3f_m$, $f_c \pm 5f_m$ etc.). The amplitude of the distortion products relative to the desired tones is a measure of the amplifier non-linearity.

Distortion also occurs at a carrier rate which results in harmonics being generated at multiples of the carrier frequency (i.e $2f_c$, $3f_c$ etc.). These are normally removed by a harmonic filter in which case the harmonics can be neglected. A frequency product is also generated at $2f_m$ as a result of the presence of distortion around even order harmonics at
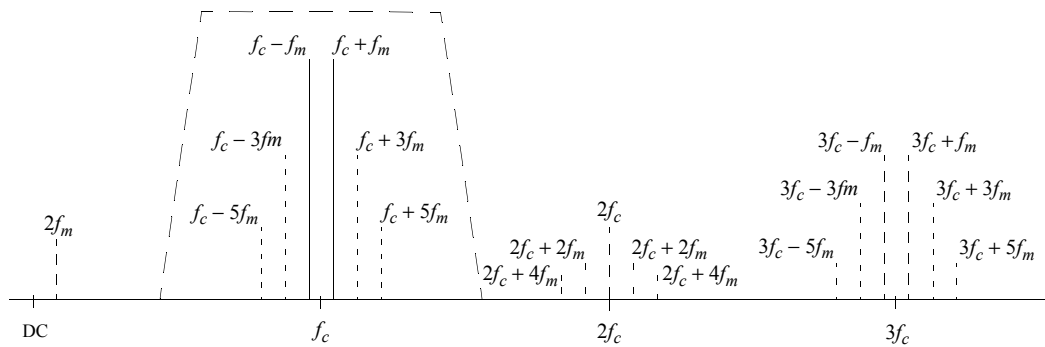
Figure 2.10: *Distortion products generated by two-tone test passing through a non-linearity; dashed box indicates zone normally viewed on spectrum analyzer. Desired signals solid, undesired distortion products dashed.*

$2f_c$, $4f_c$ etc. This product is also neglected due to the high-pass nature of the amplifier output. Occasionally even order distortion is also visible in measured two-tone tests at f_c and even order intervals ($f_c \pm 2f_m$, $f_c \pm 4f_m$ etc.). This distortion is caused by asymmetry, DC or carrier leak.

A related method used to quantify non-linearity is the third order intercept point. The intercept point graph (see figure 2.13a) is generated by performing a series of two-tone tests at different power levels. Idealized slopes of the fundamental output power (1:1 slope on a dB scale) and of the third order products (3:1 slope on a dB scale) are taken well before compression and extended right up to form an intercept point. The higher this point with respect to the operating point the more linear is the system. The intercept point approach is applicable for weak non-linearities, however some of this work deals with strong non-linearities and hence the raw two-tone test is used to assess the performance of linearization schemes.

2.4 ACI RESTRICTIONS

The usual cause of ACI is distortion in the amplification system but other causes exist, such as leakage from the Nyquist filter in the modulation. The situation shown in figure
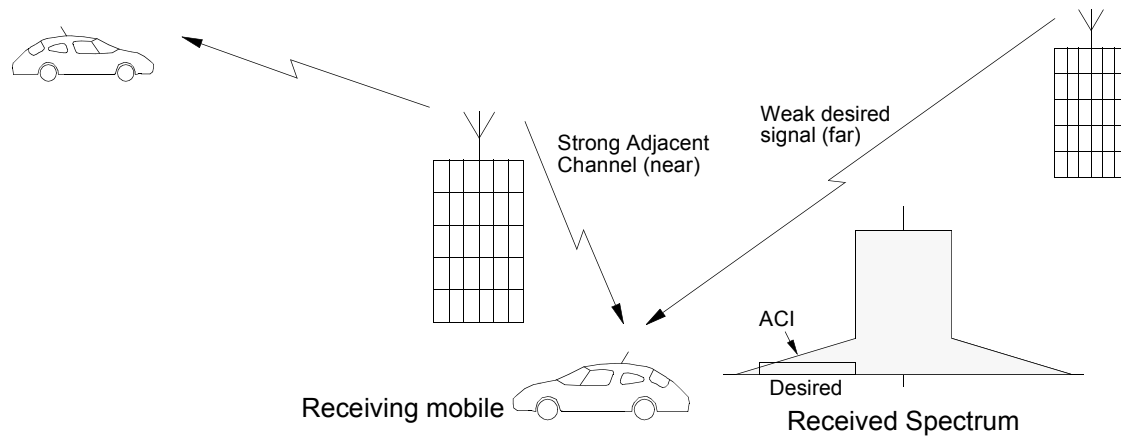
Figure 2.11: *Near-far problem in a mobile communications scenario where ACI from a strong (near) adjacent channel interferes with a weak (far) desired signal.*

2.11 demonstrates the near-far problem as it relates to ACI. The problem occurs when the receiver attempts to receive a weak signal (i.e far) in the presence of a strong (i.e near) adjacent channel transmission. If the ACI specification in the transmitter is too high the weak signal will be swamped.

The level of ACI is a specification set in all mobile communication applications and some examples are given in the next few sections.

2.4.1 Cellular Systems

The most immediate application for linearized power amplifiers is DAMPS. The level of ACI in the adjacent channel is −26dB and in the next adjacent channel −45dB. In other channels the ACI specification is given as −60dB. Cellular systems are able to modify frequency allocations in order to eliminate most of the near-far conditions. Although the specification seems lax, some of the ACI specification has been used up by the modulation scheme adopted and so intermodulation requirements are still quite tight.

2.4.2 Mobile Satellite

Unlike cellular systems the near-far effect does not exist with satellite systems since all

the mobiles are operated at long distances. However some operators allow users to access the satellite at different power levels which produces a pseudo near-far problem. Consequently systems such as Australian Optus Mobilesat can set ACI at −35dB in the adjacent channel and −50dB for all other channels.

2.4.3 Private Land Mobile Radio (PMR)

Most PMR systems presently in use utilize analog FM as the modulation system. As with mobile cellular there is a trend towards digital transmission which can relay data (for despatch purposes etc.) and voice. A new digital modulation system would have to co-exist with current analog users for quite some time. The scattered and uncontrolled nature of PMR basestations causes severe near-far problems and hence the ACI specification is quite tight e.g −70dB for APCO25 and −60dB for TETRA.

2.4.4 Future Systems

It is likely CDMA systems will feature prominently in future communications systems. Qualcomm's proposed CDMA cellular and mobile satellite systems for example, will require some linear amplification and wide dynamic range power control. Power control is crucial in CDMA systems and hence any linearization strategy should consider this additional requirement.

2.5 REVIEW OF AMPLIFIER LINEARIZATION TECHNIQUES

Varying degrees of distortion is always present in electronic systems. Early work in amplifier linearization focused on cross-modulation distortion present in multichannel systems and on intermodulation distortion of amplitude modulated signals. Although the linearization techniques developed here were aimed at mobile radio, much of the linearization work reviewed spans many applications including: fixed point-to-point microwave radio links, CATV (Community Antenna Television), satellite
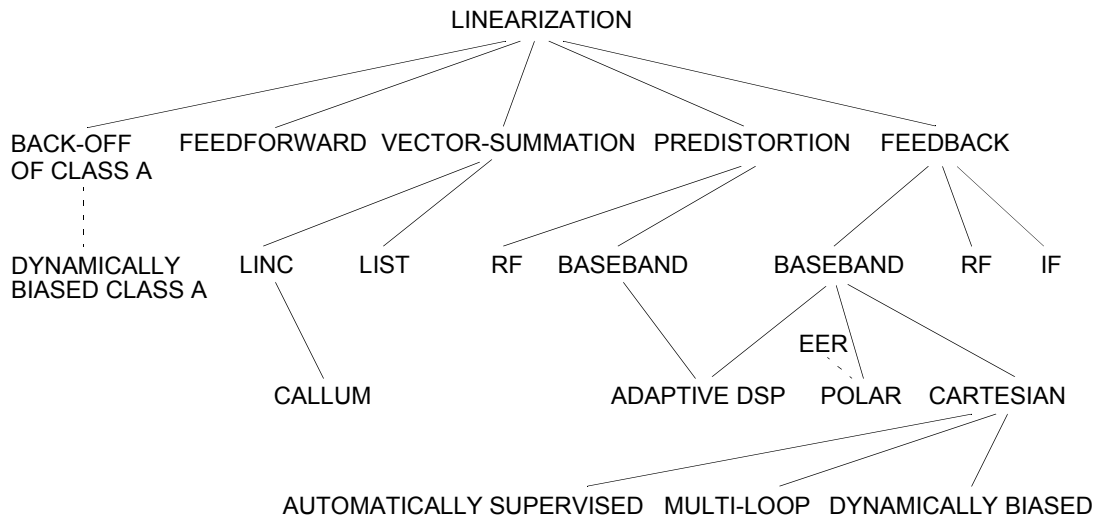
Figure 2.12: *Amplifier linearization techniques*

communications and multi-carrier basestations. In each case the objective is to improve linearity without sacrificing efficiency.

Despite the broadness of the linearization area, the linearization techniques can be roughly divided into a number of approaches - some of which draw from similar roots. Figure 2.11 shows graphically how the various linearization techniques interrelate.

2.5.1 Back-off of Class A

Amplifier back-off is the conventional approach of improving RF power amplifier linearity. The technique involves operating power amplifiers at a fraction of their saturated output power potential. The further the device is "backed-off" the better the improvement in intermodulation distortion. A 1dB back-off or reduction in output power (i.e a 1dB reduction in the fundamental frequency output power) results in a 3dB reduction in the 3rd order intermodulation distortion, a 5dB reduction in the 5th order intermodulation product and so on. This results in a 2dB, 4dB etc. improvement respectively (figure 2.12a). Since the DC power dissipation remains constant irrespective of the output power for a class A amplifier, the efficiency of the amplifier diminishes as linearity improves. Consequently to achieve the intermodulation performance desired for

(a)   *(b)*
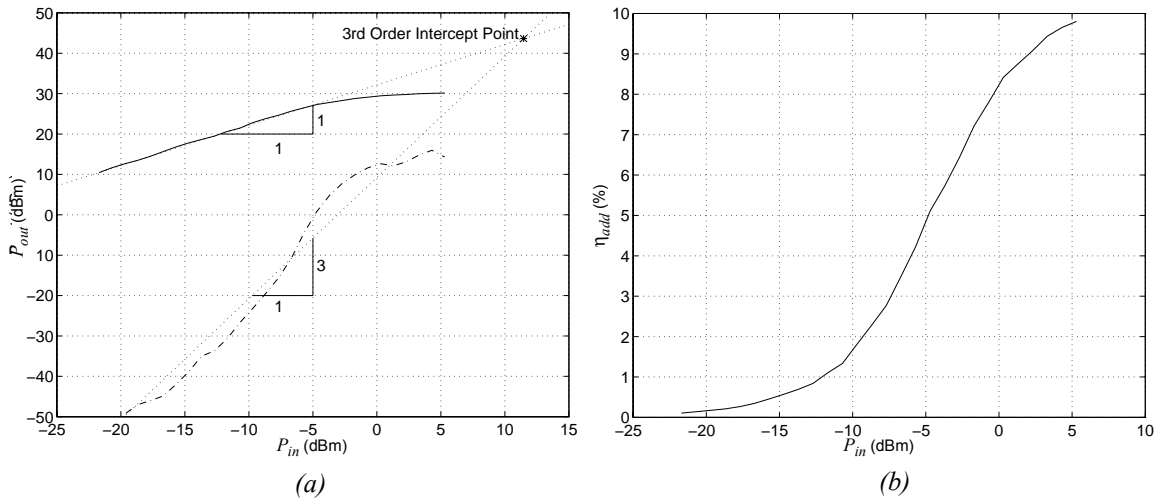
Figure 2.13: *(a) Fundamental output power (solid) and third order intermodulation distortion (dash-dot) versus input power for a two-tone test. Fundamental power rises on a one-to-one basis whereas third order power rises on a three-to-one basis (dB scale). Interception of both gradients is shown with an asterisk. (b) Power added efficiency (ηadd) versus input power under the same conditions as (a).*

most mobile communication applications the amplifier will be unduly wasting significant amounts of DC power (figure 2.12b). For many mobile applications the efficiency will be below 1%. Such a condition is highly undesirable in portable wireless applications. Further disadvantages are also incurred since the size of devices tend to be larger and thus heavier, and usually are more costly.

2.5.2 Dynamically biased Class A

This technique was introduced by Saleh[10] as a means by which the power-added efficiency of Class A Field Effect Transistor (FET) could be improved when operating with linear modulated signals. Instead of fixing the gate bias of an FET to roughly midway between the pinch off voltage (V_p) and zero volts (the condition for Class A operation), the gate bias voltage (V_g) is varied dynamically in response to the envelope of the input signal given by $V_e(t)$, such that $V_g = -V_p + V_e(t)$. This way the FET is nearly turned off when $V_e(t)$ approaches its minimum and the mean gate bias voltage is just enough to ensure the FET has sufficient dynamic range for the input signal. The benefits

of such a biasing scheme include higher power added efficiency at microwave frequencies.

2.5.3 Feedforward Linearization

Feedforward was invented as means of distortion reduction in amplifiers by Black[11]. This technique is usually applied directly at RF and is shown in figure 2.13.

The feedforward scheme consists of two sections. The first compares an attenuated version of the power amplifier (PA) output with the PA input to get the distortion generated in the PA. This distortion (given by "Error" in the diagram) is destructively combined at the output of the PA by a linear auxiliary amplifier. The resultant output is then ideally distortion free. The process has been demonstrated in the diagram for a two-tone test input. The two time delays are necessary to match any delay and frequency dependent phase shifts introduced by the respective amplifiers. Any deviation from exact amplitude and phase matching will degrade the subtraction process and subsequent distortion cancellation[12].

Amplitude and phase matching is a problem since amplifier characteristics tend to drift with temperature and time, and also vary with manufacturing tolerances. Adaptive
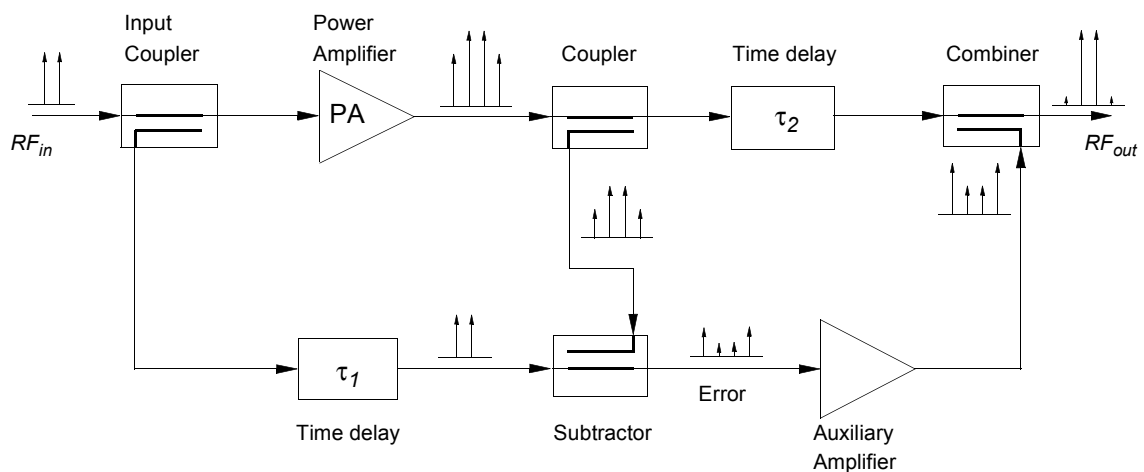
Figure 2.14: *Feedforward linearizer implemented at RF.*

techniques enable the performance of the system to be maintained despite these effects[12-13].

Efficiency of the feedforward system is reduced by the power consumption of the auxiliary amplifier which must be linear and have a high enough output power capability to overcome the loss through the output coupler.

Feedforward linearization can however deliver reasonable linearization performance (20dB-40dB improvement) over relatively wide bandwidths (3MHz-50MHz) and has the advantage of inherent stabilty[14-15].

2.5.4 Vector Summation

Vector Summation[16] is a technique which exploits the fact that the combination of two or more constant envelope signals can result in a signal with a varying envelope and phase. This arbitrary amplitude and phase modulation can be obtained by selecting the appropriate phase relationship of each of the constant envelope carriers. Amplification of constant envelope signals need not be linear and hence the use of highly efficient amplifiers is possible. The main disadvantage is the inherently lossy nature of the combining process which reduces the overall efficiency.

2.5.4.1 LINC
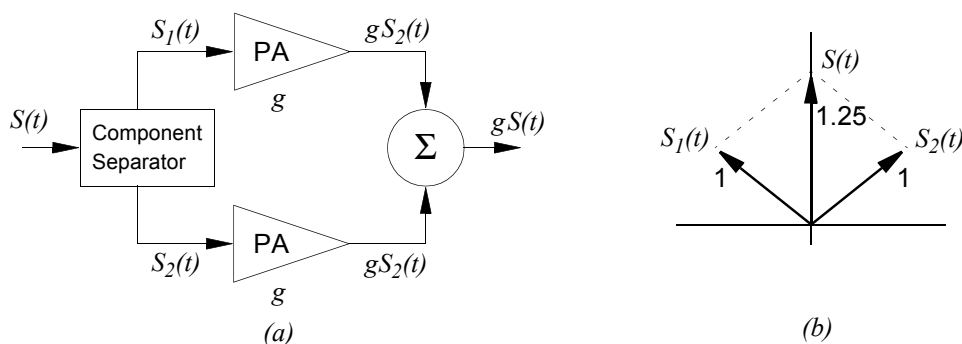
Figure 2.15: *(a) Block diagram of LINC transmitter. (b) The combination of two constant envelope vectors ($S_1(t)$ & $S_2(t)$) yields a replica ($S(t)$) of the desired output signal ($gS(t)$).*

*LI*near amplification with *N*on-linear *C*omponents (LINC)[17] is a special case of vector summation. It uses two constant envelope signals to obtain the desired output signal (figure 2.14). The component separator uses analog or DSP techniques to generate the constant envelope signals ($S_1(t)$ and $S_2(t)$) such that when amplified and then combined these signals produce the desired output signal ($gS(t)$)[17-20].

With conventional combining techniques an average combining loss of 3dB occurs reducing the maximum possible efficiency of LINC to 50%. Overall efficiencies of 21% are easily achievable[18].

The LINC technique is susceptible to amplitude and phase differences in each of the paths. Differences in these paths can severely degrade system performance [18-19] and some form of feedback is usually necessary in order to compensate for variations in the amplifiers [18, 21].

2.5.4.2 CALLUM

The Combined Analogue Locked Loop Universal Modulator (CALLUM) proposed by Bateman[21] cleverly overcomes the complexity of DSP circuits whilst simultaneously coping with amplitude and phase differences in the two paths. The technique (figure 2.15) uses two feedback loops and VCO's (Voltage Controlled Oscillators) to generate the correct constant envelope signals. Under stable operation, the VCO's automatically take
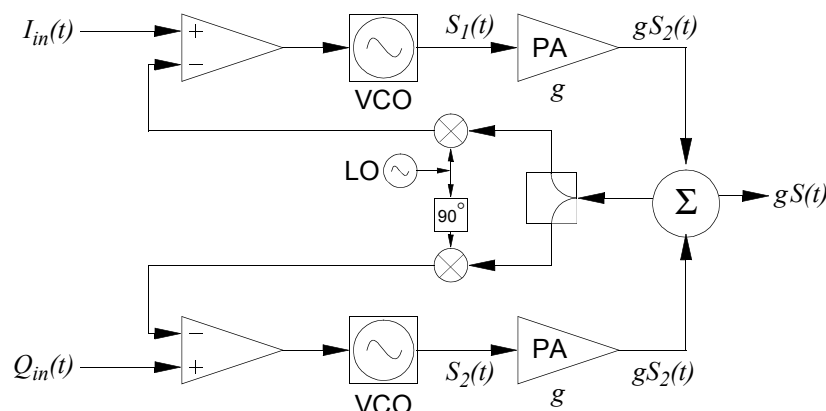
Figure 2.16: *The Combined Analogue Locked Loop Universal Modulator (CALLUM) transmitter.*

up the frequency of the Local Oscillator (LO) and therefore preform frequency translation. Furthermore the VCO's are driven to generate the necessary constant envelope LINC signals ($S_1(t)$ & $S_2(t)$) and if these oscillators are power types, they could also provide the RF power given by the RF power amplifiers in conventional LINC systems.

Bateman demonstrated 55dB of intermodulation distortion suppression was possible for a Nyquist filtered (α = 0.3) OQPSK (Offset QPSK) with a bandwidth of 30kHz. The CALLUM system does however rely on feedback which implies the potential for instability and errors introduced by the feedback gathering components (mainly in down converting mixers). Stability and further aspects of CALLUM are discussed in [22].

2.5.4.3 LIST

*LI*near amplification by *S*ampling *T*echniques (LIST)[23] is demonstrated in figure 2.16. The technique is similar to LINC in that it utilizes two constant envelope signals which are combined at the output to derive the desired linearly amplified output. The main difference to LINC is that the two signals can each only take two discrete phase values and are in effect combined in quadrature. The quadrature arrangement of the two constant envelope signals effectively gives four possible phase outputs.
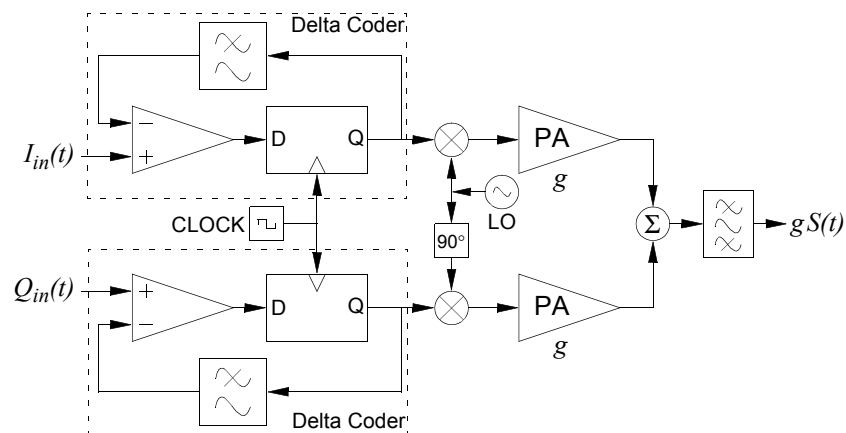
 Figure 2.17: *Linear amplification by Sampling Techniques (LIST) transmitter.*

The delta modulators shown in the dashed boxes enable any of the four possible phases to be selected in rapid secession at a rate given by the clock frequency. Filtering at the output reconstructs the signal to give the smoothed desired linearly amplified signal.

Cox[23] demonstrated that intermodulation products 40dB below the desired signals for a two-tone test (100kHz between tones) was possible for an amplifier operating at 70MHz.

The advantage with the technique is the relative ease by which the two constant envelope signals can be generated. Feedback was also proposed in [23] giving a similar improved tolerance to amplifier differences as with CALLUM. Delay in the delta coders and filtering components however reduces the amount of feedback that can practically be applied

2.5.5 Predistortion

Predistortion is a technique which modifies the input to a power amplifier such that it is complementary to the distortion characteristics of the amplifier (figure 2.17a). The cascaded response of complementary predistortion and amplifier distortion should therefore result in a linear response (figure 2.17b). The technique is generally applied at RF, IF or baseband.

2.5.5.1 RF Predistortion

Synthesizing an exact complement of an RF power amplifier at radio frequencies can be difficult. Usually an attempt is made to reduce the third order intermodulation products only by use of a cubic type canceller[24-28]. A block diagram of a cuber predistorter is

(a)   (b)
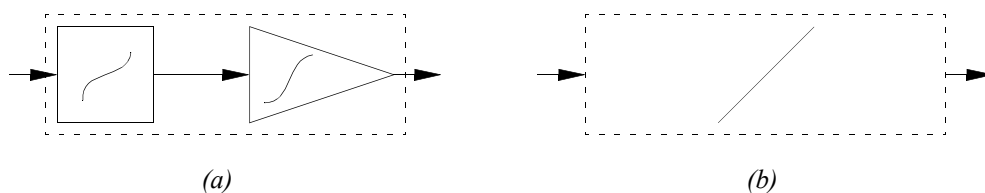
Figure 2.18: *(a) Combination of complementary predistortion and amplifier distortion yields (b) linear transfer.*
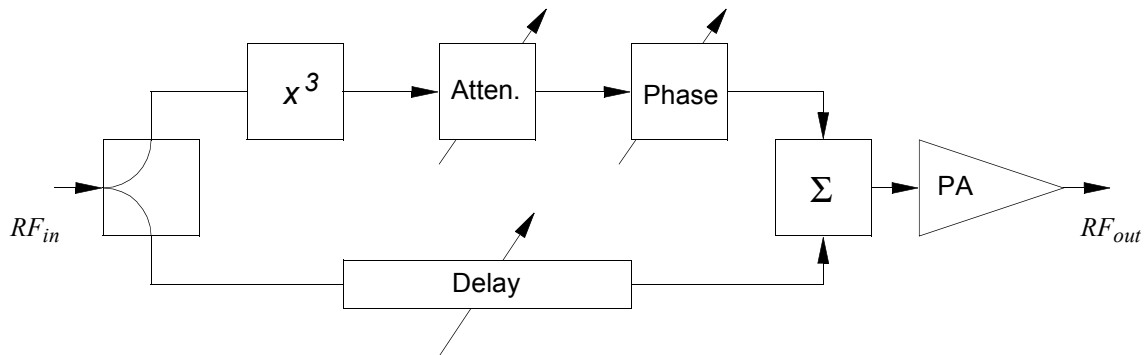
Figure 2.19: *Cubic canceller predistortion system.*

shown in figure 2.18.

A cubic law device (x^3 in the diagram) is used to generate third order distortion based on the magnitude of the RF input. This (pre)distortion is then added to a delayed version of the input and applied to the non-linear RF power amplifier. The amplitude and phase shift of the third order distortion is manipulated such that the third order distortion generated within the amplifier is cancelled. Making the adjustment adaptive can allow this technique to track drifts in the amplifier characteristics[24-25].

The cubic law device can be realized in a number of ways. Usually diodes are used with either a quadrature hybrid[25-26] or a circulator[27]. Alternatively a compressed amplifier[28] can be used.

The scheme is only suitable for weakly non-linear amplifiers since only third order distortion products are cancelled. Implementation at RF does however allow wide-band operation. Nojima[25] for example reported more than 20dB improvement in intermodulation distortion over a 25MHz bandwidth at 800MHz. Occasionally the predistortion is applied at an Intermediate Frequency (IF) to enable easier implementation for higher frequencies[29]. The potential disadvantage with IF techniques is the possible degradation introduced by the up conversion process.

There are other RF predistortion techniques and some will only be mentioned here. These

include: techniques aimed at suppressing AM/PM distortion using varactor diodes or ferrimagnetic materials[30]; and techniques which attempt to synthesize RF predistortion using circuits such as: RF driver stages whose distortion complements that of the main power amplifier; or transistor circuits which have non-linear elements in various feedback arrangements[31]. A more elaborate polynomial analog predistorter using mixers has also been proposed[32].

2.5.5.2 Baseband Predistortion Using DSP

Digital Signal Processing (DSP) offers the possibility of synthesizing complex predistortion characteristics. Because of speed limitations the predistortion must be applied at baseband and subsequently up converted. The linearization bandwidth is hence generally limited due to DSP processing. A generic DSP predistorter is shown in figure 2.19.

The forward path takes the digitized modulation signal and predistorts it in a complimentary manner to the amplifier distortion. The digital output is then converted into an analog signal for upconvertion and subsequent amplification by the non-linear RF amplifier. The upconversion process is typically performed with a quadrature modulator, however IF upconversion is possible. Optional adaptation feedback can be used to track out drifts in the amplifier and to also find the predistortion needed to achieve linear amplification.
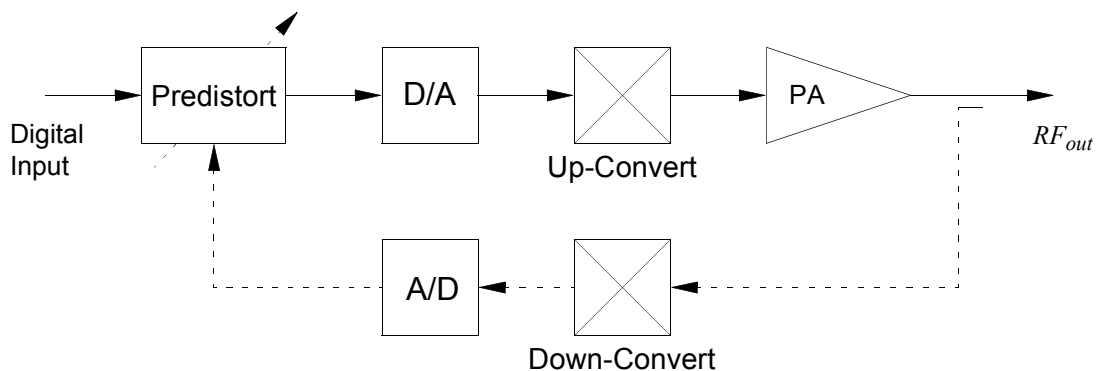
Figure 2.20: *Generic block diagram representation of an adaptive baseband DSP predistortion linearizer.*

The actual predistortion can be accomplished using polynomial representation, or with input output look up tables. Polynomial representation is the baseband equivalent[33] of the cuber predistorter described above. Since DSP offers more computational capabilities, higher order polynomials are possible resulting in a better representation of the desired predistortion. The main disadvantage with polynomial representation is the relative difficulty in having stable and effective adaptation algorithms.

The look up table predistorter is more popular for DSP implementation. The predistortion tables can take different forms. The most straightforward is the polar complex gain form shown in figure 2.20(a). This predistorter consists of two one dimensional tables. The amplitude map predistorts for the amplifier's AM/AM distortion and the phase map predistorts for the AM/PM distortion. The address of both maps is driven by the amplitude of the input signal. Faulkner[34] presented an adaptive polar predistorter using this technique. Interpolation between points in the tables allowed the use of a relatively small table size with only 64 entries. The computational effort necessary for the polar to rectangular conversion was found to be a potential problem. The overall computational load was quite high and with an ordinary DSP (TMS320C25) intermodulation distortion was reduced by 30dB over a limited 2kHz bandwidth. Another polar mapping predistorter proposed the use of cubic spline interpolation[35].

Cartesian complex gain tables avoid polar conversions and require a lower DSP processing load (figure 2.20b). Cavers[39] proposed the use of cartesian tables addressed by the signal power. Complex multiplication by the input signal is then used to apply the
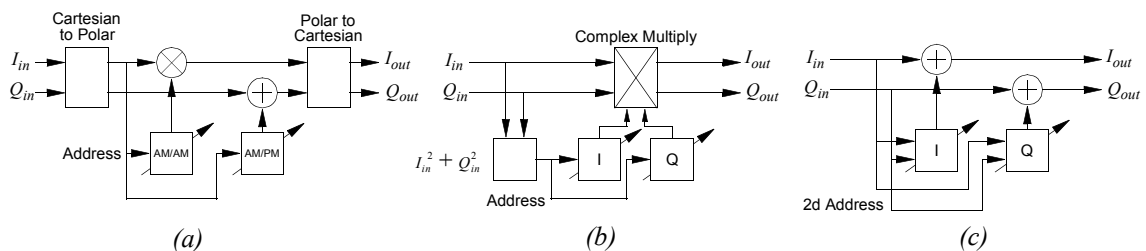
Figure 2.21: *Three examples of table based predistortion (a) Polar complex gain, (b) Cartesian complex gain, and (c) Full cartesian mapping.*

predistortion. The predistorter achieved a fast convergence time (4ms) due to the low memory requirements and a root finding secant adaptation algorithm.

Systems using complex gain tables (either cartesian or polar) cannot overcome quadrature modulation errors in the forward chain. To solve this problem Faulkner[36] proposed a circuit termed CRISIS (CRoss-coupled Intra-Symbol Interference Suppression). This circuit is capable of removing linear errors in both the up and down conversion process but requires a series of test signals.

Sundström[40-41] also proposed a complex gain based predistorter with a simpler and more robust adaptation algorithm, for which a chip was developed. The chip integrated the most important sections of the predistorter's functions including a CRISIS circuit. The application specific DSP significantly increased the modulation bandwidth (208kHz) and reduced power consumption to around 10% (100mW) of a standard DSP predistorter. The chip makes predistortion potentially viable for portable wireless applications.

Full cartesian mapping is another table based technique[37-38]. This technique requires a large amount of memory (2Mwords) in order to map an input point on the complex plane to an output point on the complex plane (figure 2.20(c)). Consequently adaptation is very slow (10sec @ 16kBits/sec) since there is a large region to be accessed repetitively before convergence occurs. Nagata's system[37] was able to achieve −60dB ACI for 32kBit/sec, π/4 Shift QPSK modulation. The system required an external phase adjuster to maintain stability but there was no need to correct for quadrature upconversion errors and hence it did not require a CRISIS circuit.

2.5.6 Feedback Linearization

Feedback was invented as a means of reducing distortion in amplifiers by Black[42]. Generic feedback is shown in figure 2.21. The input signal is amplified and filtered by the forward path consisting of loop compensation, *G(s)* and amplifier gain *g*. Distortion
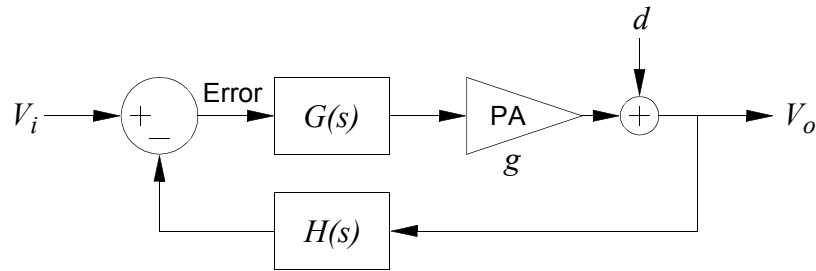
Figure 2.22: *Generic block diagram representation of feedback linearization principle*

generated within the amplifier can be modelled as an unwanted signal shown by *d*. The output is fed-back for comparison through *H(s)*. The action of the loop is such that the error is minimized forcing the output to track the input. This is best illustrated by

$$V_o = \frac{gG}{1+gGH}V_i + \frac{d}{1+gGH} \qquad (2.7)$$

As the loop gain (*gHG*) is made large two useful properties are demonstrated in the equation. The first is that the input begins to more accurately track the feedback signal regardless of the forward gain. The overall gain of the system in fact begins to primarily depend on 1/*H*. It is well known that making *H* dependent on passive stable components such as resistors will stabilize the overall gain of circuits significantly.

The second important property of feedback is demonstrated in the second term in the equation. As gain rises this term tends to zero and hence distortion is minimized. The amount of distortion reduction is given by 1 + *gGH* or the loop gain but if this is made too large instability can occur (primarily due to the fundamental limitation of delay in the systems described in this thesis).

2.5.6.1 RF Feedback

RF feedback[43-45] is the most direct application of feedback. For stability to be maintained, the bandwidth of the loop compensation is usually a very small fraction of the centre operating frequency. The loop compensation at radio frequencies therefore requires very high Quality factor filters such as cavity filters.

If suitable filters are available, the technique is capable of reasonable performance. Rosen[43] reported a 13dB improvement in third order intermodulation distortion over a 1MHz bandwidth at 3GHz. Ezzeddine[44] was able to get 8dB improvement over 3MHz bandwidth at 4GHz.

Both of the previous references cited used passive feedback networks. Ballesteros[45] proposed an active feedback network incorporating an auxiliary amplifier whose gain exhibited a peak at the compression point of the main amplifier. This enabled the loop gain to be maintained right up into compression. Another benefit with the scheme was that the forward gain of the amplifier was not reduced (as is the case with passive feedback). The active feedback system described was able to increase the output power for an ACI level of -40dB by 3.2dB in 130MHz band centred at 1GHz.

Another form of feedback linearization was presented by Hu[46]. Hu demonstrated that for a two-tone test with frequencies f_1 and f_2, low frequency feedback centred at $f_2 - f_1$ could yield a reduction in third order intermodulation distortion. This would be equivalent to placing feedback around the $2f_m$ component shown in figure 2.9. An improvement of 12dB was demonstrated at 10GHz using a tone separation of 10MHz. An analytical explanation using Volterra Series was also given.

2.5.6.2 IF Feedback

IF (Intermediate Frequency) feedback[47] is similar to RF feedback except the loop compensation is performed at a somewhat lower frequency. This relaxes the sharpness of the filter required and enables the use of lower Quality factor filters. Higher loop gains are hence possible with narrow bandwidths.

The technique presented by Voyce[47] is shown in figure 2.22. The potential problem with IF feedback is the up and down conversion process. The system shown in the figure has the up and down conversion process within the feedback loop therefore reducing errors introduced by these components. The actual comparison is done at RF (not IF) and
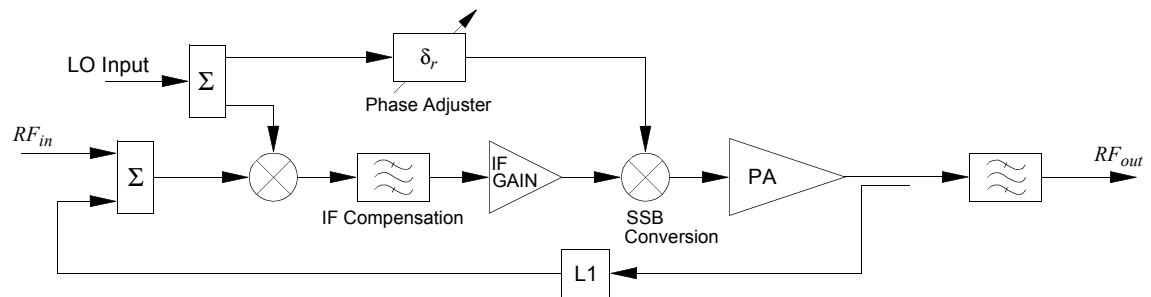
Figure 2.23: *IF feedback linearization after Voyce*[47].

so the system can be thought as an RF feedback system with IF compensation. Voyce's system was able to reduce intermodulation distortion by 12dB over a 1MHz bandwidth centred at 450MHz. The IF frequency used was 20MHz.

2.5.6.3 EER and Baseband Polar Feedback

EER (Envelope Elimination and Restoration) was developed by Kahn[48-49] as a means of efficiently transmitting Single-Side Band (SSB) modulation (a linear modulation).

The technique is shown in figure 2.23. The input is separated into two parts. A hard limiter removes the amplitude modulation of the signal and provides the phase modulation only. This constant envelope signal is then efficiently amplified by a non-linear power amplifier.

The amplitude modulation of the signal is obtained by envelope detection and applied at the power supply of the power amplifier by high level modulation. This imparts the amplitude modulation upon the phase modulated signal and reconstitutes the original
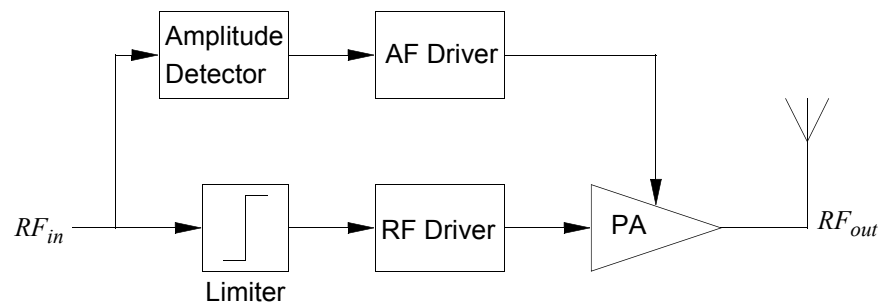
Figure 2.24: *Envelope Elimination and Restoration (EER) after Kahn*[48-49].

signal.

Kahn made improvements to the basic scheme such a the use of a phase equalizer in the limiter path to equalize the time delay between the phase modulation and amplitude modulation.

Kahn's system was improved by the introduction of feedback. This feedback is termed polar feedback since EER essentially utilizes an amplitude and phase representation of the signal. Petrovic[50] introduced the polar loop transmitter shown in figure 2.24. The operation of the transmitter is similar to EER except feedback has been applied to correct for errors in the amplitude and phase modulation process, and so the spectral purity on the output is improved. Another major difference is the use of a VCO to generate the necessary phase modulated drive for the power amplifier. By the nature of stable phase feedback, the frequency of this VCO must match that of the down converted output phase much like a Phase-Locked-Loop (PLL).

Petrovic reported some impressive results such as a spurious free output below 50dB for a two-tone test for amplifiers operating at 100MHz and 13W peak output with an efficiency of 55%. It is likely that the efficiency quoted does not consider the power consumed in the high level modulator.

Resolving the modulation in polar form does however have the problem of spectral
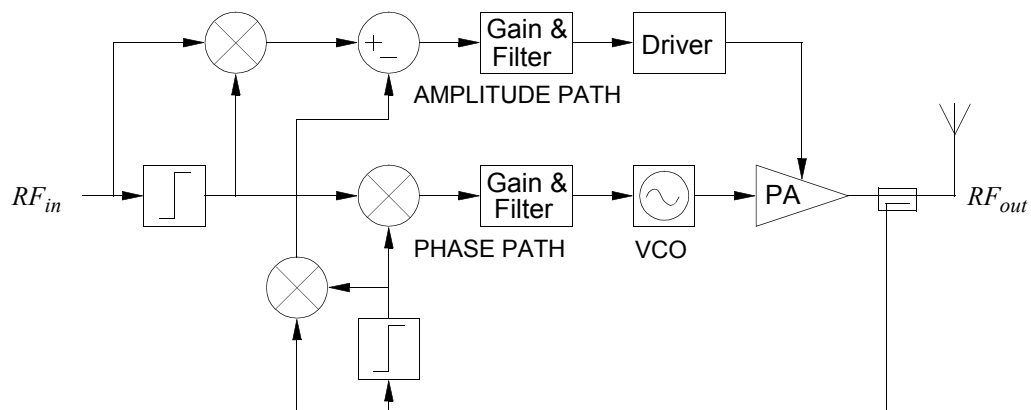
Figure 2.25: *Polar feedback loop after Petrovic*[50].

expansion. This means the spectral components of the amplitude modulation and phase modulation signals alone can be wider than the spectrum of the final output. Both the amplitude loop and phase loop must then be able to accommodate a wider bandwidth[51]. The finite bandwidth of both feedback loops therefore places a limit on how well intermodulation distortion is suppressed regardless of how much loop gain is employed. Other limiting factors are discussed and analysed in [51] and include: leakage to the output of the phase modulated carrier; timing error between the related amplitude and phase modulation functions; nonlinearity of the high level amplitude modulator; and nonlinearity of the polar resolver (i.e non-linearity in the amplitude detector and phase detector)

Efficient application of the high level amplitude modulation is a problem with the polar loop transmitter. Koch[52] suggested the use of a PWM (Pulse Width Modulated) switched-mode power supply to drive the power supply. The problem is however, the switching frequency must be made high in order to accurately track the amplitude modulation which due to bandwidth expansion has wide bandwidth. With a switching frequency of 400kHz and a measured efficiency of 90% for the switch mode, Koch reported a total efficiency of 50% for a two-tone test operating at a carrier frequency of 835MHz and an average output power of 5W. The intermodulation distortion products were 30dB down. Only the amplitude was fed back and so it is likely that further improvements in the intermodulation performance could be achieved using phase feedback also.

Chiba[53] presented an alternative amplitude only polar feedback scheme. The amplitude feedback was applied at a low level via a voltage controlled amplifier (VCA). This is advantageous since the switch mode power supply driver no longer has to handle the dual task of efficient high level modulation and applying this amplitude modulation accurately enough to provide a high degree of intermodulation distortion suppression. The switch mode power supply modulator was driven open loop. Chiba reported a total efficiency of 40% with intermodulation distortion being 50dB down for a system operating at 1.5GHz.

2.6 CARTESIAN FEEDBACK LINEARIZATION SYSTEMS

Cartesian feedback linearization which uses negative feedback of in-phase and quadrature baseband modulation, is another narrow band modulation feedback scheme. It has been given prominence here since the majority of this thesis discusses various aspects of cartesian feedback.

Petrovic[54] first proposed what is commonly referred to as cartesian feedback. The basic principle of cartesian feedback is shown in figure 2.26. The baseband inputs to the system in I and Q format, form the reference signals to the loop. The forward path of the system consists of the main control loop gain and compensation filters, a synchronous I-Q modulator, a non-linear but efficient RF power amplifier, and the antenna acting as an output load.

The feedback path obtains a portion of the transmitter output via an RF coupler, the signal from which is then synchronously demodulated. The resultant demodulated I-Q baseband
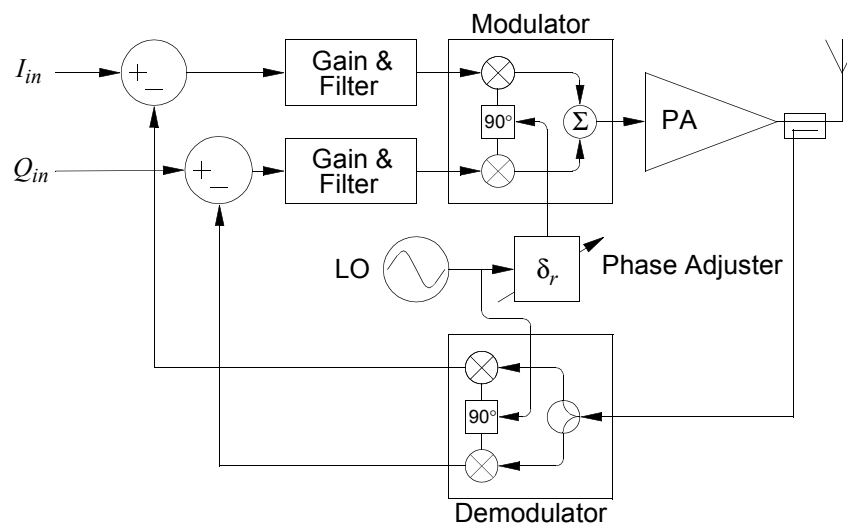
Figure 2.26: *Cartesian feedback transmitter.*

signals are used as the primary feedback signals and are subtracted from the input. The resultant error signal becomes the necessary pre-distorted drive for the non-linear amplifier. Since the output is driven to follow the input, linearization is achieved with the loop being able to automatically compensate for drifts in amplifier non-linearities due to temperature and power supply variations.

The loop control characteristics are established by the gain and the compensation filters. The level of intermodulation distortion reduction is essentially governed by the loop gain, and the compensation allows the stability and behaviour of the system to be controlled.

Synchronism between the modulator and demodulator is obtained by splitting a common RF carrier. Due to RF path differences in the forward and feedback paths, a phase adjuster (δ_r) is necessary to maintain the correct relationship between the input signals and feedback signals. Incorrect setting of the adjuster results in cross-coupling between the I and Q components, and at the extreme can invert the feedback. Common with other closed feedback loops, this technique is only conditionally stable and the setting of the adjuster with the aim of maintaining stability is one of the key problems. Amplifier non-linearities also effect stability as does excessive baseband phase shift. The setting of the adjuster and how the RF amplifier non-linearities influence this setting is discussed in chapter 4. Practical results of phase adjusting strategies are given in the next section.

As with other feedback schemes the ultimate performance of the loop is limited by the quality of feedback. Errors and distortion in the feedback gathering circuits, especially in the demodulator will create errors and distortion on the output regardless of the amount of loop gain employed.

Still, using fairly simple circuitry cartesian feedback can deliver good results and hence warrants the further investigation given in this thesis. Petrovic[54] for example was able to achieve intermodulation products 70dB below the main signal for a two-tone test with an amplifier operating at 2.5MHz for 1W PEP (Peak Envelope Power). In [55] Petrovic

reports intermodulation products 70dB below 100W PEP for a two-tone test. These results were obtained for a HF band (1.6-30MHz) transmitter. This transmitter incorporated an IF stage to enable it to operate over the many octaves which constitute the HF band. Petrovic[56] also achieved similar results for a VHF transmitter.

There are a number of other examples operating at higher frequencies. Johansson[57-58] presented detailed measured results on two transmitters operating at 900MHz. For the narrowband transmitter described, −60dB out-of-band emissions was achieved with 38% power added efficiency for a two-tone test (20kHz between tones). For the wideband transmitter Johansson reported a 20dB improvement in intermodulation distortion with 40% power added efficiency for a two-tone test (1 MHz between tones). This particular result demonstrates the feasibility of cartesian feedback to handle new forms of modulations like CDMA and wideband 16QAM.

The only limitation to the operation frequency of cartesian feedback is finding suitable components. Wilkinson[59] reported the highest frequency (1.7GHz) of operation to date. Out-of-band emission was 38dB below a PEP of 400mW for a two-tone test (4.2kHz between tones).

2.6.1 Automatically Supervised Cartesian Feedback

A well designed cartesian feedback loop is a good performer provided it is stable. Petrovic[55] first implied the use of an additional controller to set the phase adjuster in order to maintain stability. Brown[60] presented this controller as a means of maintaining stability in a HF SSB transmitter. Brown's adjuster was able to operate with the cartesian loop open or closed by measuring the phase between the feedback and the signals prior to upconversion (i.e the predistorted drive). A SSB tone (2.5kHz) was used to adjust the transmitter in open loop. After the phase error was sufficiently reduced (4°), the loop was closed and continuous phase monitoring was enabled whilst transmitting SSB voice modulation. If the phase error deviated by more than a prescribed level (25°) during

transmission, the voice modulation was interrupted and the tone re-inserted for the adjustment process to be re-preformed. Brown found that the phase setting did not deviate significantly as a function of time and hence proposed the possibility of storing the phase adjustments as a function of channel frequency in memory.

The phase detection was achieved with an XOR (Exclusive OR) gate connected between one of the demodulated feedback signals and one upconversion signal (thus limiting the phase controller to SSB signals). Two low-pass filters were used following the phase detector. The filter with the lower cutoff (5Hz) was used to monitor the transmitter whilst transmitting SSB voice modulation. The filter with the higher cutoff (1.9kHz) was used in the setting operation with the transmitter in open loop. The use of a low cutoff filter for monitoring and a higher cutoff filter for setting enabled the whole adjustment process to be performed in 40ms.

Brown's adjuster has the disadvantage that transmission is interrupted if the transmitter's phase error rises unacceptably. Periodic open loop phase adjustment, in a spare TDMA (Time Domain Multiple Access) time slot for example, is one way this problem could be overcome. Since one SSB tone is used in Brown's adjustment process no intermodulation distortion is generated during the adjusting procedure time slot.

Ohishi[61] and Kubo[62] presented another automatic phase adjuster. This adjuster was operated during TDMA ramp ups. A measurement of the demodulated phase was made during this time to provide an appropriate adjustment. Once the correct phase is set (just before the end of the ramp up period), the loop is closed and the gain gradually increased. This process of gradually increasing gain was termed soft-landing. Unlike Brown's phase adjuster, this adjuster used both demodulated lines for phase measurement allowing it to operate with any modulation. The phase was measured using a technique known as direct phase quantization.

The feedback gathering circuits pose other limitations on the ultimate performance of the

cartesian feedback system. The demodulator used to get a replica of the transmitted output, introduces DC offsets and other linear errors like gain and phase imbalance. The demodulator mixers also introduce non-linear errors such as intermodulation distortion. All of these undesirable errors appear at the transmitter output and should be minimized.

Bateman[63] proposed a circuit for the reduction of DC offsets using two analog sample and holds (one for the I channel and one for the Q). DC offset reduction was achieved by first switching off the RF power amplifier and then forcing the predistorted drive signals to zero by adding opposing DC voltages to the demodulated signals. After settling to the necessary opposing voltages, the sample and holds were switched to hold. This process took 150μs to achieve carrier leakage levels 45dB below PEP. Recalibration was required every few minutes. A successive approximation register and D/A could be substituted for the analog sample and hold to enable a long drift free hold condition.

Demodulation errors pose a similar problem to the quadrature modulator errors in polar and gain mapped adaptive predistortion systems. The use of a CRISIS like circuit could therefore be used to minimize these demodulation errors. The optimum position for this CRISIS circuit would be at the input of the cartesian feedback loop since placing a DSP circuit within the loop would unduly introduce delay.

In summary then, the practical application of cartesian feedback requires supervisory circuits. These supervisor circuits can overcome: the potential limitations of stability and the setting of the phase adjuster; and the effects of linear errors and other distortions introduced by the feedback gathering circuits. TETRA is one standard which specifically acknowledges the time required by the supervisory circuits to adjust the transmitter and hence has allocated a linearization adjustment time slot[64] in the frame structure.

2.6.2 Multi-loop Cartesian Feedback

Cartesian feedback is generally suitable for narrowband applications only. Johansson[65-
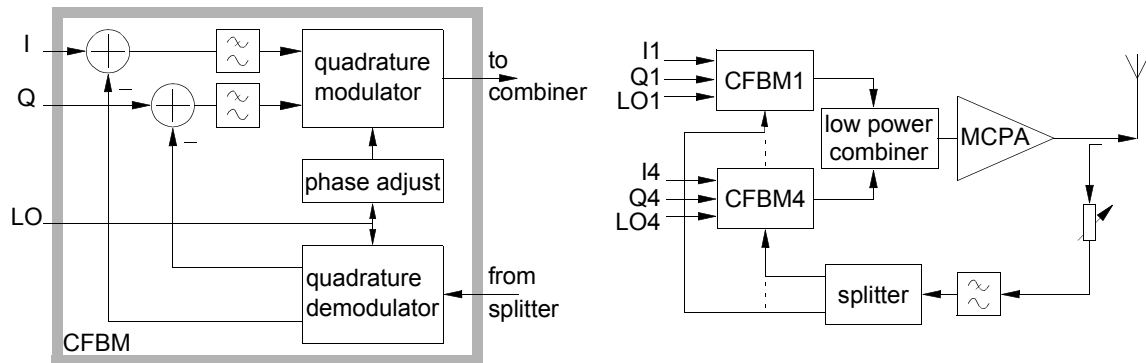
Figure 2.27: *MCPA linearization with multi-loop cartesian feedback after Johansson[65-66].*

66] presented a technique which attempted to extend the bandwidth capability of cartesian feedback. The scheme involves using several cartesian feedback modules (CFBM) operating with center frequencies across a band (figure 2.27). The intended application was Multi-Carrier Power Amplifiers (MCPA) which enable transmission of many user channels through one linear power amplifier. The loops were arranged such that the bandwidth of each loop did not overlap and hence were acting independently. This is necessary since as the loops are placed closer together in the frequency domain, the overall behaviour begins to approximate that of one loop of wide bandwidth, which in-turn then becomes restricted by the fundamental limitations of delay that limits all cartesian feedback loops.

Johansson also suggested placing cartesian feedback loops even on empty transmitter channels in order to suppress intermodulation distortion falling in these channels. Johansson placed four loops (1 MHz apart) in an experimental systems operating at 880MHz and achieved up to 30dB suppression in intermodulation distortion. Each of the loops was carrying a two-tone test with 20-26kHz separation between the tones.

2.6.3 Dynamically Biased Cartesian Feedback

RF power amplifier characteristics are strongly dependent on power and bias supplies. Smithers[67] presented a scheme of modifying the power supply so that gain, phase shift and input impedance were simultaneously linearized. This simultaneously linearized

Figure 2.28: *Dynamically biased polar loop transmitter after Smithers* [67].

point was found to be just before the onset of amplifier saturation (as a result of extensive amplifier characterization). Amplitude only polar feedback (i.e envelope feedback) was proposed as the means by which the optimum point was maintained. A further improvement was made to the scheme by measuring the amount and sign of the input reflection coefficient (with a directional coupler and a mixer) and using this information to control the feedback (figure 2.28). Smithers demonstrated constant input impedance could be maintained over the full power range with this technique. Smithers also achieved −40dB spurious output for a two-tone test and was able to maintain excellent efficiency (around 70%) for much of the power range.

The work presented in this thesis has some similarity to the work of Smithers. Comprehensive amplifier data was taken as described in the next chapter. From this data the optimum power and bias supply for best power added efficiency was determined and used in a "Dynamically Biased Cartesian Feedback" loop (figure 2.29). The dynamic bias circuits shown in the dashed box force the amplifier to operate in the most efficient way for the desired output envelope. The cartesian feedback then finely adjusts the RF amplifier input until the exact desired output is maintained. This is an important and distinct difference to Smithers' work since the linearization process is separate from the dynamic bias process. The separation of the two functions enables the application of the dynamic bias signals, particularly the power supply signal, to be relaxed. The switch-mode power supply therefore need not be accurate and so the switching frequency does

Figure 2.29: *Dynamically biased cartesian feedback transmitter as proposed in this thesis (see chapter 5 for more details).*

not have to be unduly high. Dynamically biased cartesian feedback is one of the major contributions of this thesis is discussed in more detail in chapter 5.

2.7 CONCLUSION

The pressures of limited spectrum has driven the adoption of linear modulation schemes. Efficient and linear power amplification is hence an important consideration for portable wireless applications.

This need for efficient linearized amplifiers has prompted the re-investigation and interest of various linearization schemes. Feedforward, vector summation, predistortion and feedback are linearization strategies which begin with a non-linear yet efficient power amplifier and linearize it to an acceptable level of ACI.

Of the linearization methods discussed in this chapter, CALLUM, adaptive predistortion

using DSP and cartesian feedback are the most promising techniques suitable for application in portable wireless applications. Of these, cartesian feedback was selected for study here because it had the potential for excellent performance with relatively simple circuitry suitable for both hand-held implementation and also for single channel linear basestation applications. The problems of stability offered a challenge as did the scope for improving its efficiency. These issues are discussed in more detail in chapters 3, 4 and 5. The next chapter details cartesian feedback linearization.

3 CARTESIAN FEEDBACK LINEARIZATION

The preceding chapter primarily examined contributions to the field of RF amplifier linearization made by other researchers. The remainder of the thesis is essentially concerned with contributions made by the author in cartesian feedback.

Since the basic premise of most linearization schemes is to start with an efficient yet non-linear RF power amplifier and then linearize it, it is appropriate to first examine the amplifier and the techniques used to characterize it. This is discussed in section 3.1. The amplifier is also the most dominant component in the cartesian feedback loop. Two amplifiers were used in this research, one intended for low power applications and the other for basestation applications.

Many behavioural properties of feedback systems can be predicted from the open loop frequency response. How the frequency response is modelled and how the open loop gain improves linearity is discussed in section 3.2.

Simulations were performed to demonstrate how intermodulation distortion generated by the amplifier is reduced by the application of feedback. It is shown in section 3.3 that the frequency response essentially determines the degree of improvement and the bandwidth over which it can be obtained.

Section 3.4 presents measured results from the implemented hardware. The results demonstrate the viability of cartesian feedback as a means of achieving linear amplification coupled with good efficiency. DC offsets and instability caused by poor adjustment of the RF phase adjuster are two prominent practical problems with the experimental hardware (section 3.5).

3.1 MEASUREMENT OF RF POWER AMPLIFIERS

The most dominant component in a cartesian feedback system is the RF power amplifier (PA). Measurement of this component is therefore important in deriving a suitable model for further analysis and simulation.

The nonlinearites of an RF PA are amplitude dependent. It is necessary therefore to know how the amplifier output and phase characteristics vary with input drive level.

The first attempt at RF PA characterization consisted of a vector network analyzer (HP8753C) connected via GPIB to a computer (figure 3.1). The network analyzer was used to generate a power swept input signal to the PA. The RF phase and gain of the PA was then measured as a function of input power. The computer was used to store and process the data.

It is straightforward to accurately calibrate the network analyzer for relative measurements (i.e for measurement of RF phase and gain at a fixed power level). However, the desired RF amplifier input output characteristics require absolute as well as relative accuracy. The power sweep delivered by the network analyzer should therefore be accurate and linear which is not the case. The manufacturer of the HP8753C recommends the use of a power meter to measure the power at the measurement port and set power correction values within the network analyzer. The measured nonlinearity in
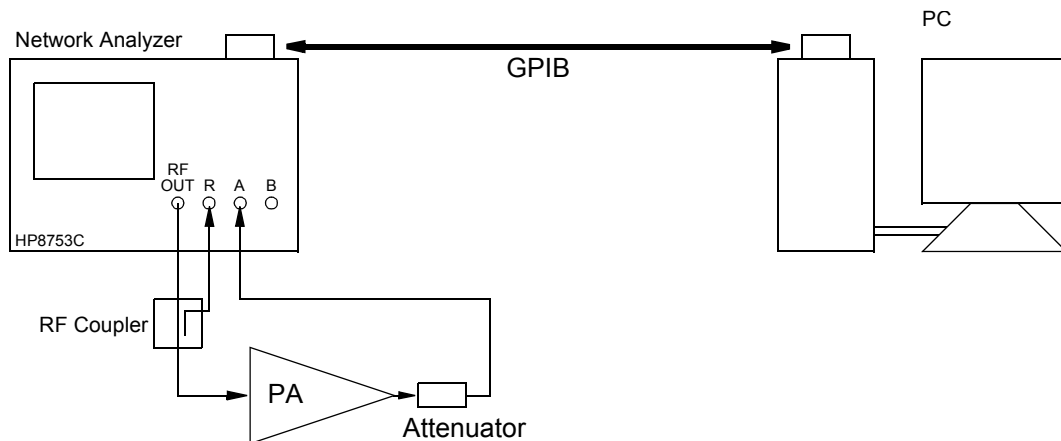
Figure 3.1: Early RF power amplifier test rig. RF connections via semirigid cable and SMA connectors.

the power sweep is shown in figure 3.2 which gives the measured output power as a function of displayed desired output power at a carrier frequency of 900MHz (as measured by a Rhode & Schwartz NRVD power meter and a Z2 linearized zero-bias-Schottky diode measurement head at the output of the RF coupler).

At low powers (from −10dBm to −8dBm) the output power delivered by the 8753C remains flat. Then at about −7dBm the power begins to ramp up reasonably linearly until higher powers are reached. The power delivered between 22dBm and 25dBm is highly non-linear. At 24.7dBm the network analyzer gives a power unlevelled indication which
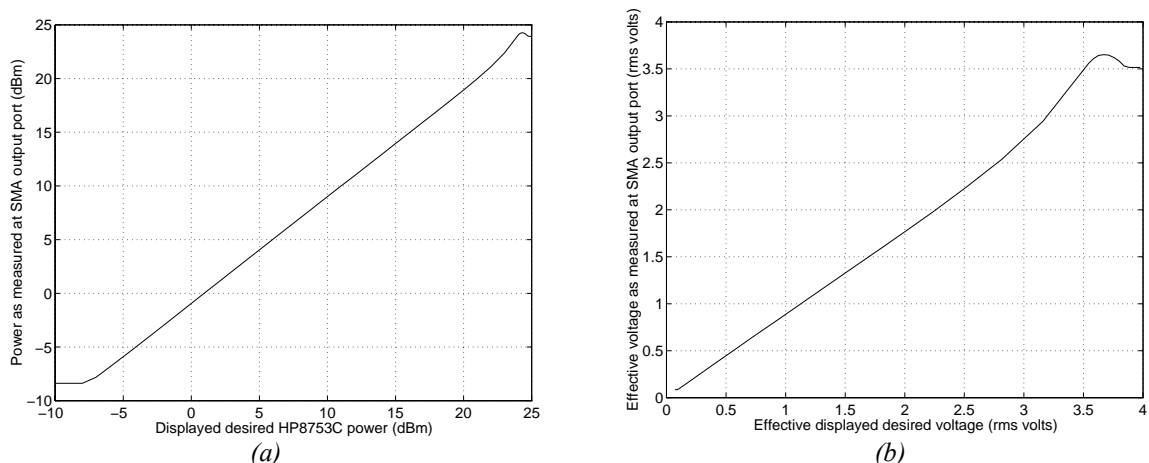
Figure 3.2: HP8753C Network Analyzer Power Sweep Non-linearity at a carrier frequency of 900MHz (a) dB scale, (b) Effective rms voltage into 50 ohms.

causes the output power to suddenly drop back to 24dBm. The high level power non-linearities are more obvious when the power is plotted in terms of equivalent rms voltage into 50Ω (figure 3.2(b)).

If left unchecked, such power level non-linearities will modify the measured characteristics of the PA.

The power levelling scheme actually adopted is shown in figure 3.3. The network analyzer is still used to provide the power sweep and measure the RF phase and gain. The addition of a power meter enables improved measurement of the PA's output power. Since a calibrated network analyzer can rather accurately measure the gain of the PA, the input power provided by the network analyzer can also be rather accurately determined (i.e P_{in}(dBm) = P_{out}(dBm) − *RF Gain*(dB)). The absolute accuracy of the input and output power is hence no longer determined by the non-linear power sweep of the HP8753C. The components separating the output of the PA from the power meter must also be calibrated.

The other additional components shown in figure 3.3 are a GPIB programmable ammeter
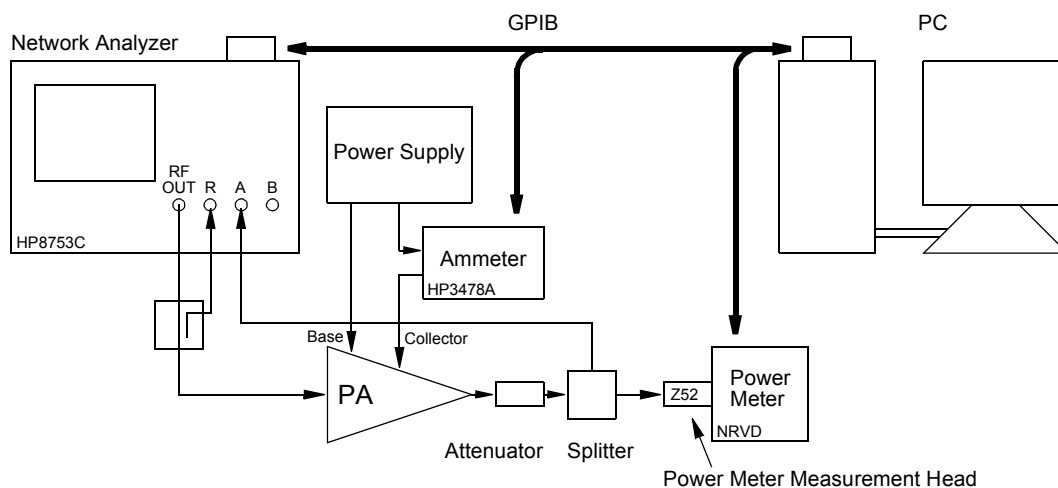
Figure 3.3: Improved RF power amplifier test rig. RF connections via semirigid cable and SMA connectors.

and a variable power supply. The ammeter is used to measure the current consumption and hence power consumption and efficiency of the PA. The variable power supply, which provides both collector bias and base bias is important for characterizing the amplifier under different V_{CC} and V_{BE} conditions. Chapter 5 discusses how bias optimization conditions can be used to improve the efficiency of a conventional cartesian feedback system.

3.1.1 Low Power Amplifier

A typical bipolar transistor (Philips BLU98) RF amplifier was constructed as described in the manufacturers data sheet (figure 3.4). The transfer characteristics using both test rigs are shown in figure 3.5. The true responses are shown in solid lines. The dashed lines indicate the erroneous responses obtained using the early test rig with the amplifier characteristics dipping at saturation. Modelling such a response in a cartesian feedback loop simulation program will change the sign of the gain and erroneously cause oscillation.

As was mentioned in chapter 2, the transfer characteristic highlights two main concerns with this type of amplifier, namely - amplitude response non-linearity and sudden phase changes (figure 3.5(*a*) & 3.5(*b*)). These effects occur most prominently at transistor turn-on (i.e. when $vbe \approx 0.7V$). Further measurements with this amplifier were taken with different bias conditions. These results are presented in chapter 5.
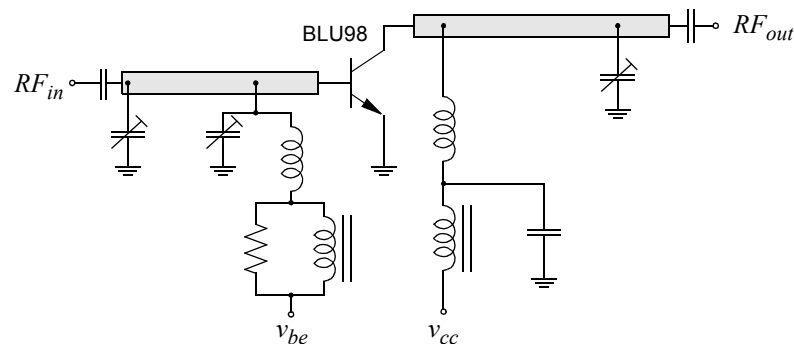
Figure 3.4: Low power BTJ RF power amplifier using BLU98.
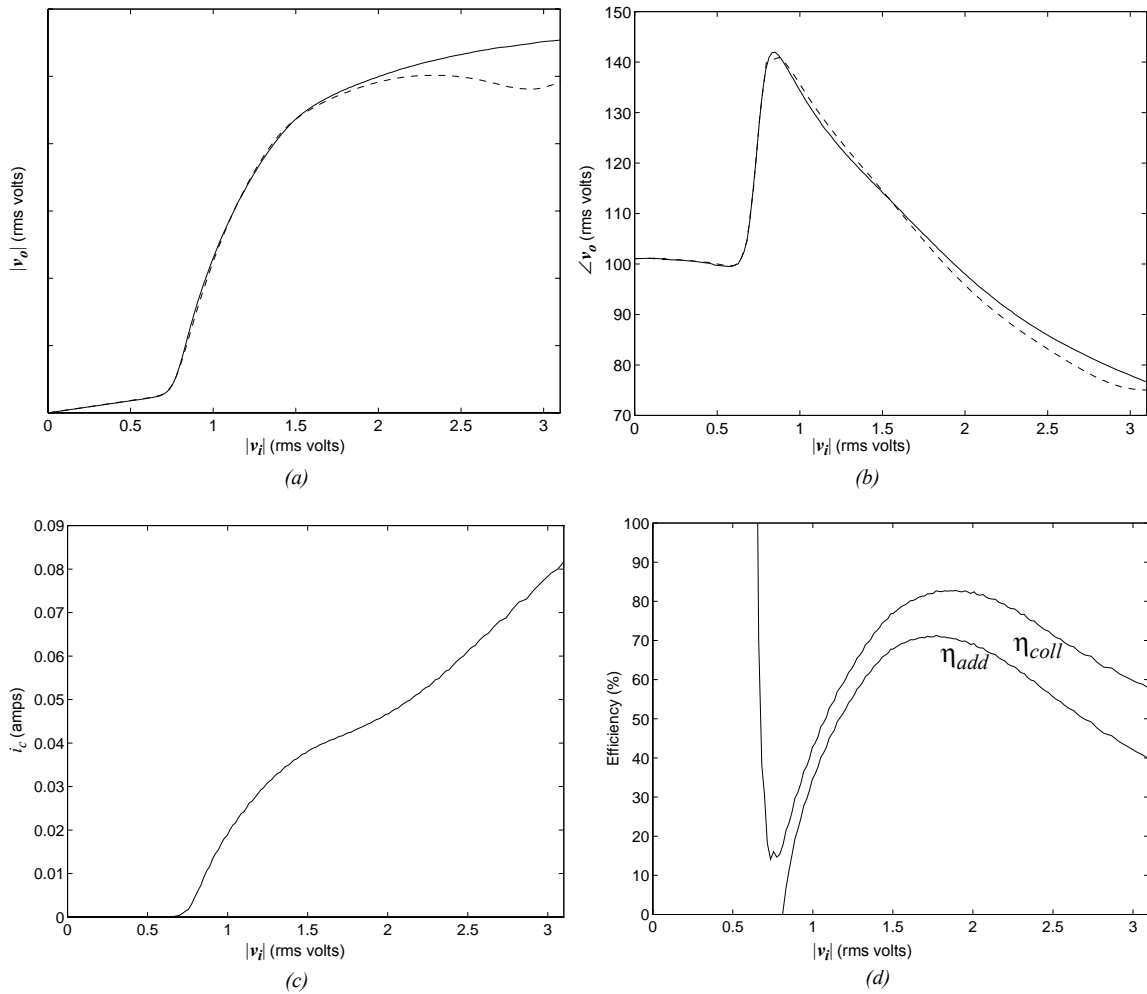
Figure 3.5: Low Power BJT RF Amplifier input-output transfer characteristics at 900MHz with v_{cc} = 13V and v_{be} = 0V. Solid traces indicate true responses and dashed traces indicate responses obtained with early test rig. (a) amplitude response, (b) phase response, (c) current consumption and (d) collector and power added efficiency.

It is evident from figure 3.5(*c*) that very little collector current flows when the input is low and the amplifier is thus off. With virtually no collector current flowing and the input effectively leaking through to the output, the collector efficiency will be high (figure 3.5(*d*)). In contrast the power added efficiency acting like an attenuator.

When the input overcomes the *vbe* drop of the BJT, the transistor turns on and collector

current begins to flow. The transistor begins to provide gain giving more realistic values of efficiency.

It should be noted that the measurement technique used here takes the static amplifier characteristics. That is, the amplifier characteristics are measured one point at a time using a CW (continuous wave) signal. Under operational conditions, the characteristics would be traversed at a modulation rate. Any memory in the amplifier caused by thermal effects and bias circuits [7] are therefore not measured by this characterization scheme. And since the linearization bandwidths considered in this work are narrowband (less than 20kHz), it has been assumed that the RF amplifier is comparatively wideband and therefore frequency induced variations in the amplifier characteristics have been neglected[6] - although delay is used in other parts of this thesis to represent some of the bandwidth restriction the amplifier does actually possess.

3.1.1.1 Tuning for Improved Efficiency

A dynamic efficiency meter was programmed using the test rig of figure 3.3. The dynamic efficiency meter displayed both collector (η_{coll}) and power added efficiency (η_{add}) on the screen of the computer in real time. The screen of the network analyzer was set to display the input reflection coefficient on a smith chart. With such a set up it was possible to optimally tune the collector circuit of the amplifier for best collector efficiency and then adjust the base circuit for best input match and power added efficiency.

3.1.2 High Power Amplifier

A 50 Watt PA (Ericsson TXPA45) intended for TDMA basestation applications was also used extensively in this research. The characteristics were obtained using essentially the same test rig as shown in figure 3.3. The only modifications from the low power case was the substitution of higher rated components, such as: an attenuator capable of dissipating 50W, and replacing the ammeter with a combination of low resistance shunt and voltmeter.
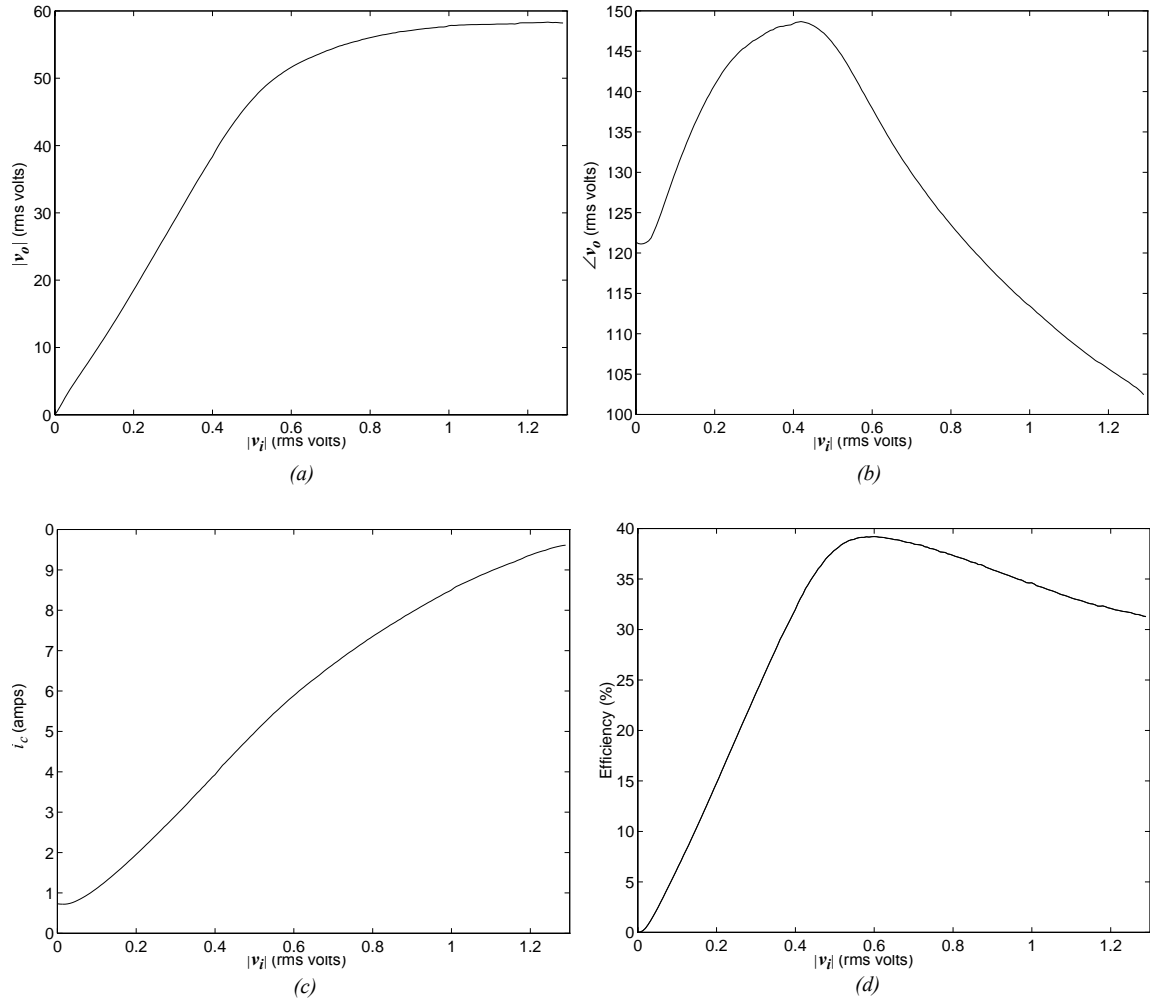
Figure 3.6: High Power TXPA45 RF Amplifier input-output transfer characteristics at 950MHz with v_{cc} = 24V. (a) amplitude response, (b) phase response, (c) amplifier current with 0.581A quiescent current for entire amplifier, (d) collector and power added efficiency (which are effectively equivalent in this case since the gain of the amplifier is high (40dB)).

The amplifier responses as presented in figure 3.6 show how some quiescent bias can eliminate much of the turn-on region distortion at the expense of some loss in efficiency for amplifiers using BJT's. In general TDMA applications demand some degree of linearity to avoid ramp-up distortion.

3.2 FREQUENCY RESPONSE

After the PA characteristics, the next most important cartesian feedback parameter is the open loop frequency response of the system. The open loop frequency response governs the degree and bandwidth of the distortion reduction [42]. The higher the loop gain the greater the reduction. Traditional frequency response techniques can be applied to the cartesian feedback loop and offer a useful simplified starting point for further analysis. An equation to illustrate this for a cartesian feedback loop (as obtained from figure 3.7) can be written with all variables being complex as,

$$Y(t) = \frac{G_A X(t)}{1 + G_A H_f} + \frac{d_A(t)}{1 + G_A H_f} - \frac{d_f(t) G_A H_f}{1 + G_A H_f}, \tag{3.1}$$

where *Y(t)* represents the transmitter output and *X(t)* represents the input signal. The open-loop gain G_A, is comprised of all the forward gains in the cartesian feedback system i.e (as shown in figure 3.7) the baseband amplifiers and filters (*G(s)*), the modulator, driver, and RF power amplifier ($ge^{j\delta}$), and the transmission delay ($e^{j\omega\tau}$). $d_A(t)$ models the distortion introduced by all of these forward gain components. The feedback transfer function H_f which is comprised of the RF directional coupler and demodulator, also has an associated distortion component $d_f(t)$. The expression highlights how $d_A(t)$ which includes the RF amplifier non-linearity, is approximately reduced by the amount of loop
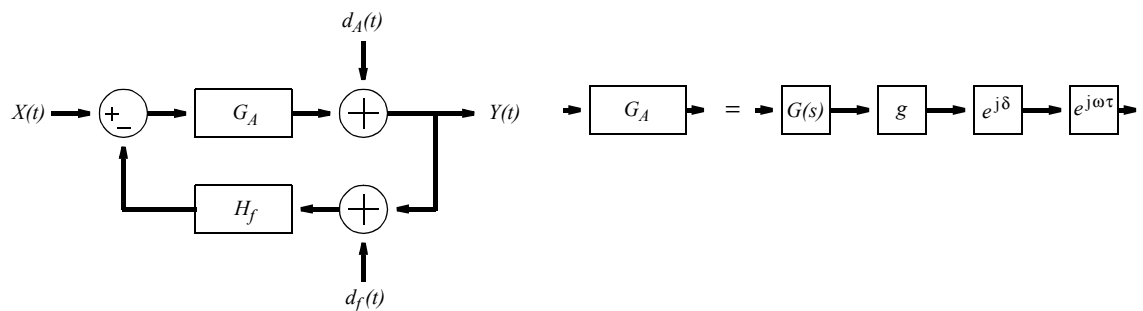
Figure 3.7: Complex baseband representation of cartesian feedback loop modelling gains and distortion. Bold lines signify complex quantities i.e. two lines. Forward gain, G_A, is comprised of the gain in the baseband amplifiers and filters G(s), the gain and RF phase rotation of the RF amplifier and upconvert chain, $ge^{j\delta}$, and a delay, $e^{j\omega\tau}$.

gain G_AH_f. A loop gain of 35dB, for example, will reduce output intermodulation products by approximately 35dB. The loop still however remains sensitive to distortion generated in the feedback path ($d_f(t)$) which is not changed by the amount of loop gain. This highlights the need for the feedback gathering components to be highly linear and also of low noise[57]. All of the distortion quantities except that produced by the amplifier are generally small compared to the output signal and consist of terms which are either constant (such as noise power level, DC offset or carrier leak) or are signal dependent such as the amplifier intermodulation distortion. This section only considers the effects of amplifier distortion which can be reduced by the action of the feedback loop (i.e $d_f(t)$ is assumed to be 0).

The modulation bandwidths discussed in this thesis are narrowband (10's kHz) relative to the RF component bandwidths in the loop (10's MHz). It is therefore reasonable to assume that for low frequencies the loop response will be dominated by the compensation filter. The RF components do however have a finite bandwidth. The finite bandwidth is caused by high frequency poles and zeros due to the filtering distributed across the RF components. The simplest way to reproduce both the low frequency requirements and high frequency characteristics is to model the loop compensation directly combined with a time delay. In the early stage of this work the delay was approximated from data sheets and RF component measurements. Later the delay was measured from the system implemented in section 3.4.

Consider the calculated bode response shown in figure 3.8 of a system with a single pole p at a pole location frequency given in radians per second, a DC gain term K and a time delay τ given in seconds. The transfer function is given by

$$G(s) = \frac{Kp}{s+p} e^{-\tau s} \tag{3.2}$$

Assuming at this stage, the cartesian feedback components are wideband, linear and no cross-coupling exists between the I and Q paths (i.e $\delta = 0$ in $e^{j\delta}$ of figure 3.7), then the
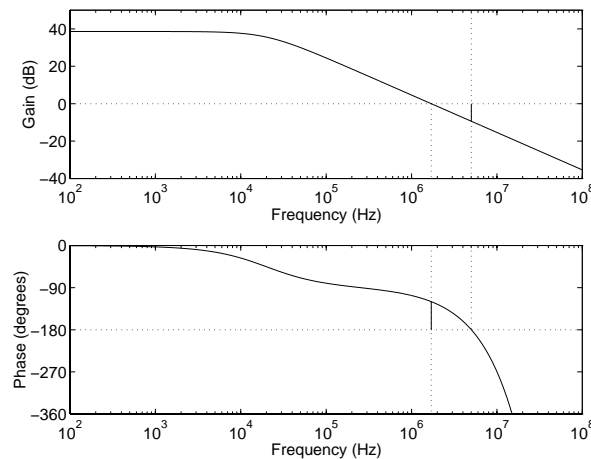
Figure 3.8: Bode Response of G(s) with a single pole at 20kHz, a DC gain of 85.2 (38.6dB), and a 50ns delay. The phase margin as drawn is 60°, and the gain margin as drawn is 9.4dB.

pole represents the dominant pole purposely introduced by the baseband filters. The DC gain represents the loop gain which includes the gain of the baseband filters and the gain of the RF stages, and the delay concisely models phase shift introduced by high frequency poles and zeros in addition to actual transmissive delay. Using classical bode techniques it is therefore possible to determine the gain and phase margins for different combinations of gains and delay (table 3.1).

Table 3.1: Some example *G(s)* transfer functions

Pole Frequency, (kHz)	Phase Margin, (degrees)	Gain Margin, (dB)	DC Gain	System Delay (ns)
20	20	2.2	195.2	50
20	30	3.5	167.6	50
20	40	5.1	140.0	50
20	50	7.0	112.5	50
20	60	9.4	85.2	50
20	70	12.7	58.3	50

3.2.1 Gain Maximization

Since the forward loop gain reduces distortion produced in the PA, it is desirable to maximize gain over as large a bandwidth as possible. This can be achieved by introducing more elaborate compensation transfer functions consisting of many poles and zeros.

Figure 3.9 shows a possible alternative compensation filter response (solid lines) compared to the single pole compensation described previously (dot-dashed lines). With two poles and one zero, the loop gain (and hence distortion reduction) has been increased by 10dB whilst the stability as measured by the gain and phase margins is essentially unchanged. The main drawback is that the phase response indicates relatively less stability over one decade.

Although increasing the compensation complexity has some benefits in terms of increasing loop gain, single pole compensation was favoured in this research in order to facilitate the comprehensive stability analysis given in the next chapter.
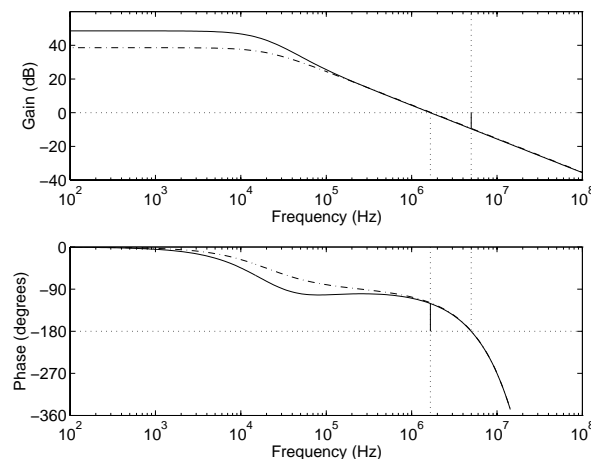
Figure 3.9: Bode response comparison of loop compensation filters G(s). The dot-dashed lines give the bode response of the single pole (20kHz) and delay (50ns) previously described. The solid lines give the bode response of a compensation filter with two poles at 20kHz, a zero at 65kHz, a 50ns delay and 10dB more gain than the single pole filter. The phase margin as drawn is 59°, and the gain margin as drawn is 9.6dB.

3.3 TIME DOMAIN SIMULATIONS

With the two main parameters of the cartesian feedback system characterized it is now possible to perform simulations to demonstrate the distortion reducing ability of cartesian feedback. A block diagram of the simulation program is shown in figure 3.10. The simulation was implemented using complex quantities and complex baseband representation.

Although the power sweep non-linearity in the measuring system was removed through the use of a power meter (section 3.1), the resulting data is unevenly spaced (due to the uneven output provided by the network analyzer at higher output levels). The data obtained of the RF amplifier was therefore first spline fitted to give evenly spaced table values. This reduced the simulation time without compromising accuracy. Linear interpolation was used in the simulations to obtain values in between table entries.

The loop compensation filter was converted from the s-plane representation of equation 3.2 to the z-domain and then into a difference equation suitable for time domain simulation. The 50ns delay in the system was achieved with one unit sample delay (z^{-1}) which gave a 20MHz sample rate.
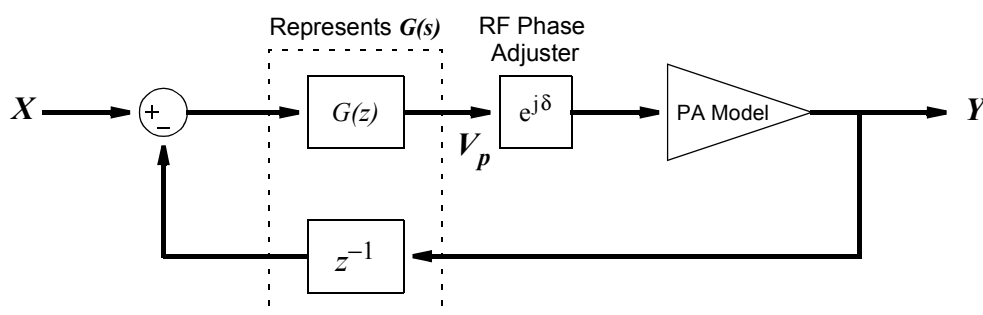
*Figure 3.10: Block diagram of cartesian feedback digital simulation. **X** is the complex input, **Y** is the complex output, and V_p is the complex predistorted drive voltage. The bold lines describe complex quantities. The PA model is obtained from measured characteristics. The combination of G(z) and z^{-1} represent the sampled version of **G(s)**. The RF phase adjuster is implemented with a complex rotation $e^{j\delta}$.*

The transformation from the s-plane to the z-plane implementation for digital time domain simulation can be performed a number of ways. Figure 3.11 shows a comparison of the single pole transfer function (*G(s)* without the delay) with two alternative digital filter implementations.

The dashed lines give the response of an equivalent digital filter implementation using the impulse invariant approach. This technique gives an accurate filter matching for the impulse response at the sampling instants. The magnitude response as shown in the figure is also well matched, however the phase response deviates significantly. This deviation would make stability aspects of the cartesian feedback loop difficult to predict through simulation. The impulse invariant technique of digital filter implementation yields a single pole in the z-domain equivalent to the single pole in the s-plane.

Another well known approach to digital filter implementation is the bilinear transform. The magnitude and phase response are well matched across most of the band. The effects of the frequency warping are only apparent near half the sample rate. Since the sample rate in this thesis is relatively high (20MHz) in order to simulate the sorts of delay encountered in a typical hardware implementation, the effects of this warping are

(a)   *(b)*
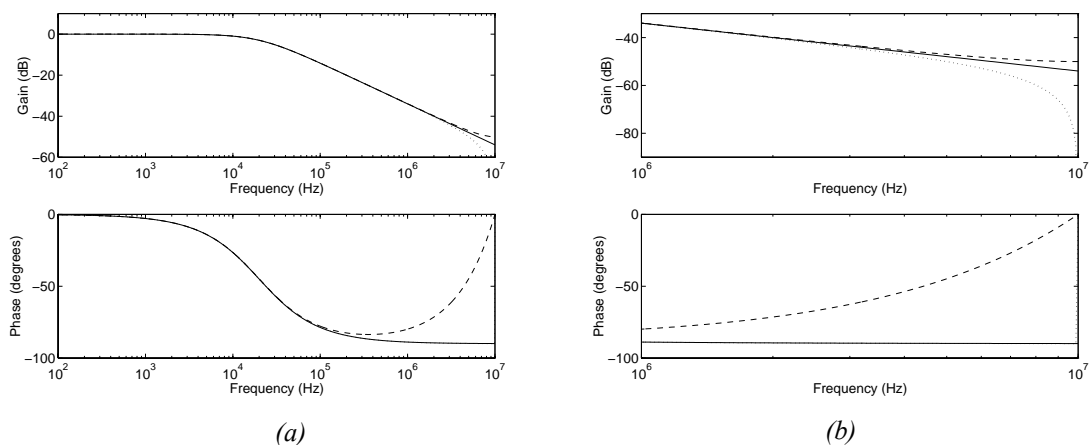
Figure 3.11: Comparison between analog G(s) without delay (solid lines) with digital domain versions, G(z) (without delay). Impulse invariant generated filter (dashed lines) has accurate amplitude matching but the phase deviates significantly. Bilinear transform generated filter (dotted lines) has accurate gain and phase matching. (a) wideband response up to $f_S/2$, (b) same as (a) with only last decade shown.

negligible in the modulation bands considered (the possibility of aliasing is also reduced with such a high sample rate). The bilinear transform method of digital filter implementation was therefore chosen for the time domain simulations discussed in this thesis. The bilinear transform yields a digital filter with a single pole in the z-domain equivalent to the single pole in the s-plane, and a zero at half the sample rate.

The results from the simulations are presented in both the frequency and time domain in the next section. Since the simulations involve a non-linearity within a feedback loop, the simulations must be performed in the time domain. Time domain waveforms visually demonstrate system operation. Results in the frequency domain however are more useful in assessing the level of intermodulation distortion reduction.

An FFT (Fast Fourier Transform) was used to obtain the frequency domain plots from the time domain signals at the end of the time domain simulation. The use of an FFT forces the number of samples in the simulation to be 2^n. The nature of the FFT effectively takes these samples and cascades them endlessly in a repeated continuous stream. It is therefore important to ensure the first sample and last sample do not give a discontinuity and cause spurious spectral components to emerge. Windowing progressively tapers the input to the FFT such that the first and last samples are zero. Although this stops discontinuity, the windowing function disperses the previously discrete spectral components across several frequencies.

It is preferable to avoid the problems with the FFT process by carefully arranging the input signal such that it repeats an integer multiple of times within the number of samples. For a two-tone test this is easily achieved if the modulation frequency (Hz) of the baseband tone is

$$f_m = cycles \times \frac{f_s}{2^n}$$

(3.3)

where *cycles* is a number of integer sine waves which fit within 2^n samples at a sample frequency of f_s (Hz). If the simulation variables are chosen such that equation 3.3 is

satisfied, there will be no discontinuity and hence windowing will not be required to obtain an accurate spectrum.

Aspects of simulation discussed in this section are also treated in [4].

3.3.1 Intermodulation Distortion Reduction

The first series of simulations were performed to examine the distortion reducing abilities of cartesian feedback. The results of a simulated two-tone test for the low power amplifier are given in figure 3.12. A complex envelope two-tone test was generated by injecting a sine wave into the In-Phase channel of the input i.e the real part of X. The frequency chosen, 4.8828125kHz, satisfied equation 3.3, with a sample rate of 20MHz, 8 cycles and 2^{15} samples. The loop filter ($G(s)$) used was as shown in figure 3.8 and the phase adjuster was set to $-105°$ (negative mean of the amplifier phase response of figure 3.5(b)).

The action of the closed loop feedback attempts to minimize the error between the output and the input. For the output to be close to the input, the amplifier must be driven with a predistortion voltage V_p, which is complementary to the amplifier distortion. This voltage is shown in figure 3.12(a). The real part of V_p shows how the turn-on region demands a rapid change when passing through zero due to the low PA output in this region. If the system was driven harder the peaks of this waveform would have saturated. AM/PM distortion causes the RF phase of the amplifier to vary with the amplifier drive. This variation cannot be removed by a fixed phase adjuster and hence some components are expected in the imaginary part of V_p. The spectrum of V_p (figure 3.12(*c*)) shows that V_p contains sufficient high order intermodulation products which, when applied in the correct phase, reduce intermodulation distortion generated in the PA.

The output of the cartesian feedback system is shown in the solid traces of figure 3.12(*b*). The output is clearly a good replica of the input. How good this replica really is, is shown by the spectrum (solid line) in figure 3.12(*d*). The worst case intermodulation product is $-$
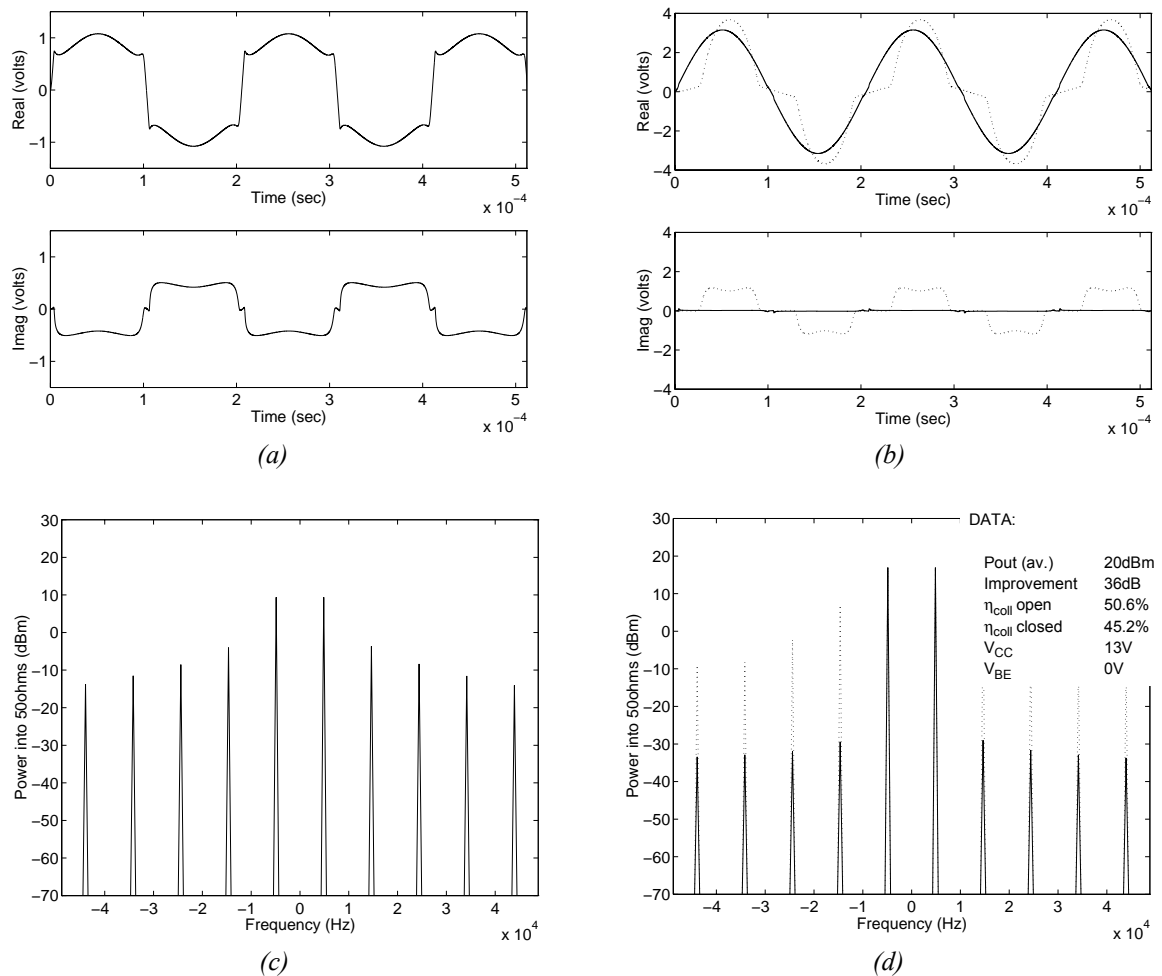
Figure 3.12: Simulated cartesian feedback with low power amplifier responses for a two-tone test. (a) Predistorted drive voltage V_p and appropriate spectrum (c), (b) Open (dotted) and closed loop output voltage with appropriate spectrums (d). The worst case intermodulation product is −46dB below the desired signals.

46dB below the desired signal. The dotted traces on the output plots show the unlinearized output before the application of feedback. The difference between the open loop case and closed loop case is 36dB. This approximately corresponds with the loop gain of the system described by figure 3.8 at 4.88kHz.

The insert in figure 3.12(*d*) gives additional data obtained from the simulation. It is important to specify the output power in any linearization exercise since the level of
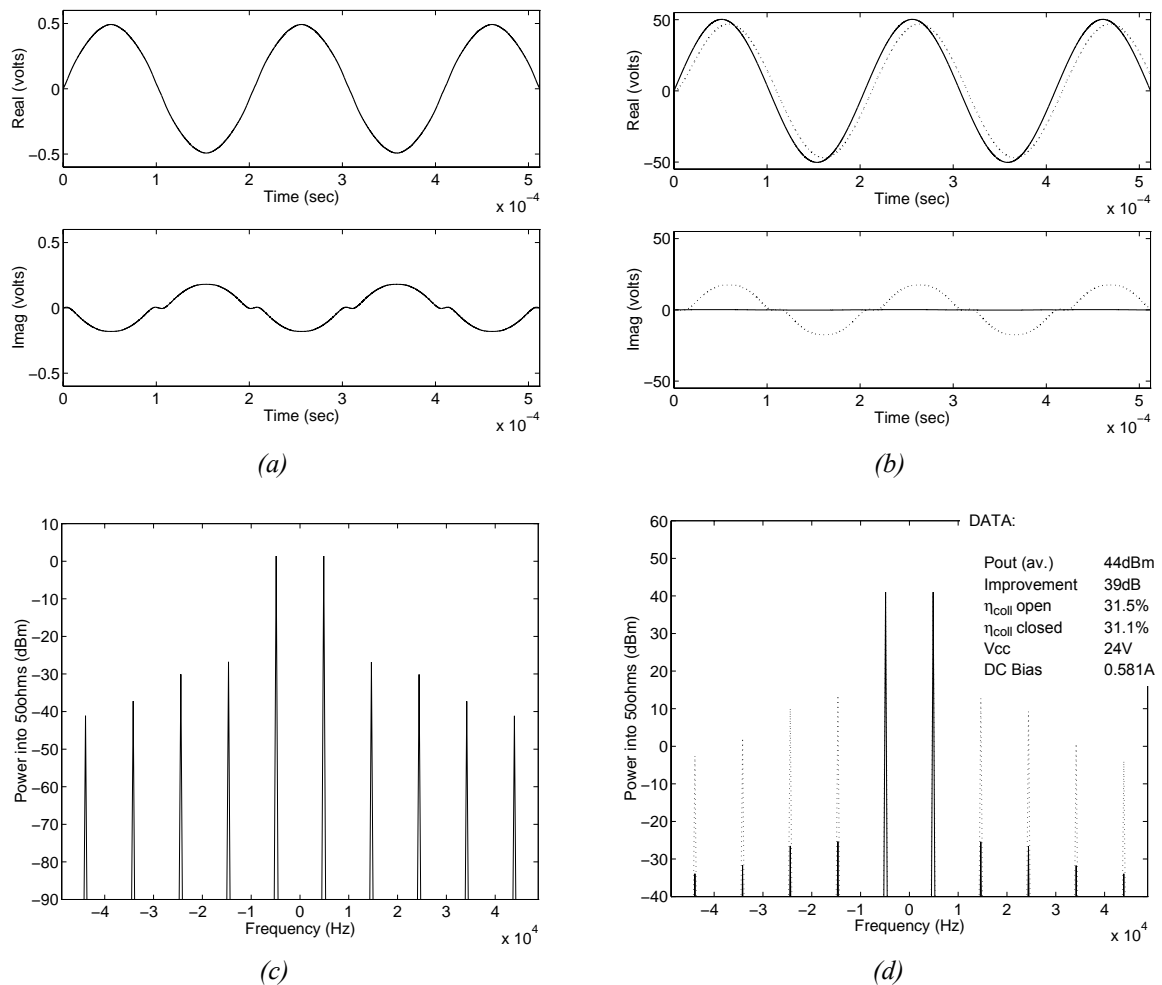
Figure 3.13: Simulated cartesian feedback with high power amplifier responses for a two-tone test. (a) Predistorted drive voltage V_p and appropriate spectrum (c), (b) Open (dotted) and closed loop output voltage with appropriate spectrums (d). The worst case intermodulation product is $-67dB$ below the desired signals. The reduced distortion (compared to fig 3.12) is due to the class AB biasing of the

intermodulation distortion is highly dependent on the output power. Since the collector current of the PA was also characterized, it was possible to simulate the efficiency of the system before and after the application of feedback. The limited 5% reduction in collector efficiency highlights the advantages of linearizing a non-linear yet efficient amplifier.

Simulations were also performed with the high power amplifier model. These results are shown in figure 3.13. This time the loop gain was increased to match the frequency response of the 50° phase margin entry of table 3.1 and the phase adjuster was set to −

118°. This amplifier is biased in class AB which reduces the original level of distortion, leading to a lower absolute distortion after the application of feedback. This is shown by the lack of sharp discontinuities in V_p and by the before and after traces of figures 3.12(*b*) and 3.12(*d*). The drawback is a reduction in efficiency. Still, a collector efficiency (which in this case is also power added efficiency due to the high gain of the amplifier) of 31% is quite good compared to the option of Class A amplification.

3.3.1.1 Effective Amplifier Gain

Simulations were performed with varying degrees of loop gain. It was verified that a change in the loop gain resulted in an exact change in the ability of the cartesian feedback loop to suppress intermodulation distortion provided the output power remained constant. The loop gain itself is comprised of the linear filter gain and the gain of the amplifier. To predict the degree of intermodulation distortion suppression, the gain of the amplifier must be known. For substantially non-linear amplifiers, like the low power amplifier, the amplifier gain is difficult to assess.

A series of simulations were performed to find the contribution of amplifier's gain in reducing distortion. Figure 3.14 shows the results of these simulations. The solid line
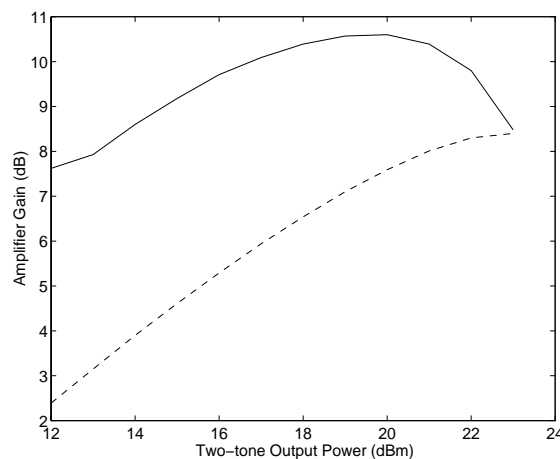
Figure 3.14: Amplifier gain versus output power (two-tone signal). Effective Amplifier Gain as measured by the amount of distortion reduction (solid line). Dashed line is the gain as measured by harmonic linearization i.e the fundamental output power divided by the fundamental input power.

shows the proportion of loop gain attributed to the amplifier. This gain was determined from

$$EAG = \frac{\left(10^{\left(\frac{IM_{imp}}{20}\right)}\right) - 1}{K} \tag{3.4}$$

where *EAG* (Effective Amplifier Gain) is the linear gain component the amplifier effectively contributes to the distortion reducing process, IM_{imp} is the amount of open to closed loop improvement in the third order intermodulation distortion product (dB) (measured with a low frequency two-tone test well within the filter bandwidth), and *K* is the gain in *G(s)* (equation 3.2). The solid trace shows there is approximately a 3dB variation in the effective gain of the amplifier for the power output range shown. This 3dB variation will change the ability of the cartesian feedback loop to reduce distortion depending of the output power level.

The dashed lines are an attempt to somehow measure the effective amplifier gain without actually doing open and closed loop cartesian feedback simulations. The trace was generated by measuring the gain from input to output for the fundamental component of a two-tone test. This method of characterizing the gain of non-linear systems is referred to as harmonic linearization[68]. The term linearization in this context refers to the process of modelling non-linear systems as equivalent linear systems.

The harmonic linearization approach does not accurately predict the amplifier's contribution to cartesian loop gain. This could be due to the fact that harmonic linearization assumes that the distortion products generated by the non-linearity are filtered out by the loop filter. This is not the case in cartesian feedback where the distortion is purposely designed to pass through the filter in order to try to eliminate it from the output by the action of feedback.

3.3.2 Instability

Like all feedback systems cartesian feedback has the potential to become unstable. Instability occurs whenever the feedback from the output becomes positive for whatever reason. In the cartesian feedback loop, the loop filtering and delay can cause the feedback to be positive at some frequency. If the gain is positive at this time (i.e negative gain margin) instability will result.

Another potential threat to stability is the setting of the phase adjuster. Figure 3.15 shows wideband spectra of two unstable situations for the low power amplifier with the simulation parameters the same as those presented in figure 3.12, except for the setting of the phase adjuster. Figure 3.15(*a*) has the phase adjuster set to +60° above −105° and figure 3.15(*b*) has the phase adjuster offset by −70° from −105°. The spectra show how instability causes spurious products to rise up at the least stable frequencies in the system. For this system the region of potential instability is around 1.8MHz and approximately corresponds to the 0dB crossing frequency of figure 3.8.

The instability results because the misadjustment of the phase adjuster provokes cross-coupling between the In-phase and Quadrature channels. The misadjustment can also
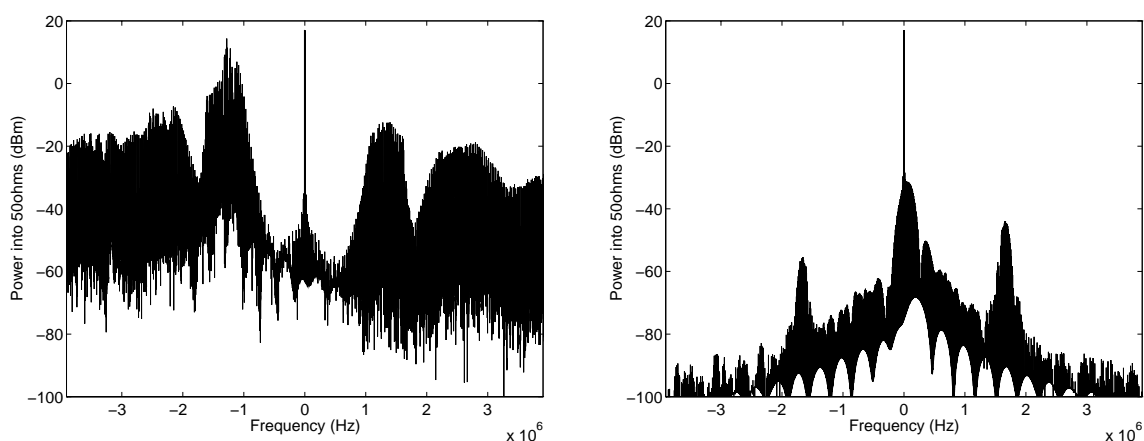
Figure 3.15: Wideband spectrums of simulated cartesian feedback with a two-tone test. The simulation conditions are the same as those use to generate figure 3.12 except (a) phase adjuster set to +60° above −105° and (b) phase adjuster offset by −70° from −105°.

cause the I and Q channels to be interchanged or at worst both channels can be inverted. It is logical to assume then that at intermediate stages of cross-coupling the stability will be degraded. Additionally as the phase adjuster error increases, the noise floor will tend to rise around the least stable frequencies before continuous oscillation occurs.

The unstable wideband spectra highlight the potential for interference to other channels using the same band. The spectra also show that for more positive phase adjustments (e.g +60° from −105°) the instability will cause spurious oscillation to rise on the left side of the spectrum. For more negative phase adjustments the spurious components tend to rise on the right side.

The previous discussion on effective amplifier gain eluded to the difficulty in assessing non-linear components. The effective gain is only suitable for approximating the level of intermodulation distortion reduction a loop is capable of. A more rigorous amplifier gain model is needed to accurately determine the stability of a system. Also, how the amplifier interacts with the phase adjuster in the cartesian feedback loop has a bearing on stability. These issues are comprehensively examined in the next chapter.

3.4 IMPLEMENTATION

The physical realization of the cartesian feedback system described in section 2.6 is discussed in this section. The measurements presented here are comparable to those simulated in the previous section.

A block diagram of the experimental hardware as applied to the low power amplifier is shown in figure 3.16. The baseband processing components consist of six operational amplifiers (three per channel). These op-amps were responsible for amplifying the signals from the demodulator and subtracting them from the input signals. The total voltage gain of the three op-amps was 58dB. Since the op-amps have a finite gain bandwidth product
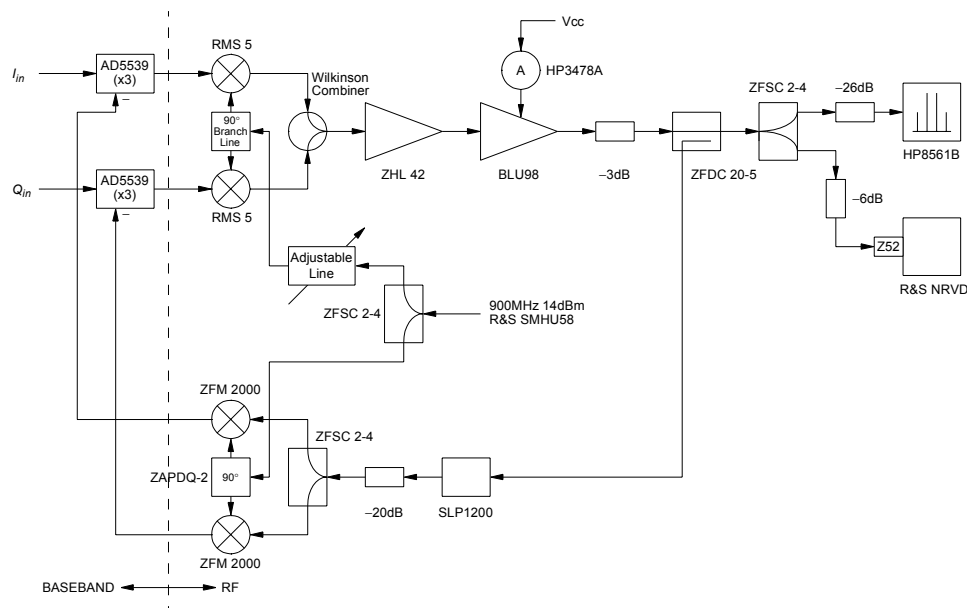
Figure 3.16: Block diagram of experimental hardware. RF component part numbers are "Mini-Circuits" unless otherwise indicated.

(1.4GHz in this case), phase shift will be introduced by the closed loop transfer function. With 58dB of gain the measured phase shift through these op-amp circuits was $-45°$ at 3.3MHz. This phase was modelled as a delay of 38ns ($1/[360/45 \times 3.3\text{MHz}]$). The rest of the hardware in the loop was RF and had an effective delay of around 12ns. The total system delay was then modelled as 38ns + 12ns = 50ns.

The upconverting quadrature modulator was constructed with passive mixers, splitters and combiners in a stripline structure. The driver stage was a class A unit with 35dB of gain and a 1dB compression point of around 28dBm. This was more than capable of driving the PA stage which is described in section 3.1.1. The output from this amplifier is applied to two output devices via an attenuator, a directional coupler, a splitter and more attentuators. The spectrum analyzer was used to monitor the intermodulation performance of the cartesian feedback system. The power meter was used to accurately determine the average output power. When combined with the power supply voltage and current consumption, this enabled the calculation of efficiency.

Accurate measurement of power at RF involves many considerations. First the power

measurement head must be accurate at the frequency and ambient temperature of operation. This is within the control of the manufacturers. The measurement head chosen must also be suitable for the application. A thermal sensing head was used for these measurements since the modulation was not CW. The insertion loss between the PA output and the measurement interface of the power sensing head was also carefully measured and allowed for.

The output coupler was used to sense a portion of the RF output for feedback. The RF feedback was filtered to remove any reminents of carrier harmonics (1.8GHz and beyond). The demodulator consisting of a splitter, two high performance mixers and a quadrature hybrid, is sensitive to the input level applied. The attenuator proceeding the demodulator is therefore used to set the appropriate level for demodulation. If this level is too high, then the mixers will introduce distortion which will corrupt the feedback signals, and generate undesired distortion at the output of the transmitter which cannot be reduced by the action of feedback. If the RF feedback signal is too low, then the demodulated signals will be corrupted by noise and become susceptible to DC offsets. This is a classic noise distortion trade-off. There exists an optimum level at which the demodulation mixers can be driven. Johansson[69, 75] has examined this problem and found the optimum level to give 75dB dynamic range for similar hardware to that described here.

The other RF components in the experimental system provide the local oscillator signals for both the modulator and demodulator. A line stretcher was used to adjust the relative RF phase difference, δ, between the modulator and demodulator.

3.4.1 Measured Performance

The results from the hardware using a two-tone test are given in figure 3.17. The conditions for these measurements are similar to those of the simulation results given in figure 3.12. The measurements agree closely with those predicted by the simulation as is highlighted by table 3.2. The simulations are close to the measurements (2dB & 4%) as

<div align="center">(a)   (b)</div>

Figure 3.17: Measured two-tone test for the low power amplifier with no base bias. (a) Measured output spectrum; Open-loop performance (dotted) and closed-loop performance (solid). The worst case intermodulation component is approximately 48dB down from desired signals. (b) Measured time domain waveforms in real and imaginary format. Predistorted drive (top two traces) and desired output (bottom two traces).

result of the accurate characterization process and ensuring the operation of both the simulations and measurements at the same output power and hence over the same region in the amplifier.

The measurements confirm that the distortion is minimized by the action the feedback without destroying the inherent efficiency of the unlinearized PA.

The effects of applying some DC bias on the base of the transistor is shown in figures 3.18 and 3.20. The turn-on gap is avoided and hence the intermodulation performance is

Table 3.2: Two-tone test results summary for low power amplifier

	Simulation $V_{BE} = 0V$	Measured $V_{BE} = 0V$	Measured $V_{BE} = 0.7V$
IMworst Open Loop	−10dBc	−12dBc	−32dBc
IMworst Closed Loop	−46dBc	−48dBc	−66dBc
IM improvement	36dB	36dB	34dB
η_{coll} Open Loop	50.6%	54.2%	36.2%

```
ATTEN    10dB      VAVG   10        MKR   -65.83dB
RL   0dBm                10dB/         -5.0kHz
                                            DATA:

                                            Pout (av.)    20dBm
    MKR                                     Improvement   34dB
   -5.0.    kHz                             η_coll open   36.2%
D  -65.83   dB                              η_coll closed 35.8%
                                            V_CC          13V
X                                           V_BE          0.7V


CENTER    900.0000MHz         SPAN    100.0kHz
*RBW    300Hz       VBW  300Hz      SWP   3.0sec
```

(a) *(b)*

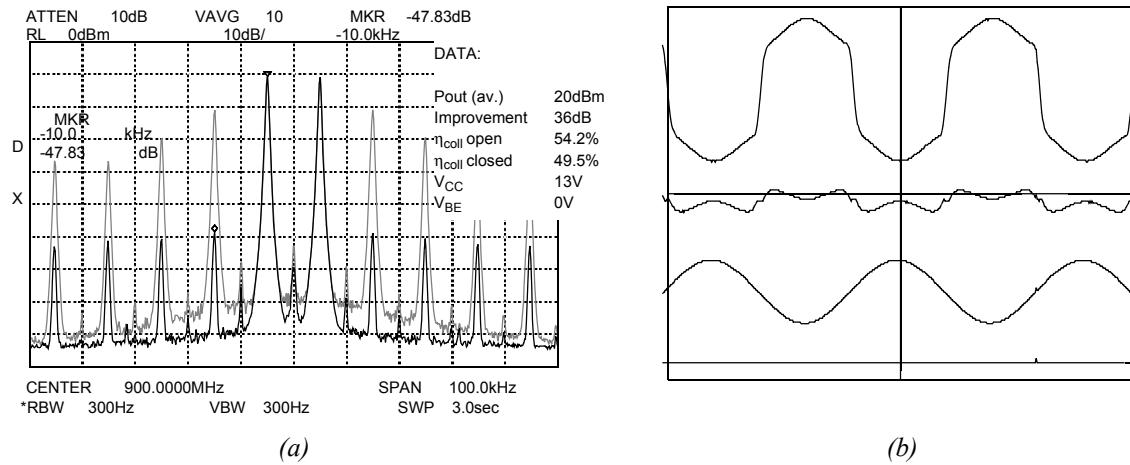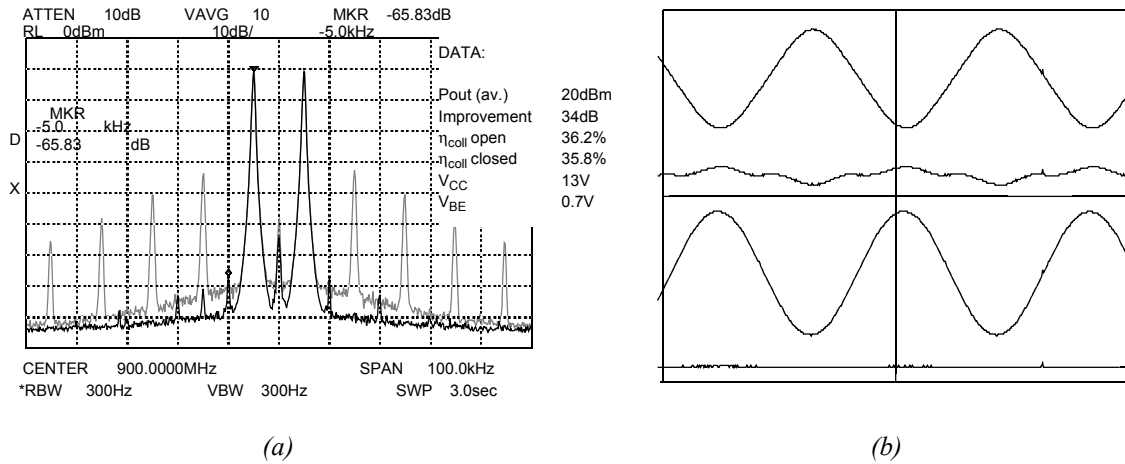*Figure 3.18: Measured two-tone test for the low power amplifier with base bias. (a) Measured output spectrum; Open-loop performance (dotted) and closed-loop performance (solid). The worst case intermodulation component is approximately 66dB down from desired signals. (b) Measured time domain waveforms in real and imaginary format. Predistorted drive (top two traces) and desired output (bottom two traces).*

improved at the expense of a reduction in efficiency. The achieved efficiency of 36% is still quite good whilst the worst case intermodulation product of −66dBc is suitable for many linearly modulated mobile communications applications.

Figure 3.19 shows an output spectrum using the low power amplifier without base bias and filtered π/4 QPSK modulation. Because this type of modulation avoids the


```
ATTEN    10dB      VAVG   50        MKR   -61.83dB
RL   0dBm                10dB/         -6.25kHz
                                            DATA:

                                            Pout (av.)    20dBm
    MKR                                     Improvement   44dB
   -6.25.   kHz                             η_coll open   49.6%
D  -61.83   dB                              η_coll closed 42.3%
                                            V_CC          13V
X                                           V_BE          0V


CENTER    900.00000MHz        SPAN    50.00kHz
*RBW    100Hz       VBW  100Hz      SWP   11sec
```
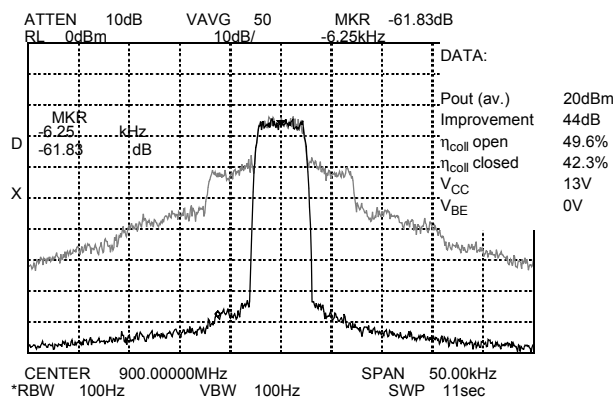
Figure 3.19: Measured output spectrum with filtered π/4 QPSK modulation for low power amplifier without base bias. Open-loop performance (dotted) and linearized closed-loop performance (solid). The intermodulation distortion is approximately 62dB down from desired signals.

troublesome zero crossing area of the BJT, distortion generated by operating through this region is avoided. Consequently excellent intermodulation distortion performance is possible without resorting to efficiency reducing bias. The resulting efficiency is quite high combined with good intermodulation distortion performance.

The hardware used to obtain the measurement for the high-power amplifier was similar to that used to obtain results with the low-power amplifier. The primary difference was the introduction of a 30dB 50W attenuator and the use of the built-in internal coupler on the amplifier for providing the feedback signal. The higher overall gain and power output (50W PEP) caused stray RF signals to be more of a problem. To minimize the effects of these stray signals metal boxes were used around all sub-blocks and semi-rigid cable was used for interconnections. Some stray effects were still noticeable however probably due to conducted RF along the shields of the semi-rigid cables which were physically positioned across a relatively large bench space.

The better AM/PM distortion allowed the use of a higher loop gain and this is reflected in the output spectrum (figure 3.20). Again, with −66dBc the linearized performance is suitable for many mobile communications applications.
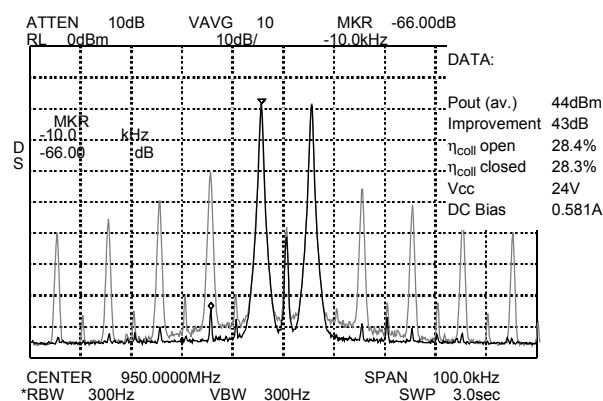
Figure 3.20: Measured output spectrum with a two-tone test for high power amplifier (with base bias). Open-loop (dotted) and linearized closed-loop performance (solid). The worst case intermodulation component approximately 66dB down from desired signals.
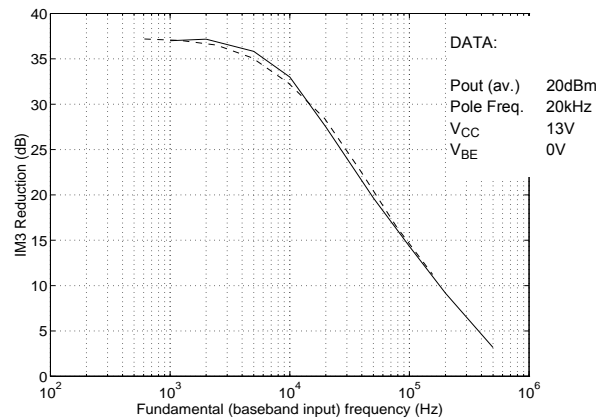
Figure 3.21: Measured (solid) and simulated (dot-dashed) improvement in third order distortion. Corner frequency of IM3 reduction is one third that of filter pole frequency. Ultimate roll-off is approximately 20dB/dec.

The loop compensation filter has a pole frequency of 20kHz. The loop gain therefore reduces as the frequency increase beyond this point. This diminishes the intermodulation improvement. This effect was measured and compared with the prediction provided by the simulation model using two-tone test signals. Figure 3.21 shows the reduction in third order intermodulation distortion products (IM3) against baseband input frequency (the frequency between one of the main tones and the carrier). In this figure the corner frequency for IM3 reduction is expected to be 20kHz/3 = 6.7kHz which highlights the need for the gain bandwidth product of the cartesian feedback loop to be sufficient for the application. Agreement between the simulation prediction and measurements was within 1dB.

3.4.2 Asymmetrical IMD

Careful examination of figure 3.20 shows that the third order intermodulation products either side of the center tones are asymmetrical for the high power TXPA45 amplifier. The exact cause of this was not investigated here since exact circuit details of the TXPA45 were not known.

Some properties and possible causes of this effect can however be discussed. First,

asymmetrical IMD in the frequency domain could be caused by the low pass filter effects of the interstage matching circuits and the active devices themselves. This is unlikely to be the cause here since the 2-tone test frequency is rather low compared to the bandwidth of the amplifier itself.

Second, asymmetrical IMD in the frequency domain is effectively hysteresis in the time domain (i.e. a memory effect). This hysteresis could be caused by self heating in the transistors (that in turn changes the gain characteristics of the devices) but the 2-tone test frequency here is probably too high to have an impact when typical thermal time constants are considered.

So the most probable cause for the asymmetry lies in another remaining possibility - the biasing circuits. These could have time constants comparable to the 2-tone test frequency and thus cause asymmetrical IMD for certain ranges of 2-tone test frequencies.

3.5 PRACTICAL CONSIDERATIONS

The results of the previous section make no reference to some of the practical problems encountered. The most prominent is the maintenance of stability followed by the removal of DC offsets. The DC offsets were removed in the hardware by fixed DC voltages to cancel the DC generated in the demodulator.

If the design of the loop is sound (i.e reasonable gain and phase margins) then stability depends primarily on the setting of the phase adjuster. Instability can have a disastrous result causing interference in many adjacent channels (figure 3.15). Both these problems have been treated with appropriate hardware in the literature [60-63].

An interesting observation made through the course of the measurements was the relationship between the current consumption of the PA as a function of the phase
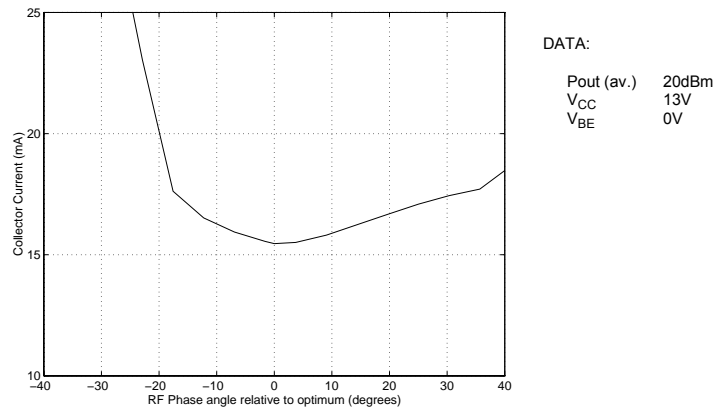
Figure 3.22: Collector current of low power amplifier in closed-loop cartesian feedback as a function of phase adjuster setting.

adjuster setting. Figure 3.22 which shows the relationship, demonstrates the possibility of optimizing the phase adjuster setting on the basis of minimum collector current.

The possible reason for this current minimum could be due to the fact that oscillations in the loop take power and this in turn requires current. It will be shown in chapter 4 that prior to continuous oscillation the noise floor tends to rise at frequencies of least stability. This increase in noise also requires current. It is visible in this amplifier due to its class of operation. Minimizing the current hence minimizes the noise and ultimately maximizes stability and efficiency. Although the collector current could be used as the sole basis for setting the phase adjuster the current could be used as additional information for control loops described in [60-62].

Although automatic phase adjustment circuits can maintain stability, the exact onset of instability has not yet been previously examined in the literature. In the next chapter a stability analysis is undertaken and is one of the major contributions of this work.

3.6 CONCLUSION

An improved means of characterizing the dominant components of a cartesian feedback

system was demonstrated and used. Specifically, a procedure which removed network analyzer power sweep uncertainty was shown to yield improved power amplifier characteristics. When placed in a simulation, the model enabled simulations to be performed which highlighted the distortion reducing ability of cartesian feedback. These simulations also enabled the performance of cartesian feedback to be accurately predicted. When compared to experimental results, the predicted simulated performance was within 2dB (IMD) and 4% (for efficiency predictions).

Care was also taken with modelling the frequency dependent components in the cartesian feedback loop. Since most of the loop components were wideband compared to the modulation bandwidth, the system was modelled with a single pole filter and a delay. The delay was designed to model the effects of high frequency poles and zeros along with actual transmissive delay. Since stability is an important issue in all feedback systems, the digital domain simulation of the frequency dependence was performed by bilinear transformation. This enabled bode responses to be accurately simulated and could hence be used as a platform for bode stability analysis.

The ability for feedback systems to reduce distortion is essentially governed by how much loop gain is present. It is advantageous then, that as high a loop gain is maintained for as broad a bandwidth as possible whilst under the constraints of stability. Adding an additional pole and zero to the simple one pole compensation filter showed that a 10dB improvement in distortion reducing loop gain was feasible.

The simulations were backed up with experimental hardware and demonstrated cartesian feedback as a means of obtaining linear amplification with good efficiency. The best results showed that with $\pi/4$ QPSK and the low power amplifier (V_{BE}=0V). It was also shown that −62dBc is achievable with a collector efficiency of 42% since $\pi/4$ QPSK modulation avoids the zero crossing region of the amplifier characteristics (unlike the two-tone test), cartesian feedback is able to greater reduce intermodulation distortion - going from 36dB improvement with a two-tone test to 44dB improvement with $\pi/4$ QPSK

modulation.

The effect of changing base bias was also examined in the measurements. It was shown that with a two-tone test, adding base bias could reduce closed loop intermodulation distortion by 18dB, however efficiency was reduced by 14% as a result. A more in-depth examination of the effects of different bias conditions is developed in chapter 5.

Through the course of the measurements a potentially useful effect was observed which could assist in the automatic adjustment of the phase adjuster by minimizing the collector current of the PA. This has not been previously reported in the literature.

The main practical problems encountered were DC offsets and instability. Instability in cartesian feedback is a critical problem worthy of further investigation. The next chapter examines the causes of instability by first using a linear approximation to the PA and then extending the analysis into a non-linear PA model. The reasons for the increase in out-of-band noise are also developed.

4 STABILITY AND NOISE ANALYSIS

Experience gained from simulations and measurements undertaken in the previous chapter highlighted the need for further investigation of cartesian feedback stability.

If the cartesian feedback loop is to be stable, it must be stable at all input signal levels. Because the amplifier characteristics change with input level, so does the degree of stability. The cartesian feedback system can be stable at one input level, but unstable at another. Bursts of oscillation can occur when the envelope of a modulated signal passes through these unstable amplitude bands.

The change in the stability margin is caused by the dynamics of the amplifier characteristics. Intuitively it can be seen that any increase in amplifier gain produces a corresponding reduction in loop gain margin. Additionally, any change in phase rotation through the amplifier produces cross coupling between the I and Q channels. It will be shown later that this also affects stability in a similar way as does reducing the phase margin.

The stability analysis is further complicated by the amplifier gain which can be expressed in two ways: the absolute gain $\left|V_o\right|/\left|V_i\right|$ and the differential gain $\Delta\left|V_o\right|/\Delta\left|V_i\right|$. In a completely linear amplifier these two terms are the same; however in a non-linear

amplifier significant differences exist. Figure 4.6(*c*) illustrates this point. At the highest power shown the differential gain has fallen to −10dB whereas the absolute gain is still high at 5dB. On the other hand when the transistor turns on, the differential gain is considerably larger than the absolute gain. Both gain terms are required for an accurate study of cartesian feedback behaviour. In addition to this, it will be demonstrated that the rate of change of amplifier phase rotation with applied input level and hence output level can also effect stability.

The aim of this chapter is to analyze cartesian feedback stability at all amplifier power levels and produce a methodology for designing these systems in a robust manner. A two stage process is used to develop the stability analysis of cartesian feedback. First a suitable amplifier model is found, and then this model is placed in the cartesian feedback loop to give the stability behaviour.

Two amplifier models were used. Both are piecewise representations of a series of operating points on the amplifier characteristics. These characteristics were obtained and presented in the previous chapter. It has also been assumed in this analysis that the amplifier is wide-band compared to the loop filtering and modulation and so frequency dependence of the RF amplifier parameters has been neglected. Although the amplifier is relatively wideband its bandwidth is however finite. The finite bandwidth introduces additional phase shift which has been modelled as extra delay. The modulator and demodulator were assumed to be ideal.

The first of the amplifier models is suitable for amplifiers with weak non-linearities. This model uses as series of complex gains (i.e. a gain magnitude and a phase) in a piecewise representation of the amplifier (section 4.1.1). The high power amplifier (TXPA45) was modelled in this part of the analysis, since it was the more linear of the two amplifiers. The second model is more elaborate, which in addition to complex gain, also has a parameter giving a measure of non-linearity at each operating point (section 4.1.2). The more non-linear low power amplifier (BLU98) was modelled for this part of the analysis.

A Multiple Input Multiple Output (MIMO) model is first developed for amplifiers with weak non-linearities (section 4.2). This model was then used to give a graphical stability analysis suitable for these amplifiers (section 4.3). It will be shown that results from this part of the analysis give a worst case stability bound when applied to amplifiers with larger non-linearities.

In section 4.4, the MIMO model is extended for use with the more non-linear amplifier model. First a series of perturbation simulations is presented to demonstrate the complex gain varies as a function of applied perturbation and is hence inadequate as the only means to model complex non-linear behaviour. Then in section 4.4.2 the non-linear model is reduced to its canonical form using linear algebra. Once in this reduced form it is then applied to a MIMO representation similar to that presented for the linear case. Section 4.6 presents a graphical stability analysis that gives an exact solution for amplifiers with both weak and strong non-linearities.

A series of time domain simulations is given in section 4.7 to the perturbation behaviour of non-linear RF power amplifiers when placed in the cartesian feedback loop, and further demonstrates why the setting of the phase adjuster tends to alter the distribution of out-of-band emissions of cartesian feedback transmitters.

Finally, section 4.8 deals with noise and presents a simple technique for minimizing the out-of-band noise components.

4.0.1 Summary of stability analysis approach

The full treatment of stability in cartesian feedback is presented in this chapter and some mathematics is involved. This section will summarize the chapter in a non-mathematical sense.
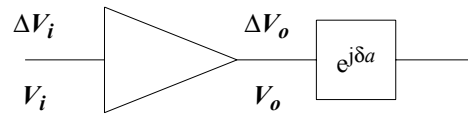
Figure 4.1: RF amplifier representation with bulk RF rotation separated.

Systems with feedback become unstable when differential perturbations, usually caused by noise (small amplitude and random phase), are propagated around the loop with ever increasing amplitudes. The differential behaviour of the loop therefore dictates the onset of instability. In the case of cartesian feedback systems, the effect of the non-linear amplifier on small perturbation signals is therefore important with the system being required to be stable for all input phases of the perturbation signal.

Stability will be assessed by considering the amplifier's response to a small perturbation signal ΔV_i, about an operating point set by the input vector V_i (bold representing complex quantities). The model is first simplified by moving the bulk RF phase rotation which exists between the forward and feedback paths, into a separate block as shown in figure 4.1. This allows the input and output vectors to be shown in phase with each other (figures 4.2(*a*)-4.2(*d*)). Using the input vector V_i as the reference for the coordinate system defines

$$\Delta V_i = \Delta a + j\Delta b \tag{4.1}$$

where Δa is in-phase with V_i, and Δb is orthogonal to V_i (figure 4.2*(a)*).

The effect of Δb is to produce a phase change in the input vector (no amplitude change),
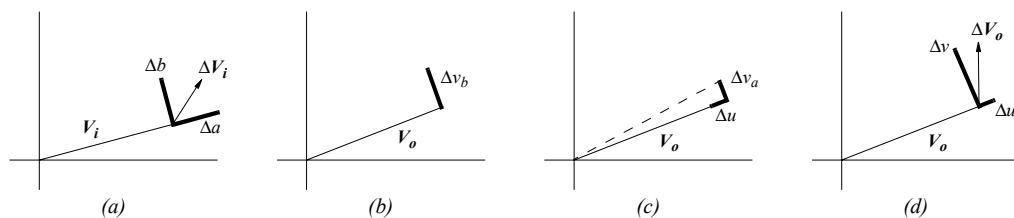
Figure 4.2: Signals and perturbations as they pass through RF amplifier. (a) Input signal and corresponding applied input perturbation. (b) Output signal with perturbation caused by phase change on input vector. (c) Output signal with perturbations caused by amplitude change on input vector. (d) Output signal with total output perturbation.

and a corresponding phase change in the output vector only, hence, the resulting output perturbation, Δv_b (figure 4.2*(b)*) is

$$\Delta v_b = \frac{|V_o|}{|V_i|}\Delta b = g_q\Delta b \tag{4.2}$$

where g_q is defined as the absolute gain.

The foremost effect of Δa is to increase the amplitude of V_o by the differential gain, g_i

$$\Delta u = \frac{\Delta|V_o|}{\Delta|V_i|}\Delta a = g_i\Delta a \tag{4.3}$$

The change in the input and hence output amplitude also causes a change in the phase (AM to PM effect) and hence an orthogonal component, Δv_a, is also generated (figure 4.2*(c)*)

$$\Delta v_a = \frac{|V_o|\Delta\angle V_o}{\Delta|V_i|}\Delta a = |V_o|g_d\Delta a \tag{4.4}$$

where g_d is the slope of the phase curve. The resulting output perturbation is then defined as (figure 4.2*(d)*)

$$\Delta V_o = \Delta u + j(\Delta v_a + \Delta v_b) = \Delta u + j\Delta v \tag{4.5}$$

This full model for the perturbation gain of the amplifier is summarized in figure 4.3 and is proven mathematically in section 4.1.

Simplifications to the model can be justified for certain types of amplifiers. The cross coupling term $|V_o|g_d$ can be neglected if this is appreciably lower than the g_i and g_q gains. Also if the difference between g_i and g_q is small they can be replaced by a single gain term g. These conditions apply to amplifiers with low turn-on distortion (Class A and AB) and operating below compression but excludes amplifiers with significant turn-on distortion such as class C amplifiers. The linearization of amplifiers with weak non-linearities is necessary in systems where the intermodulation distortion performance is strict (e.g PMR -70dB in adjacent channel). This is because the cost effective
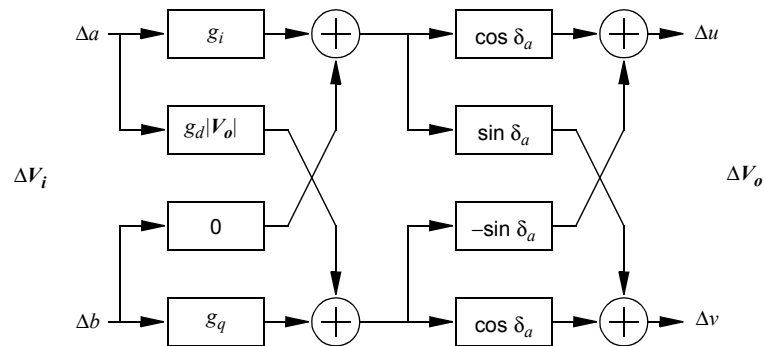
Figure 4.3: Full perturbation model of RF amplifier with bulk RF rotation separated

improvement that linearization techniques can provide is generally limited, which implies that the raw unlinearized amplifier must be reasonably linear to start with.

Figure 4.4*(a)* shows g_i, g_q and $|V_o|g_d$ plotted against V_i for the high power amplifier (figure 3.6*(a)* and figure 3.6*(b)*). The above conditions hold for input levels up to just below the 1dB compression point (solid lines). Finally figure 4.4*(b)* combines the plots of figure 3.6*(b)* and figure 4.4*(a)* to show the amplifier phase rotation as a function of amplifier gain. This plot will be used later in this chapter.

Section 4.3 uses a simplified version of the above model for cartesian feedback stability

Figure 4.4: Truncated high Power BJT RF Amplifier input-output transfer characteristics at 950MHz with v_{cc} = 24V. (a) Gains of amplifier (b) Phase versus gains in dB, the required input voltage ($|V_i|$) are marked on the curves.

analysis. It gives perfect results for linear amplifiers, good results for amplifiers with weak non-linearities and can be used as a worst case bound for amplifiers with strong non-linearities. The simplification neglects the cross-coupling term and sets the gains in both arms to the worst case (largest of g_i and g_q). The amplifier is summarized by two parameters, gain (g) and phase rotation (δ).

The MIMO cartesian feedback analysis suitable for amplifiers with weak non-linearities, process involves deriving the stability region in terms of RF phase rotation δ, and loop gain g for a cartesian feedback loop containing an ideal linear amplifier. The shape of this region when plotted on a graph (δ versus g) is dependent on the loop bandwidth requirement (pole position, p) and delay, τ.

The amplifier has a unique phase rotation and gain for each input level. These values can be superimposed on the stability graph (δ versus g) for different input levels. In this way it is easy to see if the amplifier characteristics cross or get too close to the stability boundary.

Subsequent sections of the chapter repeat the analysis using the complete (non-simplified) amplifier model. The performance can be predicted exactly for both weak and strong non-linearities, however the analysis is complex and less suitable as a design tool. Three parameters are required to describe the amplifier and this causes the stability boundary to become a stability surface. The three dimensional nature of the problem makes the graphical design approach more difficult.

4.1 A PIECEWISE AMPLIFIER MODEL

This section mathematically proves the amplifier model introduced in the previous section. The RF amplifier characteristics of the high power amplifier (TXPA45) have been reproduced in figure 4.5. Although the amplitude and phase responses of figure
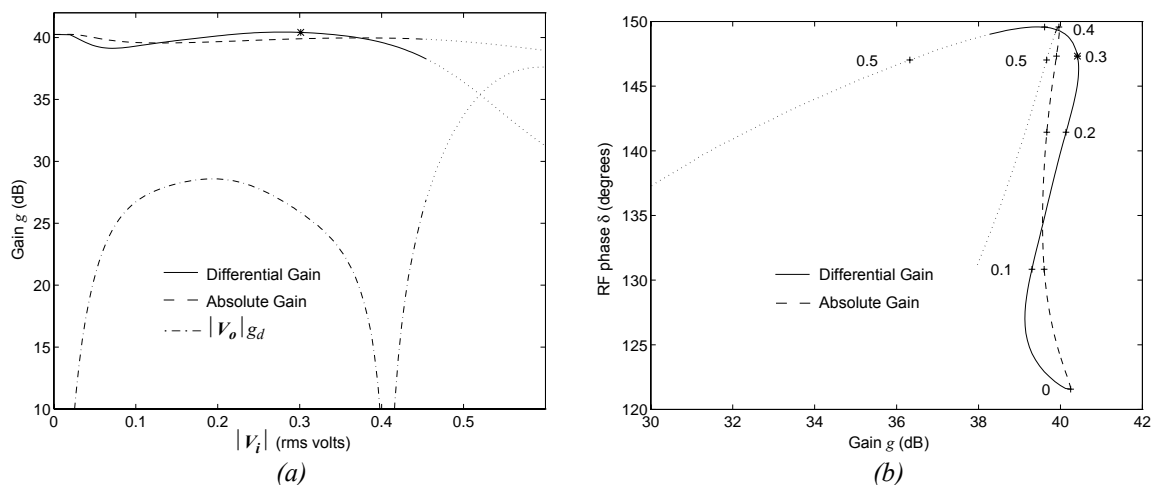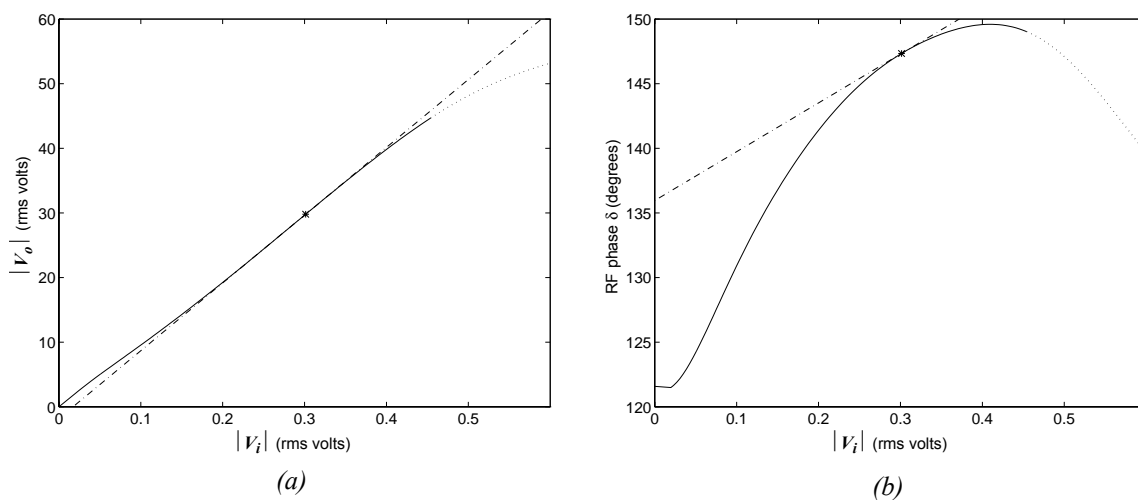
Figure 4.5: Truncated high Power BJT RF Amplifier input-output transfer characteristics at 950MHz with
v_{cc} = 24V. (a) amplitude response, (b) phase response.

4.4*(a)* and 4.4*(b)* were measured at a carrier frequency of 950MHz, they are in a form
suitable for complex baseband representation. The curves are further tailored for analysis
by the representation of RF powers as equivalent rms voltages into a 50 Ω resistor.

Most of the non-linearity in the high power amplifier exists in the saturation region. Most
of this region has been truncated in figure 4.5 since this section of the stability analysis
will only deal with amplifiers with weak non-linearities.

To cope with the weak non-linearities which do exist in the amplifier, the characteristics
can be broken up into a series of points yielding a piecewise representation. One of these
points has been superimposed on the characteristics of figure 4.5. Drawing a tangent (dot-
dashed line) at the point shown on the amplitude response gives the following expression

$$|V_o| = |V_i| g_i + c \tag{4.6}$$

where g_i is the gradient of the tangent and c is some constant. A similar tangent applied to
the phase response gives

$$\angle V_o = \angle V_i + |V_i| g_d + \delta_d + \delta_r \tag{4.7}$$

where g_d is the gradient of the tangent, δ_d is a constant RF phase rotation at that point and
δ_r is the setting of the phase adjuster shown in figure 2.25.

Equations 4.6 and 4.7 accurately describe the amplifier behaviour for small changes in V_i. Some simplifications will be made at this stage appropriate for amplifiers with weak non-linearities. These simplifications will then be progressively removed in sections 4.1.1 and 4.1.2 to yield the full non-linear model. This way the contribution of each of the non-linearities can be demonstrated.

If the amplifier in question was perfectly linear, c in equation 4.6 and g_d in equation 4.7 would both be zero. Under these assumptions combining equations 4.6 and 4.7 gives

$$V_o = |V_i| g_i e^{j(\angle V_i + \delta_d + \delta_r)} \qquad (4.8)$$

which further reduces to

$$\begin{aligned} V_o &= g_i |V_i| e^{j\angle V_i} e^{j(\delta_d + \delta_r)} \\ &= V_i g_i e^{j\delta} \end{aligned} \qquad (4.9)$$

Where for convenience $\delta = \delta_d + \delta_r$. The complex gain is the complex derivative of equation 4.9 which is

$$\frac{dV_o}{dV_i} = g_i e^{j\delta} \qquad (4.10)$$

This is an expected result and shows the magnitude of the complex gain is equal to g_i which has been termed the differential gain, and the phase of the complex gain is the RF phase rotation through the amplifier δ. Using a series of these complex gains in a piecewise approach is an approximation which is suitable for linear amplifiers only.

4.1.1 Amplifier model with amplitude non-linearities only

The results of the preceding analysis can be extended slightly to encompass a degree of amplitude non-linearity in the amplifier characteristics. This can be achieved by allowing the c variable back into the amplitude characteristics and then combining equation 4.6 and 4.7 (with $g_d = 0$)

$$V_o = (|V_i| g_i + c) e^{j(\angle V_i + \delta_d + \delta_r)} \tag{4.11}$$

Introducing $V_i = a + jb$ and $\delta = \delta_d + \delta_r$ into equation 4.11 gives

$$V_o = (\sqrt{a^2 + b^2} g_i + c)\left(\cos\left(\text{atan} \frac{b}{a} \right) + j \sin\left(\text{atan} \frac{b}{a} \right) \right) e^{j\delta} \tag{4.12}$$

which reduces to

$$V_o = \left[\left(a g_i + \frac{ca}{\sqrt{a^2 + b^2}} \right) + j\left(b g_i + \frac{cb}{\sqrt{a^2 + b^2}} \right) \right] e^{j\delta} \tag{4.13}$$

Unlike in equation 4.9, the complex derivative of equation 4.13 can not be obtained directly since applying the Cauchy-Riemman test to equation 4.13 indicates the derivative can not be determined irrespective of the path taken. The derivative to equation 4.13 must hence be obtained by partial differentiation in each of the complex dimensions. Partial differentiation for the in-phase dimension gives

$$\left. \frac{\partial V_o}{\partial a} \right|_{b = \text{constant}} = \left[\left(g_i + \frac{cb^2}{(a^2 + b^2)^{3/2}} \right) + j\left(\frac{-cab}{(a^2 + b^2)^{3/2}} \right) \right] e^{j\delta} \tag{4.14}$$

and for the quadrature dimension

$$\left. \frac{\partial V_o}{\partial b} \right|_{a = \text{constant}} = \left[\left(g_i + \frac{ca^2}{(a^2 + b^2)^{3/2}} \right) + j\left(\frac{-cab}{(a^2 + b^2)^{3/2}} \right) \right] e^{j\delta} \tag{4.15}$$

The amplifier non-linearities both depend on the input magnitude only ($|V_i|$). Assigning $|V_i| = a$ by setting $b = 0$ will simplify both equations 4.14 and 4.15 considerably. It will be shown in section 4.4.2 that although setting $b = 0$ effects the solution, the range of solutions traversed by all possible input perturbation angles ($\angle V_i = \angle[\Delta a + j\Delta b]$ used in the partial differentiation process) are the same. This is valid because the amplifier models used here are ultimately to be used in a stability analysis. And for the cartesian feedback loop to be stable it must be stable for all possible combinations of input perturbation angles.

With $b = 0$ then, equation 4.14 reduces to

$$\left.\frac{\partial V_o}{\partial a}\right|_{b\,=\,0} = g_i e^{\,j\delta} \tag{4.16}$$

and equation 4.15 reduces to

$$\left.\frac{\partial V_o}{\partial b}\right|_{\substack{a\,=\,\text{constant}\\ b\,\to\,0}} = \left(g_i + \frac{c}{a}\right)e^{\,j\delta}$$

$$= \left(g_i + \frac{c}{|V_i|}\right)e^{\,j\delta} \tag{4.17}$$

The magnitude of equation 4.17 is equivalent to the absolute gain of the amplifier and is given by

$$\frac{|V_o|}{|V_i|} = g_i + \frac{c}{|V_i|}$$

$$= g_q \tag{4.18}$$

The absolute gain is commonly obtained with an RF network analyzer that measures gain by dividing the output power by the input power.

The interesting results given by equations 4.16 and 4.17 demonstrate that amplitude non-linearity causes the gain in the in-phase channel to be different to that of the quadrature channel. Figure 4.4*(a)* is a plot of both the differential gain and absolute for the characteristics of figure 4.5. When both the differential gain and absolute gain are equivalent the amplifier is amplitude linear. This is evident by comparing equation 4.18 with $c = 0$ and the magnitude of equation 4.10. The graph shown in figure 4.4*(a)* has both gains similar at low levels where the amplifier is quite linear. At higher levels amplitude non-linearity reduces the differential gain since the rate of change of the amplitude characteristics reduces. This area of non-linearity is hence characterized by a significant difference between the two gains and is shown dotted.

The amplifier analysis so far undertaken is used in section 4.2 within a cartesian feedback model. This model uses only one gain (g) and it is assumed that the worst of either gain (g_i or g_q) is used for this parameter. For this reason both gains have been plotted against

the phase characteristic in figure 4.4*(b)*.

4.1.2 Amplifier model with amplitude and phase non-linearities

In this section, the amplifier model introduced in section 4.1 will be extended and applied to the low power amplifier. The extension is achieved by allowing g_d (rate of change of phase) into the equations. As in section 4.1 the BLU98 low power amplifier characteristics first introduced in the previous chapter have been redrawn in figure 4.6 with a similar tangent drawn at some point. The gain graph as given in figure 4.6*(c)* shows
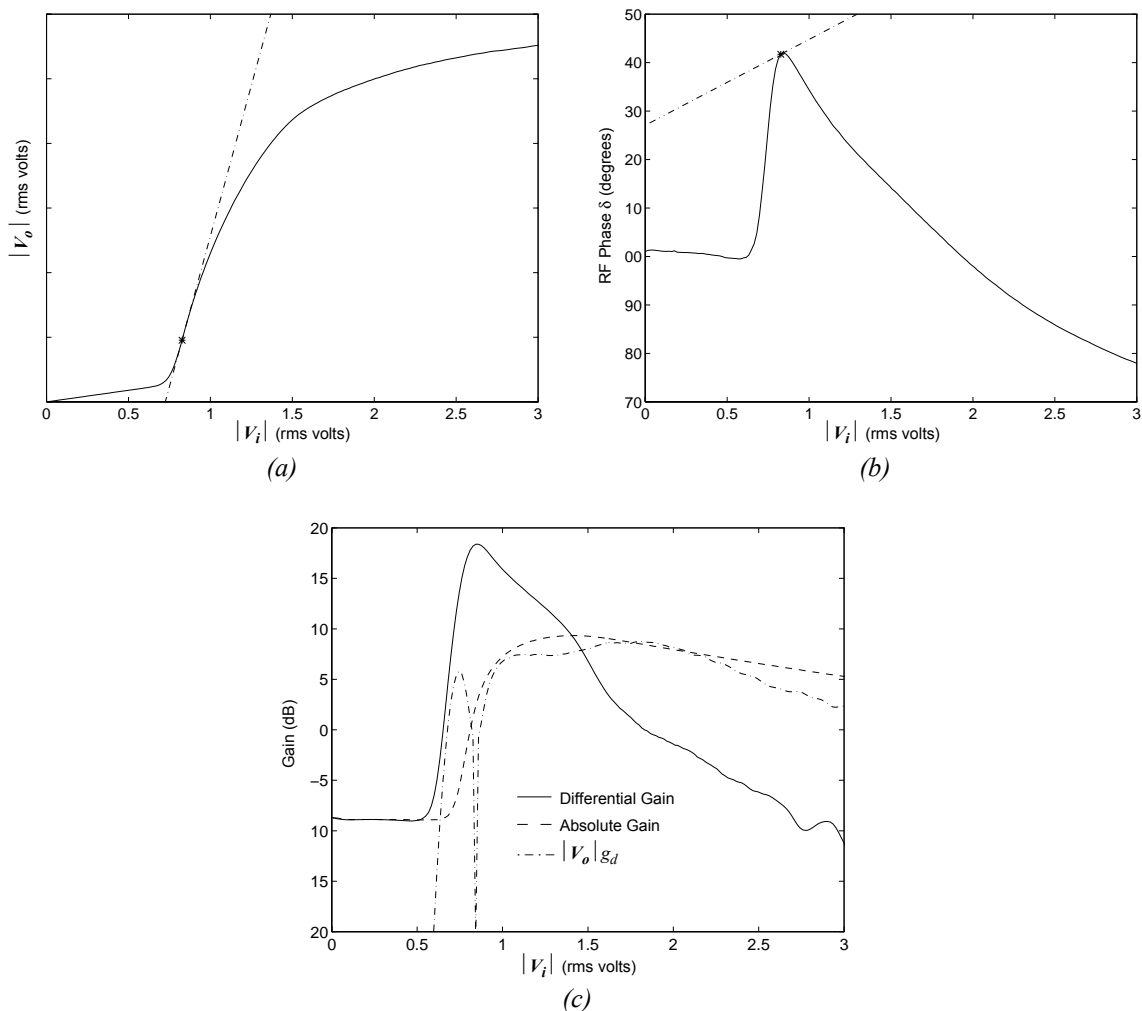
Figure 4.6: Low power BJT RF Amplifier input-output transfer characteristics at 900MHz with v_{cc} = 13V, v_{be} = 0V. (a) amplitude response, (b) phase response, (c) Gains of non-linear amplifier

that $g_d|V_o|$, the term caused by the rate of change of phase, is comparable to the other gains and hence can no-longer be neglected. So allowing all of the non-linear terms (c and g_d) into equations 4.6 and 4.7 gives

$$V_o = (\sqrt{a^2 + b^2}g_i + c)e^{j\left(\text{atan}\left(\frac{b}{a}\right) + \sqrt{a^2+b^2}g_d + \delta_d + \delta_r\right)}$$

$$= \left(a\sqrt{1 + \left(\frac{b}{a}\right)^2}g_i + c\right)e^{j\left(\text{atan}\left(\frac{b}{a}\right) + a\sqrt{1 + \left(\frac{b}{a}\right)^2}g_d + \delta_d + \delta_r\right)}$$

(4.19)

In the linear analysis of section 4.1 the partial derivatives of V_o were found and then b was set to zero. By making b approach zero first and then performing the partial differentiation, the process is made easier. With $b \to 0$ equation 4.19 then becomes

$$V_o = \left(a\left(1 - 0.5\left(\frac{b}{a}\right)^2\right)g_i + c\right)e^{j\left(\text{atan}\left(\frac{b}{a}\right) + a\left(1 - 0.5\left(\frac{b}{a}\right)^2\right)g_d + \delta_d + \delta_r\right)}$$

(4.20)

Noting first that as $b \to 0$, $V_i \to 0$, the partial derivatives are then

$$\left.\frac{\partial V_o}{\partial a}\right|_{b=0} = [g_i + jg_d(|V_i|g_i + c)]e^{j(|V_i|g_d + \delta_d + \delta_r)}$$

(4.21)

$$\left.\frac{\partial V_o}{\partial b}\right|_{\substack{a = constant \\ b \to 0}} = j\left(g_i + \frac{c}{|V_i|}\right)e^{j(|V_i|g_d + \delta_d + \delta_r)}$$

(4.22)

Indentifying from equation 4.18 $|V_o| = |V_i|g_i + c$, $g_q = g_i + \dfrac{c}{|V_i|}$ and letting $\delta_a = |V_i|g_d + \delta_d + \delta_r$ reduces equations 4.21 and 4.22 to

$$\left.\frac{\partial V_o}{\partial a}\right|_{b=0} = (g_i + jg_d|V_o|)e^{j\delta_a}$$

(4.23)

$$\left.\frac{\partial V_o}{\partial b}\right|_{\substack{a = constant \\ b \to 0}} = jg_qe^{j\delta_a}$$

(4.24)

Figure 4.7 shows how the partial derivatives obtained can be used to form a MIMO representation of the non-linear amplifier. By letting $V_o = u + jv$, equations 4.23 and 4.24 can be split into the individual MIMO gains

$$K_{11} = \left.\frac{\partial u}{\partial a}\right|_{b=0} = g_i e^{j\delta_a} \tag{4.25}$$

$$K_{12} = \left.\frac{\partial u}{\partial b}\right|_{\substack{a = constant \\ b \to 0}} = 0 \tag{4.26}$$

$$K_{21} = \left.\frac{\partial v}{\partial a}\right|_{b=0} = g_d |V_o| e^{j\delta_a} \tag{4.27}$$

$$K_{22} = \left.\frac{\partial v}{\partial b}\right|_{\substack{a = constant \\ b \to 0}} = g_q e^{j\delta_a} \tag{4.28}$$

Equations 4.25-4.28 can further be minimized by extracting the embedded phase rotation, $e^{j\delta a}$ and hence forming the model shown in figure 4.3.

The model shown in figure 4.3 is similar to the model described by equations 4.16 and 4.17 in which amplitude non-linearities only were considered. Since the effect of the rate of change of phase (g_d) is considered in this section, an additional term $g_d |V_o|$, appears. The conclusion which can be drawn is that phase non-linearity introduces an asymmetric
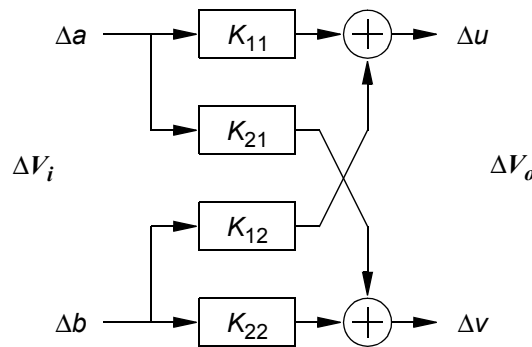
Figure 4.7: Model of non-linear amplifier obtained by partial differentiation.

cross-coupling which is dependent on the output setpoint (and from section 4.1.1, amplitude non-linearity introduces asymmetric gains).

4.2   MIMO   MODEL   OF   CARTESIAN   FEEDBACK   FOR AMPLIFIERS WITH WEAK NON-LINEARITIES

To investigate the behaviour of the amplifier model derived in section 4.1.1 inside a cartesian feedback loop, a MIMO model was employed (figure 4.8).

The RF amplifier is represented as a general block with a gain (g) and RF phase rotation (δ). The model represents one point on the amplifier characteristics. The stability analysis is obtained by considering all combinations of instantaneous gains and RF phase rotations on the amplifier characteristics (i.e a piecewise approach).

As has been stated, the model assumes that the amplifier is wideband compared to the loop filtering and modulation, and so frequency dependence of the RF amplifier characteristics has been neglected. *G(s)* represents all of the forward chain components including the loop filtering and delay.

4.2.1 Effects of Amplifier Phase Variations on Stability

In matrix form the open loop transfer function described by the MIMO model (figure 4.8)
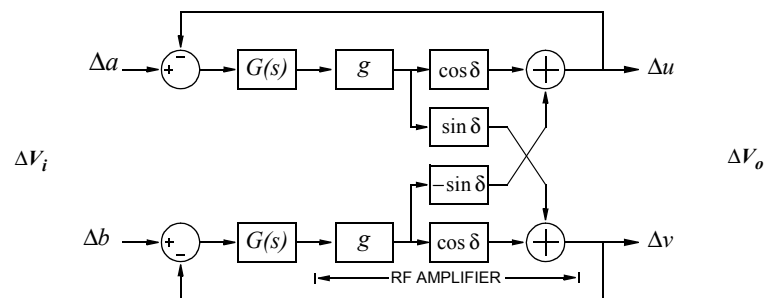
Figure 4.8: MIMO Representation of Cartesian Feedback Loop.

is given by

$$
\begin{bmatrix} \cos\delta & -\sin\delta \\ \sin\delta & \cos\delta \end{bmatrix} \begin{bmatrix} g & 0 \\ 0 & g \end{bmatrix} \begin{bmatrix} G(s) & 0 \\ 0 & G(s) \end{bmatrix}
$$
$$
= \begin{bmatrix} gG(s)\cos\delta & -gG(s)\sin\delta \\ gG(s)\sin\delta & gG(s)\cos\delta \end{bmatrix} \tag{4.29}
$$

Instability results whenever the following condition (the characteristic equation of the closed loop system) is satisfied

$$
\left| I + \begin{bmatrix} gG(s)\cos\delta & -gG(s)\sin\delta \\ gG(s)\sin\delta & gG(s)\cos\delta \end{bmatrix} \right| = 0 \tag{4.30}
$$

where the absolute signs symbolize the determinant of a matrix, and I is the identity matrix.

If instability occurs in the system, it will occur at some frequency which obviously implies the frequency dependent function of *G(s)* will be equivalent to some complex number at that frequency. Combining *G(s)* and *g* and setting this product to some complex number **G** then reduces equation 4.30 to

$$
\boldsymbol{G}^2 + 2\boldsymbol{G}\cos\delta + 1 = 0 \tag{4.31}
$$

The solution to equation 4.31 for **G** is given by

$$
\boldsymbol{G} = \frac{-2\cos\delta \pm \sqrt{4\cos\delta^2 - 4}}{2} \tag{4.32}
$$

This solution is complex since the expression within the square root is negative or zero. **G** is therefore given by

$$
\boldsymbol{G} = \frac{-2\cos\delta}{2} \pm j\frac{\sqrt{4 - 4\cos\delta^2}}{2} \tag{4.33}
$$
$$
= -\cos\delta \pm j\sin\delta
$$

Since the magnitude of $gG(s)$ is one at the frequency where the phase margin is measured it follows then that the angle of equation 4.33 is related to the phase margin of $gG(s)$ by

$$\angle(gG(s)) = \angle(-\cos\delta \pm j\sin\delta)$$
$$\Rightarrow \pm(\text{Phase Margin of } [gG(s)] - \pi) = \pm(|\delta| - \pi) \qquad (4.34)$$
$$\therefore \text{ Phase Margin of } [gG(s)] = pm_G = |\delta|$$

The amount of RF phase rotation (δ) which can be tolerated before instability results will be termed δm_G and is

$$\delta m_G = pm_G - |\delta| \qquad (4.35)$$

Stability is insured provided δm_G remains positive. Instability occurs ($\delta m_G \leq 0$) whenever the amount of RF phase rotation completely consumes the phase margin of $gG(s)$. This does not indicate that RF phase rotation and baseband phase shift are equivalent.

4.2.2 The Difference between RF Phase Rotation and Baseband Phase Shift

RF phase rotation causes cross-coupling (as shown in figure 4.8) whereas baseband phase shift results is a phase shift in a time sense. The difference is best demonstrated in figure 4.9 The solid line represents the phase shift as a function of positive and negative frequency for the first order transfer function given in Chapter 3 (equation 3.2). The graphs were obtained by taking the double-sided FFT (Fast Fourier Transform) of the impulse response of the transfer function.

Adding more delay in the transfer function effectively increases the slope of the linear phase component and hence symmetrically pushes both sides of the phase response closer to $\pm 180°$ respectively (dashed line). Delay or baseband phase shift hence directly reduces the stability of the system by subtracting away from the original phase margin of the system (pm_G).

RF phase rotation also reduces stability and in the manner shown by the dot-dashed traces. Only one side of the phase response suffers a degradation in stability (closer to
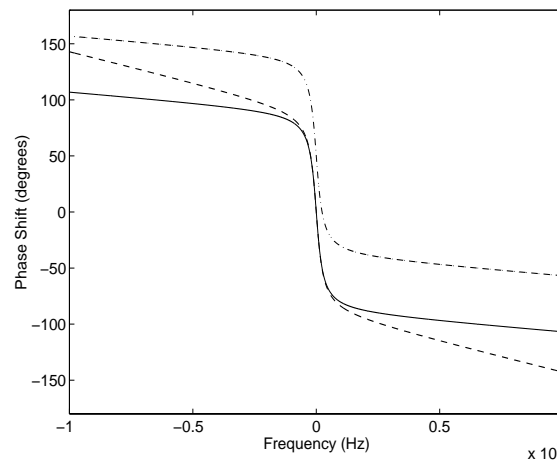
Figure 4.9: Demonstration of the difference between baseband phase shift and RF phase rotation. Original phase response (solid) and modified phase responses as a result of baseband phase shift (dashed) and as a result of RF phase rotation (dash-dot). Complex envelope representation - 0Hz on the graph represents the carrier frequency.

+180° in this case). While the other side becomes more stable (further away from −180°). The stability degradation is equivalent to the amount of RF phase rotation imposed. Therefore when the amount of RF phase rotation equals the original phase margin, pm_G, one side of the response will have a zero phase margin and instability will result (on this side of the spectrum).

The figure can also explain how only a complex tone (SSB tone) experiences the same phase shift whether it experiences an RF phase rotation or a baseband phase shift.

It is possible to have two systems with the same δm_G each having a different combination of pm_G and $|\delta|$. Both will be able tolerate the same amount of RF phase variation since both have the same δm_G but the closed loop responses of the two systems will not be exactly the same despite the fact both have the same stability margin.

4.2.3 Effects of Amplifier Gain Variations on Stability

In addition to amplifier phase variations discussed previously, the RF amplifier introduces gain variations. This directly modifies the loop gain parameter *g* of the MIMO

model. To account for this gain change the phase margin of *gG(s)* must be able to be calculated as a function of *g*. This can be accomplished by equating *G(s)* to some numeric transfer function such as that given in Chapter 3 (equation 3.2).

The phase margin of *gG(s)* (with *G(s)* of the type given by equation 3.2) is given by

$$pm_G = \pi + \operatorname{atan}\frac{\omega_{0dB}}{-p} - \omega_{0dB}\tau \text{ (radians)} \tag{4.36}$$

where:

$$\omega_{0dB} = p\sqrt{K^2 g^2 - 1} \text{ (radians/sec)} \tag{4.37}$$

ω_{0dB} is the gain crossover frequency for controller transfer functions of the type given by equation 3.2. The gain margin can also be found by finding how much loop gain (gK) in equation 4.37 will force pm_G in equation 4.36 to 0.

It is evident from the preceding therefore, that cross-coupling, as is introduced by the AM/PM distortion of the RF amplifier and error in the adjustment of δ_r (see figure 2.25) will degrade the system stability. Increases in gain as introduced by amplifier AM/AM distortion will also degrade system stability since equations 4.36 and 4.37 show that increases in gain reduce the phase margin and hence stability.

4.3 A GRAPHICAL STABILITY ANALYSIS SUITABLE FOR AMPLIFIERS WITH WEAK NON-LINEARITIES

A graphical interpretation of equation 4.35 and its two supporting equations equation 4.36 and 4.29 was used to form the conditions for stability as shown in figure 4.10. The stability boundary was generated by combining equation 4.35 and 4.36 to give

$$|\delta| = \pi + \operatorname{atan}\frac{\omega_{0dB}}{-p} - \omega_{0dB}\tau \text{ (radians)} \tag{4.38}$$

with ω_{0dB} given by equation 4.37. The delay was set to 50ns and the pole frequency was
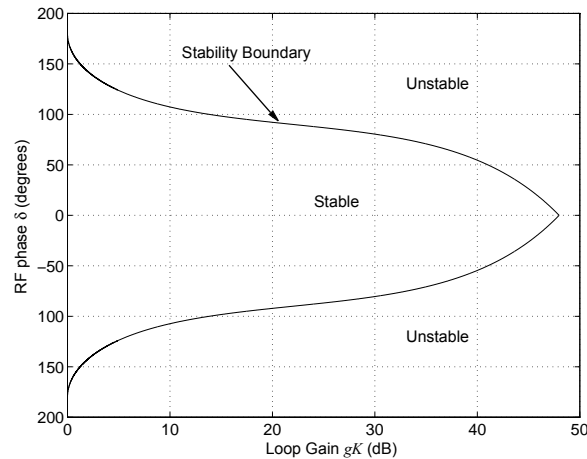
Figure 4.10: Graphical conditions for linear amplifier stability. Stability is ensured provided amplifier operation is within the stability boundary. Conditions: τ=50ns, p=20kHz.

set to 126krad/sec (20kHz) in equation 4.36 and 4.37 respectively. These are typical values from experimental hardware described in chapter 3. Within the stability boundary shown the cartesian feedback loop is stable.

To demonstrate the use and significance of the graph the amplifier gain and phase responses of the high power amplifier (figure 4.4*(b)*) can be directly superimposed upon the curve of figure 4.10.

Setting the RF phase adjuster of figure 2.25 and equation 4.7, δ_r to $-135°$, and the DC gain (K) to 3.4dB places the amplifier traces in the position shown in figure 4.11 (a blown-up version of figure 4.10). An asterisk placed on approximately the worst stability point highlights how specific stability factors can be determined. The gain margin can be found by measuring the horizontal distance from the asterisk to the stability boundary. In other words this distance gives the amount of additional gain the system can tolerate before instability occurs and is 2.9dB in this example. The vertical distance to the stability boundary gives the amount of RF phase rotation which can be accommodated before instability results. This distance, is the δ margin or δm_G, and indicates $+22°$ of RF phase rotation can be accommodated before the system becomes unstable.
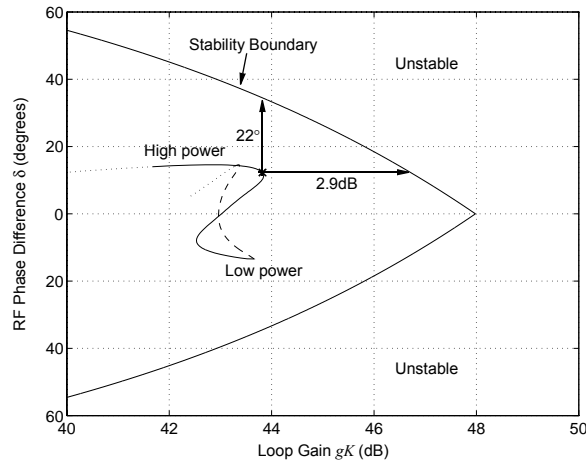
Figure 4.11: Close-up view of the graphical conditions for linear amplifier stability with amplifier characteristics superimposed. Gain and δ margins are indicated by numbered arrows.

The technique is quite versatile and allows the placement of amplifier characteristics operating under different system conditions - so as δ_r is varied, the characteristics are moved in a vertical direction, and as *K* is varied, the characteristics are moved in a horizontal direction.

Figure 4.12 gives two examples of instability caused with by different adjustment of the phase rotator. Figure 4.12*(a)* shows that positive adjustments from the optimum value

(a)   *(b)*
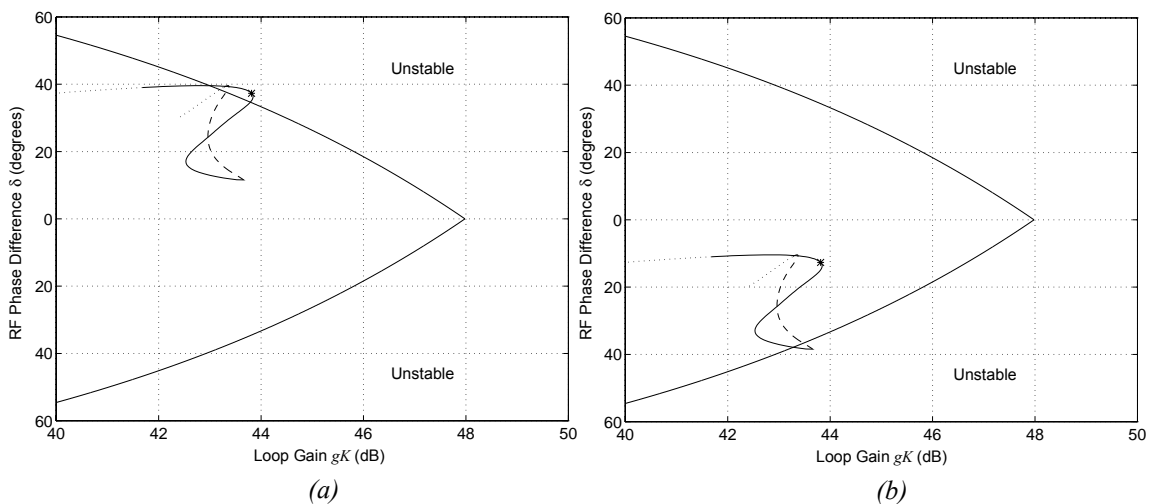
Figure 4.12: (a) Phase rotator set +25° from optimum causes instability at high out put powers. (b) Phase rotator set −25° from optimum causes instability at low output levels.

will cause instability at higher output levels, whereas shown in 4.10*(b)*, negative adjustments from optimum cause instability at low output levels. These general predictions about BJT based power amplifiers have been verified experimentally with the BLU98 low power amplifier and shown in figure 4.19.

4.3.1 A Universally Applicable Graphical Technique

Equation 4.35, plotted in its essential form with the amplifier characteristics superimposed is shown in figure 4.13. The graph is universally applicable because the phase margin of any transfer function (pm_G) can be applied irrespective of the nature of this transfer function (i.e whether it contains various combinations of multiple poles and zeros, different delay and gain).

The secondary axis shown below the main graph of figure 4.13 demonstrates a simple technique by which the universal graph can be utilized. If the gain is sufficiently large for the single pole example given, then equation 4.37 can be expressed by
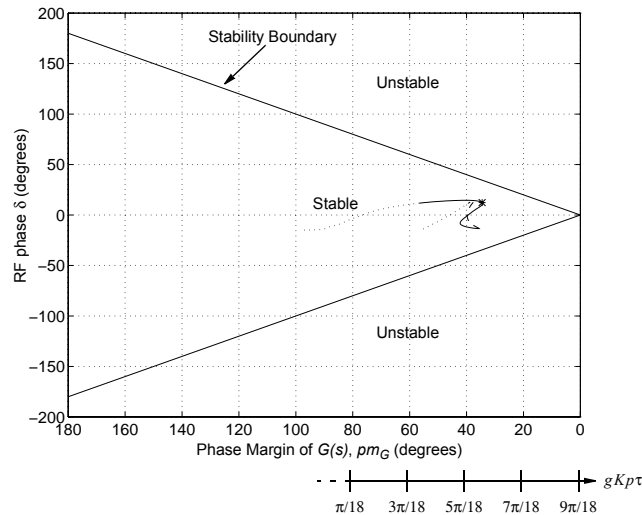
Figure 4.13: Universally applicable graphical conditions for linear amplifier stability. Additional axis allows selection of gain, pole frequency and delay for first order loops. The delay term is interchangeable with gKp and is an undesirable stability reducing quantity.

$$\omega_{0dB} \approx p\,g\,K \tag{4.39}$$

Also if ω_{0dB} is much greater than p then the pole will contribute $-\pi/2$ at ω_{0dB}. Equation 4.36 can thus be reduced to

$$pm_G \approx \frac{\pi}{2} - p\,gK\tau \tag{4.40}$$

It is this expression which allows the additional axis to be drawn. Note gK in the expression and shown on the axis is not in dB.

4.3.2 Summary of Amplifier and other Effects on Stability

Equation 4.40 and the secondary axis drawn below the graph of figure 4.13 shows clearly that for a desired or given phase margin, gK, p, and τ are interchangeable. Both gain (gK) and bandwidth (p) are desirable quantities to make large, but since τ is interchangeable with the other quantities, it consumes the phase margin directly. This is undesirable because it places a limit on how large the gain bandwidth combination can be made whilst maintaining a given phase margin. Delay is therefore the limiting factor in cartesian feedback linearization systems.

The delay modelled here was defined as comprising both a true transmissive type delay in addition to pole-zero induced delay i.e. filtering and finite bandwidth induced delay. Of these two delay types, the filtering induced delay dominated, with the transmissive delay representing only 1-2ns of the 50ns delay obtained from the experimental hardware presented. To increase the amount of gain bandwidth then, it is desirable to reduce the filtering induced delay. This can be achieved by widening the bandwidth of the components which comprise the cartesian feedback loop. The main bandwidth reducing components within the loop are the baseband (op-amp) circuits and RF power amplifier. The baseband circuit delays can be reduced by using even wider bandwidth circuits but this usually implies an increase in power consumption. Broadening the RF amplifier bandwidth has the potential to shave tens of nanoseconds off the loop delay and this should be an essential requirement in the design of the RF power amplifier. In contrast,

reducing the transmissive delay by reducing size (e.g. circuit integration) would yield only a minor improvement.

The amplifier characteristics also have an impact on stability. It was also shown in section 4.2.2 and in the stability boundary figures (figures 4.11-4.13) that RF phase rotation reduces stability. Adjusting the RF phase rotator is therefore important in placing the amplifier characteristics in a position which has the maximum distance from any stability boundary. But the distortion of the amplifier itself sets the amount of movement of the and phase. Reducing the amount of AM/AM and AM/PM distortion reduces the movement (with an ideal linear amplifier being represented as a point on the characteristics i.e. no movement at all), and yields an obvious conclusion that it is easier to linearize a more linear amplifier. This indicates that highly non-linear amplifiers, such as the BLU98 low power amplifier operated with no or little base bias, are not really suitable for practical cartesian feedback systems.

4.4 MIMO MODEL OF CARTESIAN FEEDBACK FOR NON-LINEAR AMPLIFIERS

This section applies the MIMO analysis to the non-linear amplifier model mathematically derived in section 4.2.2. In section 4.4.1 swept phase perturbations are applied at some point on the low power amplifier characteristic. The complex gain is shown to vary as a function of perturbation angle. This result demonstrates how the complex gain varies with applied perturbation and is used in section 4.7. Before being applied to the cartesian feedback MIMO model (section 4.4.3) the non-linear amplifier model is first reduced to its essential canonical form.

4.4.1 Complex Gain and Perturbations

It was found in section 4.1 that non-linearity caused the complex gain to be non-unique
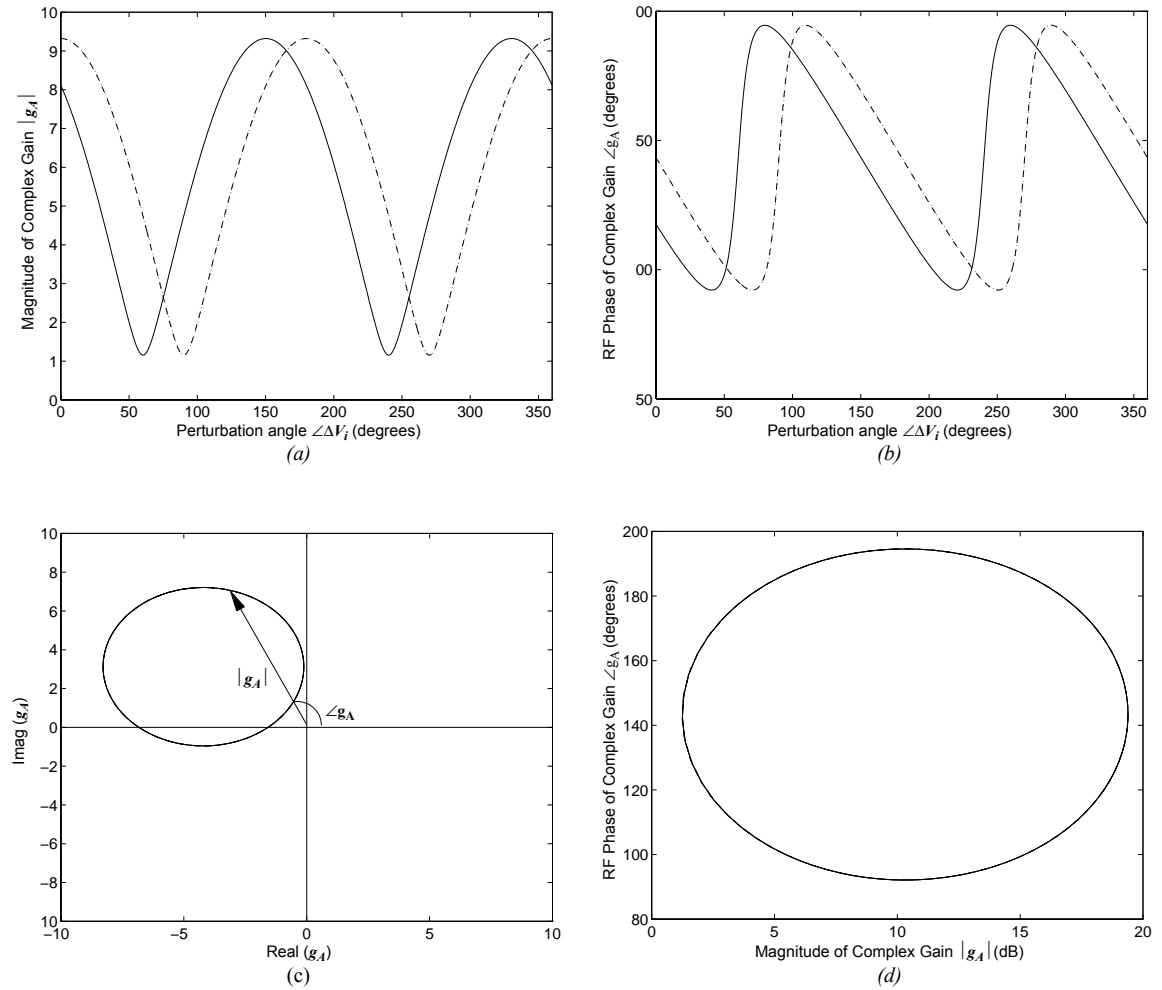
Figure 4.14: Variation in complex gain as a result of a complex rotating perturbation. (a) Magnitude of complex gain, (b) phase of complex gain, (c) complex plot of (a) and (b), (d) polar plot of (a) and (b). Two cases are shown: complex gain when input signal phase is $\angle V_i = 30°$(solid) and input phase $\angle V_i = 0°$ (dashed).

and dependent on the perturbation direction. The point on the amplifier characteristics marked with an asterisk in figure 4.6, will be chosen to demonstrate how the complex gain is affected by a complex perturbation. The complex gain at a particular setpoint $\left| V_i \right|$ is defined as

$$g_A(\left| V_i \right|) = \left. \frac{\Delta V_o}{\Delta V_i} \right|_{\left| V_i \right|} \tag{4.41}$$

with ΔV_i (the perturbation) small.

Sweeping the phase of the perturbation ($\angle\Delta V_i$) at the point marked with the asterisk (with $\angle V_i$ arbitrarily set to $-30°$) resulted in the solid line plots of figure 4.14. The complex gain versus angle ($\angle\Delta V_i$) is shown in magnitude and phase format in figure 4.14(a) and 4.14(b) respectively. Figure 4.14(c) shows the complex gain in cartesian coordinates and figure 4.13(d) shows the complex gain in magnitude (dB) and phase (degrees) format. Since the complex gain changes with the phase of the perturbation, a single unique complex derivative does not exist at this point. In other words the complex derivative depends on the path taken as ΔV_i approaches zero.

4.4.2 Reduction of Non-linear Amplifier Model

When excited by a constant magnitude perturbation with sweeping phase (i.e. the input is a circle), the non-linear model produces an elliptical output. An ellipse is generated whenever the gains in the real and imaginary channels are dissimilar, and/or when the phase shift in the quadrature de/modulator is not 90°[70-71]. It will be shown then that it is feasible to model all elliptical behaviour by appropriate selection of a set of dissimilar real and imaginary gains and a phase rotation only.

In matrix form figure 4.3 is

$$\begin{bmatrix} \Delta u \\ \Delta v \end{bmatrix} = \begin{bmatrix} \cos\delta_a & -\sin\delta_a \\ \sin\delta_a & \cos\delta_a \end{bmatrix} \begin{bmatrix} g_i & 0 \\ g_d|V_o| & g_q \end{bmatrix} \begin{bmatrix} \Delta a \\ \Delta b \end{bmatrix} \tag{4.42}$$

To simplify equation 4.42 the gain matrix given by

$$\begin{bmatrix} g_i & 0 \\ g_d|V_o| & g_q \end{bmatrix} \tag{4.43}$$

must be reorganized such that it can be written in two parts, one part containing another phase rotation to be added to δ_a, and another part consisting of two dissimilar gains in the in-phase and quadrature channels. In matrix terminology the aim then, is to diagonalize the transformation matrix of equation 4.43.

From linear algebra it is well known that a symmetrical transformation matrix is easily diagonalized by use of the Principle Axes Theorem[72]:

$$A = PDP^{-1} = PDP^{t} \tag{4.44}$$

where A is some $n \times n$ symmetric matrix, P is an orthogonal matrix and D is a diagonal matrix (^{t} represents the transpose of a matrix). If the columns of P are composed of the eigenvectors of A, then D will be composed of the corresponding eigenvalues of A. To make use of this, the transformation matrix of equation 4.43 must first be made symmetrical. This is readily achieved by introducing a phase rotation to equation 4.43 until symmetry is achieved.

$$\begin{bmatrix} \cos\beta & -\sin\beta \\ \sin\beta & \cos\beta \end{bmatrix} \begin{bmatrix} \cos\beta & \sin\beta \\ -\sin\beta & \cos\beta \end{bmatrix} \begin{bmatrix} g_i & 0 \\ g_d|V_o| & g_q \end{bmatrix} = \begin{bmatrix} g_i & 0 \\ g_d|V_o| & g_q \end{bmatrix} \tag{4.45}$$

Separating equation 4.45 gives

$$BA = \begin{bmatrix} g_i & 0 \\ g_d|V_o| & g_q \end{bmatrix}$$

$$B = \begin{bmatrix} \cos\beta & -\sin\beta \\ \sin\beta & \cos\beta \end{bmatrix} \qquad A = \begin{bmatrix} \cos\beta & \sin\beta \\ -\sin\beta & \cos\beta \end{bmatrix} \begin{bmatrix} g_i & 0 \\ g_d|V_o| & g_q \end{bmatrix} \tag{4.46}$$

For A to be symmetrical then

$$\begin{bmatrix} \cos\beta & \sin\beta \\ -\sin\beta & \cos\beta \end{bmatrix} \begin{bmatrix} g_i & 0 \\ g_d|V_o| & g_q \end{bmatrix} = \begin{bmatrix} w & x \\ x & y \end{bmatrix} = A \tag{4.47}$$

giving

$$\begin{aligned} w &= g_i\cos\beta + g_d|V_o|\sin\beta \\ x &= g_q\sin\beta \\ &= -g_i\sin\beta + g_d|V_o|\cos\beta \\ y &= g_q\cos\beta \end{aligned} \tag{4.48}$$

From equation 4.48 then

$$\beta = \text{atan}\left(\frac{g_d|V_o|}{g_i + g_q}\right) \tag{4.49}$$

A solution for β in matrix B hence provides the first step (i.e the phase rotation), in the reorganisation of equation 4.43. The second step is achieved by finding the eigenvalues of the symmetricized matrix i.e

$$\left\|\begin{bmatrix} w - \lambda & x \\ x & w - \lambda \end{bmatrix}\right\| = 0 \tag{4.50}$$

which implies,

$$\lambda = \frac{(w + y) \pm \sqrt{(w - y)^2 + 4x^2}}{2} \tag{4.51}$$

Rearranging equation 4.48

$$w = \frac{g_i^2 + g_i g_q + (g_d|V_o|)^2}{\sqrt{(g_i + g_q)^2 + (g_d|V_o|)^2}}$$

$$x = \frac{g_q g_d|V_o|}{\sqrt{(g_i + g_q)^2 + (g_d|V_o|)^2}} \tag{4.52}$$

$$y = \frac{g_i g_q + g_q^2}{\sqrt{(g_i + g_q)^2 + (g_d|V_o|)^2}}$$

and substituting into equation 4.51 gives

$$\lambda_1 = \frac{\sqrt{(g_i + g_q)^2 + (g_d|V_o|)^2} + \sqrt{(g_i - g_q)^2 + (g_d|V_o|)^2}}{2}$$

$$\lambda_2 = \frac{\sqrt{(g_i + g_q)^2 + (g_d|V_o|)^2} - \sqrt{(g_i - g_q)^2 + (g_d|V_o|)^2}}{2} \tag{4.53}$$

The diagonal matrix is then

$$D = \begin{bmatrix} \lambda_1 & 0 \\ 0 & \lambda_2 \end{bmatrix} \tag{4.54}$$

Equation 4.54 is actually a representation of matrix A in canonical form. The P^t and P^{-1}

matrix basically represent a rotation in the co-ordinate axes and back again respectively, and in this context simply means a relative shift on the perturbation phases. Therefore dropping P^t and P^{-1} at this stage strips off unnecessary information regarding the position of the amplifier characteristics relative to the perturbation angle. In fact, since the diagonalization process provides the canonical form of matrix A, the perturbation amplifier characteristics are shifted such that the maximum gain occurs at a perturbation phase of zero. This is demonstrated in figure 4.14. This model of amplifier gain (figure 4.3) was numerically verified for the point given in figure 4.6. This comparison in figure 4.14 shows that although the model does not exactly match the amplifier response, it does traverse the same vector given in figures 4.14*(c)* and 4.14*(d)*. The only difference between the models is a relative shift in the input perturbation phase. This difference results from the reduction made by letting $b = 0$ in equation 4.23 which forces $\angle V_i = 0°$ (compared to $\angle V_i = 30°$ for the solid trace in figure 4.14). Setting $b = 0$ effectively removes any information about the phase of V_i. Since the model is ultimately to be used in a stability analysis, the model is valid because the cartesian loop must be stable for *all* possible input perturbation phases, $\angle \Delta V_i$, and hence a relative shift in the input perturbation phase is irrelevant. What is important is the fact that the model traverses the same complex gain vectors as those generated by equation 4.41 as shown in figures 4.14*(c)* and 4.14*(d)*.

The model is then

$$\begin{bmatrix} \Delta u \\ \Delta v \end{bmatrix} = \begin{bmatrix} \cos(\delta_a + \beta) & -\sin(\delta_a + \beta) \\ \sin(\delta_a + \beta) & \cos(\delta_a + \beta) \end{bmatrix} \begin{bmatrix} \lambda_1 & 0 \\ 0 & \lambda_2 \end{bmatrix} \begin{bmatrix} \Delta a \\ \Delta b \end{bmatrix} \qquad (4.55)$$

Although the models given by equations 4.42 and 4.55 are not equal in terms of a point-to-point mapping, both trace out the same ellipse when excited by a sweeping perturbation. Since the elliptic vectors are invariant then the areas encircled by these vectors must also be the same. The geometrical interpretation of the determinant of a transformation matrix is the ratio or gain in area as a result of the transformation. Since

the change in area is the same for both models then it follows that the determinants of both models are also equivalent.

$$\left\| \begin{bmatrix} \cos\delta_a & -\sin\delta_a \\ \sin\delta_a & \cos\delta_a \end{bmatrix} \begin{bmatrix} g_i & 0 \\ g_d|V_o| & g_q \end{bmatrix} \right\| = \left\| \begin{bmatrix} \cos(\delta_a+\beta) & -\sin(\delta_a+\beta) \\ \sin(\delta_a+\beta) & \cos(\delta_a+\beta) \end{bmatrix} \begin{bmatrix} \lambda_1 & 0 \\ 0 & \lambda_2 \end{bmatrix} \right\|$$

$$\Rightarrow \left\| \begin{bmatrix} g_i & 0 \\ g_d|V_o| & g_q \end{bmatrix} \right\| = \left\| \begin{bmatrix} \lambda_1 & 0 \\ 0 & \lambda_2 \end{bmatrix} \right\| \tag{4.56}$$

$$\therefore \quad g_i g_q = \lambda_1 \lambda_2$$

The result of equation 4.56 can be used to yield another reduction by setting

$$g = \sqrt{g_i g_q} \tag{4.57}$$

and letting

$$g_n = \frac{\lambda_1}{g} = \frac{g}{\lambda_2} \tag{4.58}$$

giving

$$\lambda_1 = g g_n$$

$$\lambda_2 = \frac{g}{g_n} \tag{4.59}$$

The diagonal matrix of equation 4.54 can thus be expressed in terms of g_n and the reciprocal of g_n. And to finally summarize the model then

$$\begin{bmatrix} \Delta u \\ \Delta v \end{bmatrix} = \begin{bmatrix} \cos\delta & -\sin\delta \\ \sin\delta & \cos\delta \end{bmatrix} \begin{bmatrix} g_n & 0 \\ 0 & 1/g_n \end{bmatrix} g \begin{bmatrix} \Delta a \\ \Delta b \end{bmatrix} \tag{4.60}$$

where:

$$g_n = \frac{\sqrt{(g_i+g_q)^2 + (g_d|V_o|)^2} + \sqrt{(g_i-g_q)^2 + (g_d|V_o|)^2}}{2\sqrt{g_i g_q}} \tag{4.61}$$

$$(g = \sqrt{g_i g_q})$$

$$\delta = g_d|V_o| + \delta_d + \text{atan}\left(\frac{g_d|V_o|}{g_i+g_q} \right) \tag{4.62}$$

This end result was numerically verified and superimposed on the traces of figure 4.14. For the example point (figure 4.6) the values above are $g_n = 2.84$, $g = 3.28$ and $\delta = 2.50$ radians.

4.4.3 MIMO Model of Cartesian Feedback with non-linear amplifiers

Placing the final non-linear amplifier model developed in the previous section in a cartesian feedback loop allows the system to be represented by the MIMO model shown in figure 4.15. This figure shows the amplifier model given by equations 4.60-4.62 within a cartesian feedback loop composed of compensation filters given by *G(s)*.

Again, instability results whenever the characteristic equation of the closed loop system is satisfied

$$\left| I + \begin{bmatrix} \cos\delta & -\sin\delta \\ \sin\delta & \cos\delta \end{bmatrix} \begin{bmatrix} g_n & 0 \\ 0 & 1/g_n \end{bmatrix} \begin{bmatrix} G(s) & 0 \\ 0 & G(s) \end{bmatrix} g \right| = 0 \qquad (4.63)$$

where the absolute symbolises the determinant of a matrix, and I is the identity matrix.

As in section 4.2.1, if instability occurs in the system, it will occur at some frequency which implies the frequency dependent function of *G(s)* will be equivalent to some complex number. Combining *G(s)* and *g* and setting this product to some complex number **G** then reduces equation 4.63 to
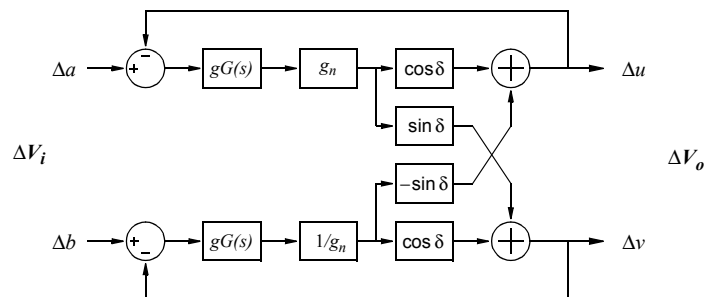
Figure 4.15: MIMO representation of cartesian feedback loop with non-linear amplifier final model.

$$G^2 + (g_n + 1/g_n)G\cos\delta + 1 = 0 \tag{4.64}$$

There are numerous possible combinations of G, g_n and δ which will satisfy equation 4.64 and result in instability. Looking first at the solution for G gives

$$G = \frac{-(g_n + 1/g_n)\cos\delta \pm \sqrt{(g_n + 1/g_n)^2 \cos\delta^2 - 4}}{2} \tag{4.65}$$

There are two possible types of solution to equation 4.65 depending on the value of the expression within the square root. The solution to equation 4.65 will be real provided

$$|\delta| < \text{acos}\left(\frac{2}{g_n + 1/g_n}\right) \tag{4.66}$$

or alternatively complex if

$$|\delta| > \text{acos}\left(\frac{2}{g_n + 1/g_n}\right) \tag{4.67}$$

The boundary condition for these solutions is defined as

$$\delta_b = \pm\text{acos}\left(\frac{2}{g_n + 1/g_n}\right) \tag{4.68}$$

When equation 4.66 is satisfied and hence the expression within the square root is positive, the two possible solutions for G will always be negative. This implies the phase of G will be $\pm\pi$ with two possible magnitudes and G is hence given directly by 4.65.

It should be noted that G has a phase of $\pm\pi$ at the frequency where the gain margin of $gG(s)$ is calculated. This enables the solution to be related back to $gG(s)$ and so the instability condition given by equation 4.65 is thus reduced to

$$G = \frac{1}{gm_G}\angle \pm\pi \qquad |\delta| < |\delta_b| \tag{4.69}$$

where gm_G is the gain margin of $gG(s)$ and is not in dB.

The result of equation 4.69 can now be applied to equation 4.65 to give the stability conditions in terms of gm_G and g_n. Instability therefore results when δ is equal to

$$\delta_s = \pm\text{acos}\left(\frac{(1/gm_G)^2 + 1}{(1/gm_G)(g_n + 1/g_n)}\right) \qquad |\delta| < |\delta_b| \qquad (4.70)$$

When equation 4.67 is satisfied and hence the expression within the square root is negative, the two possible solutions for **G** will always be complex. The complex solution to the quadratic given by equation 4.64 is

$$\mathbf{G} = \frac{-(g_n + 1/g_n)\cos\delta \pm j\sqrt{4 - (g_n + 1/g_n)^2\cos\delta^2}}{2} \qquad |\delta| > |\delta_b| \qquad (4.71)$$

It is easy to show that provided $|\delta| > |\delta_b|$ the magnitude of **G** in equation 4.71 will always be one. Again it should be noted that **G** has a magnitude of one at the frequency where the phase margin of $gG(s)$ is calculated. This enables the solution to be related back to $gG(s)$ and so the instability condition given by equation 4.71 is thus reduced to

$$\mathbf{G} = 1\angle(pm_G - \pi) = e^{j(pm_G - \pi)} \qquad |\delta| > |\delta_b| \qquad (4.72)$$

where pm_G is the phase margin of $gG(s)$ in radians.

The result of equation 4.72 can now be applied to equation 4.64 to give the stability conditions in terms of pm_G and g_n. Instability therefore results when δ is equal to:

$$\delta_s = \pm\text{acos}\left(\frac{[e^{j2(pm_G - \pi)}]^2 + 1}{-e^{j(pm_G - \pi)}(g_n + 1/g_n)}\right) \qquad |\delta| > |\delta_b| \qquad (4.73)$$

The preceding results (equations 4.70 and 4.73) can now be combined to give the amount of RF phase rotation which can be tolerated before instability results. This quantity, termed δm_G, is hence given by

$$\delta m_G = \mathrm{acos}\left(\frac{(1/gm_G)^2 + 1}{(1/gm_G)(g_n + 1/g_n)}\right) - |\delta| \qquad |\delta| < |\delta_b| \qquad (4.74)$$

$$\delta m_G = \mathrm{acos}\left(\frac{[e^{j2(pm_G - \pi)}]^2 + 1}{-e^{j(pm_G - \pi)}(g_n + 1/g_n)}\right) - |\delta| \qquad |\delta| > |\delta_b| \qquad (4.75)$$

Stability is insured provided δm_G remains positive. Instability occurs ($\delta m_G \leq 0$) whenever the amount of RF phase rotation completely consumes the gain and phase margins of *gG(s)* in accordance with either equation 4.74 or equation 4.75. The form of *gG(s)* is hence immaterial, and so all that really matters are the gain and phase margins.

4.6 A GRAPHICAL STABILITY ANALYSIS SUITABLE FOR NON-LINEAR AMPLIFIERS

The results of the previous section provide the basis for developing a graphical stability analysis for the non-linear amplifier model. This can be again demonstrated by equating *gG(s)* to the numeric transfer function given in equation 3.2.

From section 4.2.3 the phase margin of *gG(s)* with *G(s)* of the type given by equation 3.2, is given by equations 4.38 and 4.39. And the gain margin of *gG(s)* is given by

$$gm_G = \frac{\sqrt{p^2 + \omega_\pi^2}}{Kgp} \qquad (4.76)$$

where ω_π is the phase crossover frequency in radians/sec (and gm_G is not in dB). Since the phase crossover frequency is generally much greater than the pole frequency, it can be assumed that the pole contributes $-\pi/2$ at the phase crossover frequency and hence the remainder (also $\pi/2$) is contributed by the time delay giving

$$\omega_\pi \approx \frac{\pi}{2\tau} \tag{4.77}$$

The component variables of equations 4.70 and 4.73 are now defined and hence enable the stability boundary given by these equations to be plotted. Introducing 4.77 and 4.76 into 4.70 gives

$$\delta_s = \pm\text{acos}\left(\frac{\dfrac{(Kgp)^2}{\dfrac{\pi^2}{4\tau^2}+p^2}+1}{\dfrac{Kgp}{\sqrt{\dfrac{\pi^2}{4\tau^2}+p^2}}(g_n+1/g_n)}\right) \qquad |\delta| < |\delta_b| \tag{4.78}$$

$$= f_{|\delta|<|\delta_b|}(k,g,g_n)\big|_{\tau,p}$$

Introducing 4.38 and 4.39 into 4.73 gives

$$\delta_s = \pm\text{acos}\left(\frac{\left[e^{j2(\text{atan}(-p\sqrt{k^2g^2-1})-\tau p\sqrt{k^2g^2-1})}\right]^2+1}{-e^{j(\text{atan}(-p\sqrt{k^2g^2-1})-\tau p\sqrt{k^2g^2-1})}(g_n+1/g_n)}\right) \qquad |\delta| > |\delta_b| \tag{4.79}$$

$$= f_{|\delta|>|\delta_b|}(k,g,g_n)\big|_{\tau,p}$$

This stability boundary is however multi-dimensional as are the amplifier characteristics. The three amplifier parameters g, δ and g_n are plotted in figure 4.16 as a function of amplifier output voltage. It is possible to plot these amplifier characteristics as functions of each other in three dimensions. This however would make the resulting figure difficult to utilize. An alternative two dimensional method adopted here is shown in figure 4.17. The numbered contours represent the stability boundaries given by equations 4.70 and 4.73 for the values of g_n shown (i.e 1,1.5, 2, 2.5 & 2.8). Within these boundaries the system is stable, and outside it is unstable. The pole frequency, p was set to 20kHz and the delay, τ was set to 50ns in the gain and phase margin equations (4.38-4.39 and 4.76-4.77). The amplifier characteristic which is superimposed, was obtained by plotting the δ
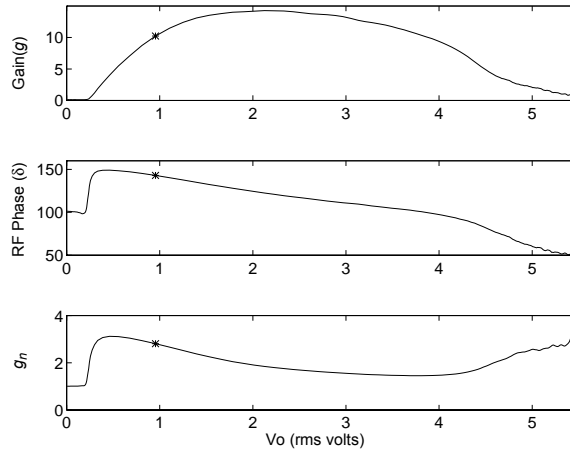
Figure 4.16: RF amplifier model parameters as a function of desired output for BLU98 low power amplifier.

characteristic of figure 4.17 against the *g* characteristic multiplied by the g_n characteristic and *K* on a dB scale (i.e δ versus *gKgn*). The markings on the amplifier characteristics give the third dimension and identify which g_n value applies at a given point.

Setting the RF phase adjuster of figure 2.25, δ_r to $-105°$ and the DC gain (*K*) to 14 (22.9dB) places the amplifier traces in the position shown in figure 4.17. An asterisk placed on the point mentioned previously ($g_n = 2.84$, $g = 3.28$ and $\delta = 2.50$ radians) highlights how specific stability factors can be determined. The gain margin can be found
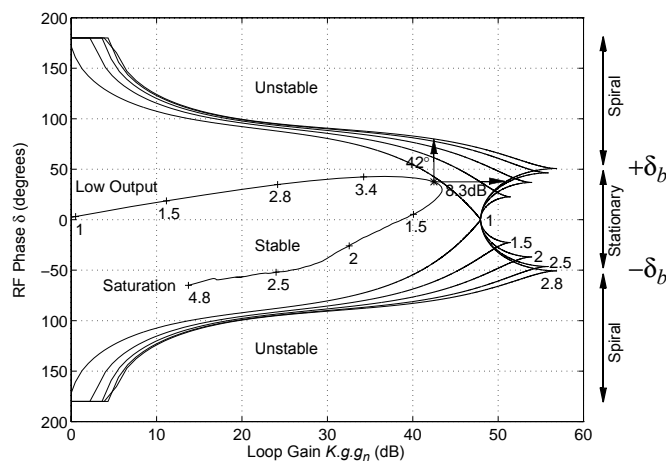
Figure 4.17: Graphical conditions for non-linear amplifier stability. Numbers indicate g_n values. δ_b shown on right is for $g_n=2.8$.

by measuring the horizontal distance from the asterisk to the stability boundary for g_n = 2.84 (marked with "2.8"). In other words this distance gives the amount of additional gain the system can tolerate before instability occurs and is 8.3dB in this example. The vertical distance to the same stability boundary gives the amount of RF phase which can be accommodated before instability results. This distance, is the δ margin or δm_G, and indicates 42° of RF phase rotation can be accommodated before the system becomes unstable.

The technique is similarly versatile to the linear approach and allows the placement of amplifier characteristics operating under different system conditions - so again, as δ_r is varied, the characteristics are moved in a vertical direction, and as K is varied, the characteristics are moved in a horizontal direction. The inner-most stability boundary (g_n = 1) represents the stability boundary derived in section 4.3. This boundary actually represents the worst case stability boundary and can be used in a simplified conservative stability analysis. This worst case boundary is also the same as that derived for amplifiers with weak non-linearities in section 4.3.

The graphical technique can also account for the burst like instability experienced just past zero-crossing in practical cartesian feedback systems. The point considered represents the situation just after the transistor switches on. From figure 4.17 it is clear that this point and the region around it has the greatest potential for instability with the δ_r setting used ($\delta_r = -105°$). This can also be demonstrated using the approach shown in figure 4.18 which is obtained by applying equations 4.74 and 4.75. The three traces indicate the amount of δ the system can tolerate before instability results for the three settings of δ_r shown in the figure.

The case with $\delta_r = -105°$ is in fact the optimum setting for the phase adjuster and is equivalent to the placement of the amplifier presented in 4.17. When the phase adjuster is adjusted by +45° above optimum the system will burst into instability at a point just after the transistor turns on (instability is indicated by negative δm_G). Alternatively when
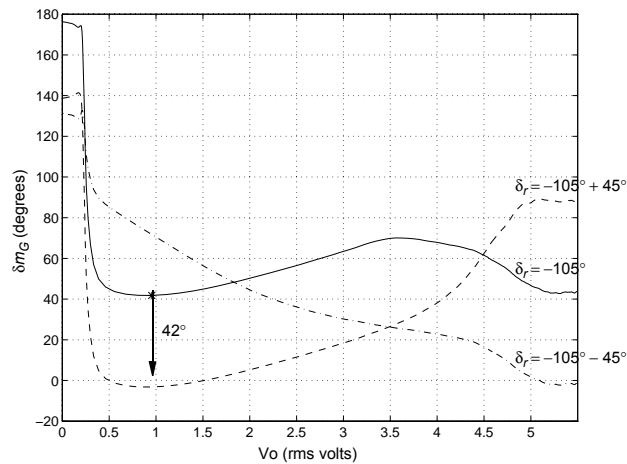
Figure 4.18: δm_G (RF phase margin) as a function of desired output for three different settings of phase adjuster. Regions below 0° indicate instability.

adjusted by −45° below optimum the instability now occurs near the saturation region of the transistor amplifier. Instability near the saturation region can also be predicted by equation 4.18 since the amplifier characteristics are shown to approach the stability boundary at saturation. This was checked experimentally and shown in figure 4.19. The top two traces are the baseband in-phase and quadrature components of the cartesian
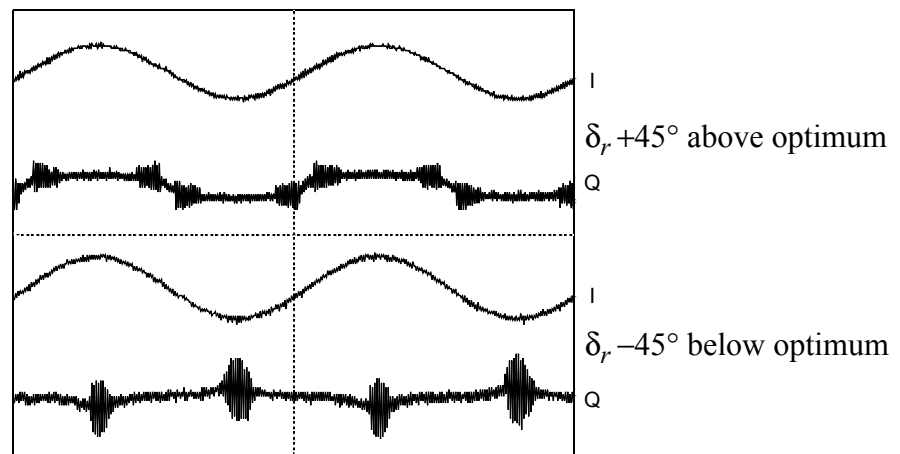
Figure 4.19: Measured confirmation of instability regions. Top two traces are in-phase and quadrature outputs (I and Q respectively) for higher than optimum phase adjustments. Bottom two traces are in-phase and quadrature outputs for lower than optimum phase adjustments. Q scales are ten times I scales. Oscillations are clearly seen on the more sensitive Q channels.

loop's demodulated feedback and hence represent the RF amplifier's output. These two traces demonstrate the first case when the RF adjuster is adjusted positive of the optimum and clearly show the burst-like instability which results as predicted in both figures 4.17 and 4.18. The bottom two traces were obtained with the phase adjuster set negative of optimum. In this instance the output is shown to saturate in an unstable manner - again as predicted in figures 4.17and 4.18.

4.7 TIME DOMAIN SIMULATIONS OF CARTESIAN FEEDBACK WITH NON-LINEAR AMPLIFIERS

The analysis performed in the previous section utilized a piecewise perturbation technique based around a series of setpoints. In this section a series of time domain simulations are presented to examine how the applied perturbations behave under different amplifier setpoint conditions.

The cartesian feedback simulation model is shown in figure 4.20. The bold lines indicate complex in-phase and quadrature signals. To examine the consequences of applying a perturbation, first a setpoint is applied to the input of the amplifier via V_{si}. This setpoint generates a corresponding output which is removed by V_{so}. Removing the setpoint "bias" at the output enables the effects of an applied perturbation to be easily observed. Furthermore, the input voltage V_i was set to zero so that the complex loop compensation given by $G(s)$ would not have to charge to some value, and hence this allowed quick

Figure 4.20: Block diagram of simulation model used in time-domain perturbation simulations (thick lines and bold font indicates complex quantities).

establishment of the desired setpoint.

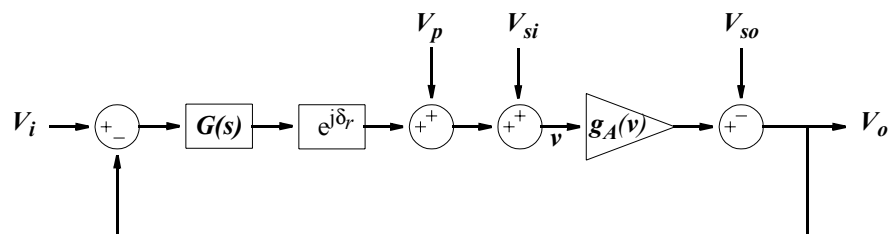A small complex perturbation on the amplitude was applied and added to the input amplitude via V_p. The function $g_A(v)$ represents the RF power amplifier and is essentially an implementation of equations 4.8 and 4.9 The low power BLU amplifier was used for the simulation model in this section. The phase adjuster (δ_r) models complex phase rotations needed to adjust out RF phase rotations of the amplifier. Since, from figure 4.15*(b)*, the average phase of the amplifier at the marked setpoint is 143° (2.50 radians), the central value of δ_r was set to −143° to compensate. Other conditions at the setpoint are $V_{si} = 0.83\angle{-30°}$, $V_{so} = 0.95\angle{113°}$ (same conditions to generate the curves of figure 4.14), and V_p, the perturbation signal was very small.

The non-linear amplifier characteristics result in two modes of operation occurring in cartesian feedback loops. The modes will be termed here as being spiral mode and stationary mode.

4.7.1 Spiral Mode

When the phase adjuster in figure 4.20 δ_r is made equal to 79° greater than the central value (i.e $\delta_r > 79°-143°$) the perturbation decays in a spiral manner given by figure 4.21*(a)*. This figure shows the real and imaginary component of the signal v given in figure 4.20 just after the system is hit with a small perturbation (V_p). The perturbation is visible by the dotted line emanating from the centre of the figure at 20°. Following the perturbation the loop provides an initial adjustment (the jump from the top of perturbation to this initial adjustment is not shown in the figure for clarity) which then decays spirally in a clockwise direction as given by the arrow. The reason for this spiral decay can be gathered from the perturbation angle dependent nature of the phase of the amplifier complex gain given in figure 4.14*(b)* and repeated here for convenience in figure 4.22.

The perturbation will be followed around the loop. Starting at a perturbation angle of 20°
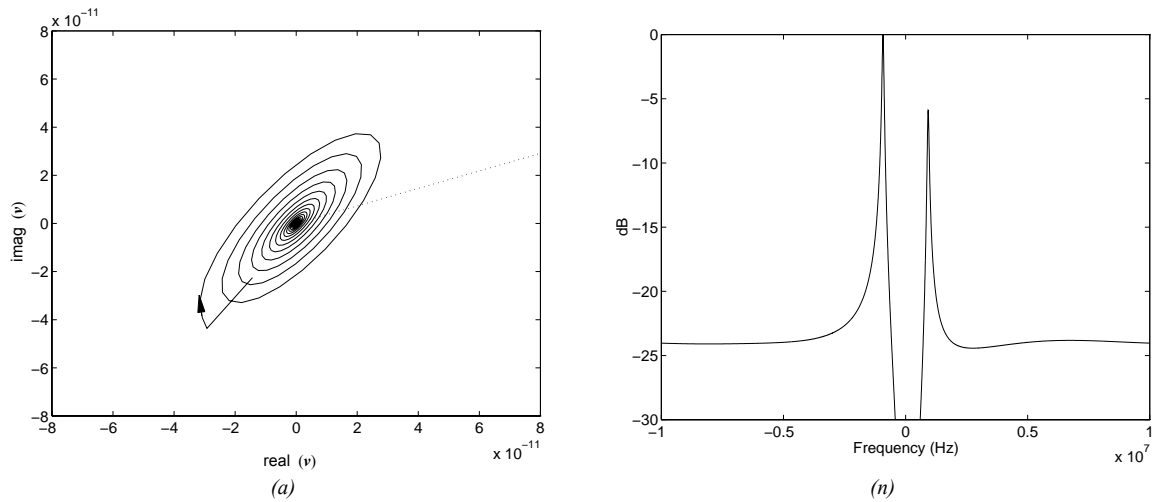
*Figure 4.21: Spiral mode perturbation decay. (a) **v** in the time domain and (b) in the frequency domain.*

gives the resultant phase rotation through the RF amplifier from the solid trace of figure 4.22 as 103°. Subsequent to the perturbation then, the RF phase of the output of the amplifier, $g_A(v)$ in figure 4.20 is given as 20° + 103° = 123°. Following the amplifier the signal undergoes a subtraction of V_{so} which completely cancels the amplified result of the bias signal V_{si}, V_{so} will not effect the phase (or the amplitude) of the perturbation at the amplifier output. Since V_i is 0, going around the loop of figure 4.20 simply inverts the signal as it arrives at the input of the compensation circuit $G(s)$. $G(s)$ is time dependent and does not introduce cross coupling between the real and imaginary axes. Although this
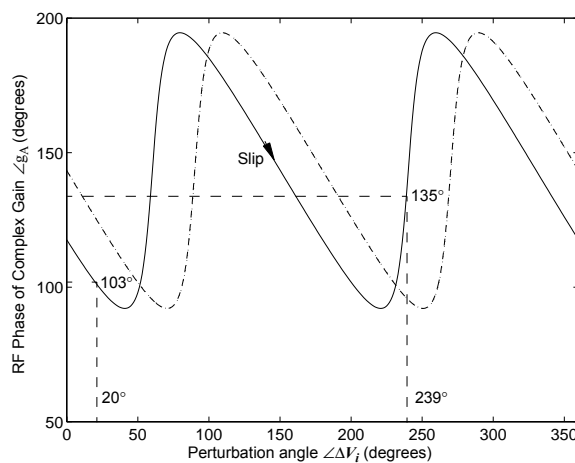
Figure 4.22: Phase of non-linear amplifier complex gain at one operating point for a sweeping perturbation (from figure 4.14(b)) used to demonstrate spiraling decay of perturbation.

time dependence will slow down the phase changes through the loop, for this exercise the effect of *G(s)* will be initially neglected (and so the figures quoted below do not directly relate to figure 4.21(*a*)). The RF phase (a complex rotation) of the signal is then assumed to be unmodified by the transfer function. δ_r is a complex phase rotation and so the RF phase at the correctly biased input of the amplifier is $123° - 180° - 143° + 79° = -121°$. Now with an input perturbation angle of $-121°$ ($239°$) the RF phase rotation through the amplifier from figure 4.22 is $135°$. The RF phase at the output of the amplifier is then $-121° + 135° = 14°$. Note, both the phase of the input of the amplifier ($20° \rightarrow -121°$) and the phase of the output of the amplifier ($123° \rightarrow 14°$) have followed phases which are changing clockwise i.e moving from positive phases to less positive phases. The output phase can again be followed around the loop in the same way and will yield yet another input perturbation which in turn will yield another RF output phase and so on. It is evident then that the complex phase of the loop will continuously slip along the response of figure 4.22.

With the introduction of the time dependence of *G(s)*, this slipping will be slowed, smoothed and made continuous (as shown in figure 4.21(*a*)). Ultimately the magnitude of the disturbing perturbation will dissipate by the action of stable closed loop feedback. In the process of the amplitude being corrected for, the phase will be continuously changing and so a spiralling decay results. Through a similar procedure it is possible to show that with the phase adjusted to be less than the central value i.e $<143°-79°$ the spiral will rotate in an anticlockwise direction.

Figure 4.21(*b*) is an FFT of the output and demonstrates the way in which a clockwise decaying spiral results in higher frequency components on the left hand side of the spectrum. Noise present in practical cartesian feedback systems causes an infinite number of random perturbations. It would be expected then that if the loop exhibits spiralling behaviour at most points on the amplifier characteristic then the adjustment of the phase adjuster δ_r will determine if and on what side of the output spectrum noise will tend to rise. The discussion above indicates that higher δ_r adjustments will result in clockwise

spiralling and hence increase the noise on the left side of the spectrum. Alternatively, lower δ_r adjustments will yield an increase in noise on the right side of the spectrum.

The authors of [61] have measured the effect of the phase adjuster setting on the output spectrum. They found that higher phase adjustments yielded increases in noise on the right side of the spectrum and vice-versa. This is opposite to what is expected from the discussion above. The difference is a result of definitions. In this work the phase adjuster (δ_r) is modelled in the forward path whereas in [61] the phase adjuster was placed in the feedback path.

In section 4.2.2, the difference between an RF phase rotation and a baseband phase shift was presented. Figure 4.9 given in that section, also agrees with the conclusions of the spiral mode simulations i.e that higher δ_r adjustments will increase the noise on the left side of the spectrum since the left side become less stable (and vice versa).

4.7.2 Stationary Mode

When the phase adjuster δ_r in figure 4.20 is made equal to 40° greater than the central phase the perturbation decays in a manner shown in figure 4.23(*a*). The perturbation is again visible by the line emanating from the centre of the figure at 20°.
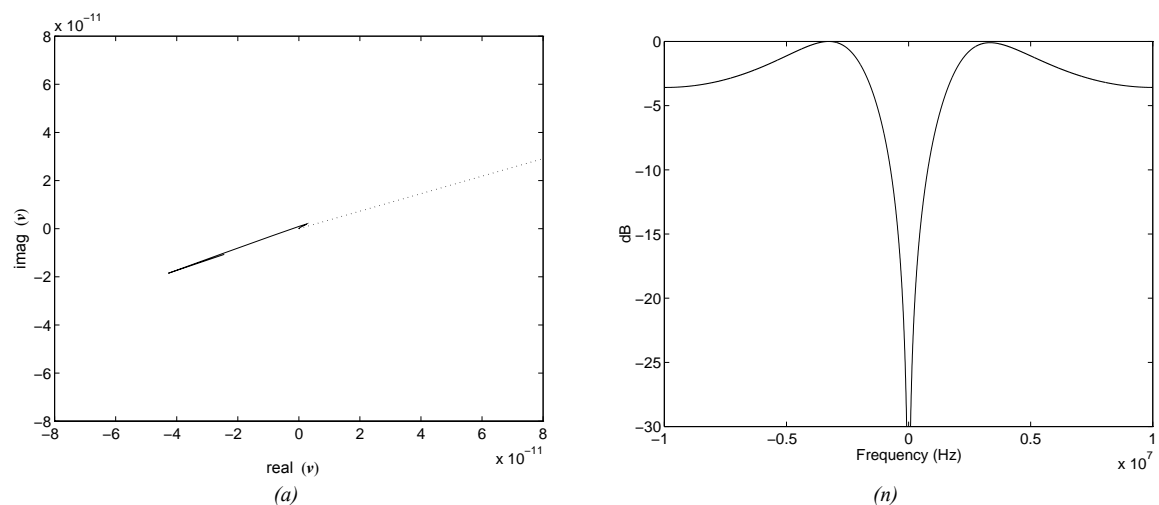
*Figure 4.23: Stationary mode perturbation decay. (a) **v** in the time domain and (b) in the frequency domain.*

The reason for this one dimensional decay can again be gathered from the perturbation angle dependent nature of the RF phase of the amplifier complex gain is again reproduced in figure 4.24. Starting at a perturbation angle of 20° gives the same resultant RF output phase as in section 4.7.1, i.e 20° + 103° = 123°. Following this phase around in the same way as in section 4.7.1 gives the RF phase at the correctly biased input of the amplifier as 123°− 180° −143° + 40° = −160°. Now with an input perturbation angle of −160° (200°) the RF phase through the amplifier (from figure 4.24) is 103° resulting in the RF phase at the output to be −57°. This phase can be followed around the loop in the same way giving −57°− 180°−143°+ 40° = −340° at the input of the amplifier. A perturbation phase of − 340° which is equivalent to 20° will continue the cycle and hence the system ends up toggling between two points on the characteristics of figure 4.24. These points ($\angle v = 20°$ or 200°) both have the same RF phase through the amplifier which from figure 4.24 is 103°. This phase is the opposite phase to that of the phase adjuster (i.e −(−143° + 40°)) so that the RF phase through the entire forward path is 0°. The amplifier is driven by the action of the loop in such a manner as to keep the RF phase through the amplifier fixed and opposite to that of the phase adjuster. It is clear from figure 4.24 that the same RF phase through the amplifier repeats at input perturbation phase intervals of 180°. Since this is the phase inversion which the RF output phase experiences as it passes around the feedback loop the systems decays in one fixed dimension.
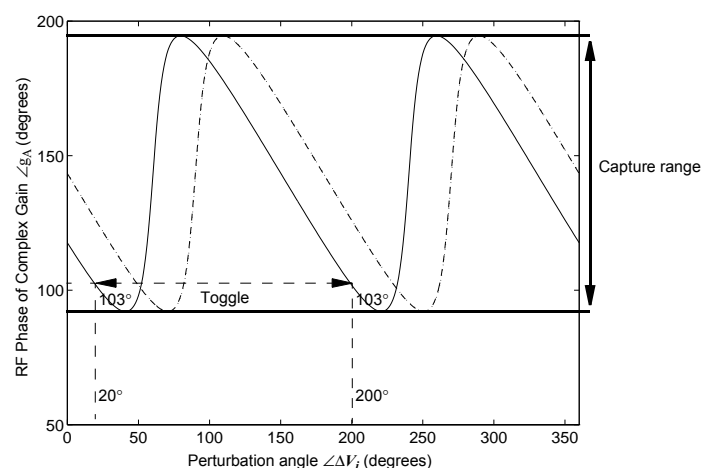
Figure 4.24: Phase of non-linear amplifier complex gain at one operating point for a sweeping perturbation (from figure 4.14(b)) used to demonstrate stationary decay of perturbation.

G(s) will slow down the establishment of the necessary conditions to provide the opposite phase described. The settings used in this section were chosen to enable quick establishment of this phase so that the phases quoted above could be easily presented.

This mode of operation has been termed stationary mode because the amplifier behaves as if it has one fixed RF phase rotation and also one fixed gain. It is possible then to model the amplifier under these conditions as one fixed or stationary complex gain which is dependent on the setting the phase adjuster. This however would not be practical and would not cover the spiral mode of operation.

The stationary mode of operation occurs whenever the adjustment of the phase adjuster is within the range of possible output phases. From figure 4.24 this range is $\pm 51°$ from the central phase. When the phase adjuster is set within this "capture" range the loop behaviour will be stationary with the amplifier being driven so that it complements the setting of the RF phase adjuster. Outside this range the loop behaviour will be spiral.

Figure 4.23(*b*) is an FFT of the output and demonstrates the way in which a one dimensional decay results in the frequency components to be essentially the same on either side of the spectrum.

4.7.3 Spiral and Stationary Modes on Graphical Stability Boundaries

In sections 4.7.1 and 4.7.2 the spiral and stationary modes of cartesian feedback operation were demonstrated. These modes can be clearly distinguished in figure 4.17. The stability boundaries where g_n does not equal one all have "horns". With $|\delta| < |\delta_b|$ (in between the horns) the system will behave in stationary mode and when $|\delta| > |\delta_b|$ the system will operate in spiral mode. This has been illustrated in figure 4.17 for $g_n = 2.84$.

The δ value at which the horns occur are the various δ_b angles for the g_n's shown. These δ_b values can be calculated by equation 4.68. The example presented in section 4.7.1 and

4.7.2 has a g_n value of 2.84 (as indicated by the asterisk of figure 4.17). With such a g_n, δ_b is equal to 51°. This δ_b angle is in fact the capture angle discussed in section 4.7.2.

When $g_n = 1$, $\delta_b = 0$, which implies the inner stability boundary has both horns at 0. It is possible to show that the operation of the loop when $g_n = 1$ is in spiral mode but these spirals are infinitely small and hence the system behaves as if the amplifier were in fact operating in stationary mode.

4.8 NOISE CONSIDERATIONS

Although stability is an important consideration, it has been found experimentally that systems with low stability margins exhibit increased levels of out-of-band noise.

The block diagram of 4.25(*a*) represents a complex noise model of a cartesian feedback system. The loop gain has been split into three components with appropriate noise sources. K_0 normalizes the closed loop gain to unity. K_1 represents gain prior to the loop compensation *G(s)* and the RF amplifier gain is represented by K_2. L_3 models the
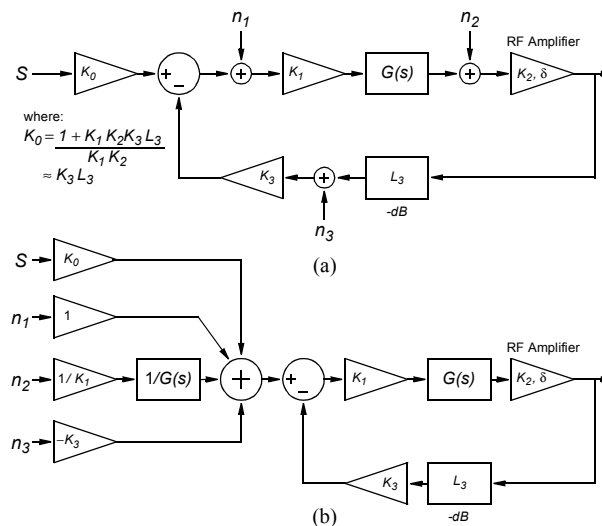
Figure 4.25: (a) Complex noise model of cartesian feedback loop showing distribution of loop gain and appropriate noise sources. (b) Rearranged complex noise model with noise referred to the input.

attenuation required to reduce RF feedback signals to levels appropriate for demodulation with the subsequent gain necessary represented by K_3.

This block diagram can be rearranged so that the noise can be referred back to the input (figure 4.25(*b*)). At some stage, all noise sources pass through the closed loop transfer function of the cartesian feedback loop. Setting the RF phase δ to zero, $g = 1$ and *G(s)* with $pm_G = 30°$ (DC gain, $K = 167.7$ (44.5dB), pole frequency = 126krad/sec (20kHz), & delay, $\tau = 50$ns) gives the magnitude response and phase response of figure 4.26. This response clearly demonstrates a peaking effect in the closed loop response for systems with low stability margins (e.g. $pm_G = 30°$)

Figure 4.27 shows two measured spectra of the experimental cartesian feedback system using the high power amplifier (TXPA45). The increase in out-of-band noise is visible as peaks in the noise floor (these peaks appear broader than the solid closed loop magnitude response of figure 4.26 because a linear frequency scale is used in figure 4.27). Cartesian feedback systems then, should be designed to be more than just stable. There must be sufficient stability margin to limit the peaking in the out-of-band noise spectrum to a reasonable level.

It is difficult to analyse how the peaking is affected exactly by changes in δ and g but it is
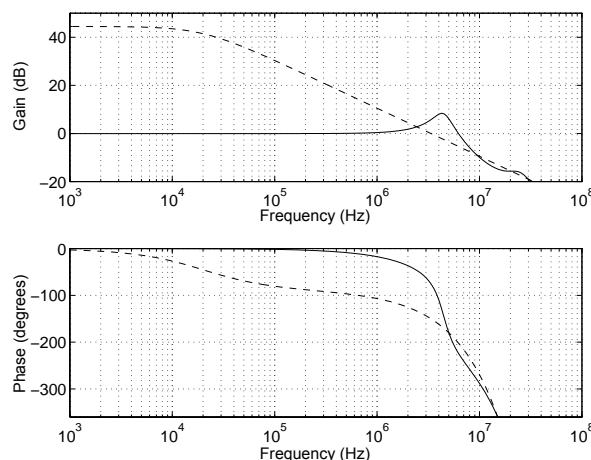
Figure 4.26: Open loop (dashed) and closed loop response of single pole system with delay. Amplitude peaking is evident in closed loop response.

```
ATTEN     20dB        VAVG    2
RL    10.0dBm              10dB/
```

```
CENTER      950.00MHz                 SPAN     20.00MHz
*RBW    30kHz           *VBW    300Hz        SWP     6.0sec
```
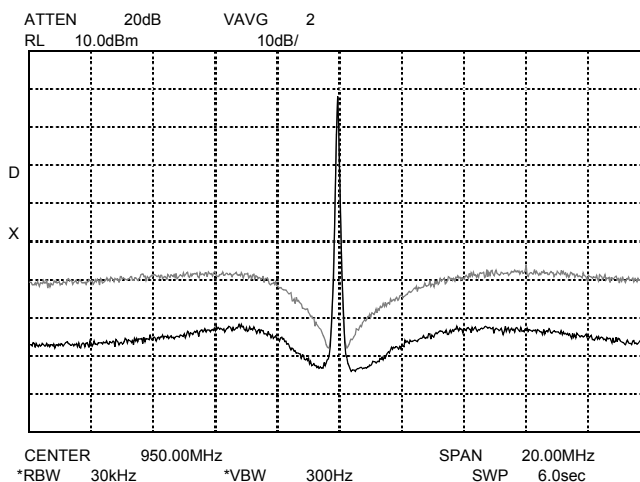
Figure 4.27: Measured wideband spectrum of a cartesian feedback transmitter. Lighter trace indicates filtering placed close to the subtraction point. Darker trace shows improved out-of-band noise performance with the loop filter further up the amplifier chain. Some peaking is also evident.

possible to determine how the peaking is affected by the selection of $G(s)$, with $\delta = 0°$ and $g = 1$. Under these conditions the closed loop transfer function is given by

$$T(s)\big|_{\substack{\delta\,=\,0° \\ g\,=\,1}} = \frac{G(s)}{1 + G(s)} = \frac{Kp\,e^{-\tau s}}{s + p + Kp\,e^{-\tau s}} \tag{4.80}$$

Now the peak of equation 4.80 occurs when the magnitude of the denominator approaches its minimum. Substituting $s = j\omega$ in the denominator gives

$$|(den.)|^2 = (p + Kp\cos(\omega\tau))^2 + (\omega - Kp\sin(\omega\tau))^2 \tag{4.81}$$

To find the condition for no peaking the derivative with frequency of equation 4.81 must be found and made greater than or equal to zero. Note, a rising closed loop response corresponds to a falling denominator.

$$\frac{d|(den.)|^2}{d\omega} = 2(\omega - \omega\tau Kp\cos(\omega\tau) - (\tau Kp^2 + Kp)\sin(\omega\tau)) \tag{4.82}$$

Rearranging the terms (by taking ω out and multiplying the last term by τ/τ) gives

$$\frac{d|(den.)|^2}{d\omega} = 2\omega\left[1 - \tau Kp\cos(\omega\tau) - (\tau^2 Kp^2 + \tau Kp)\frac{\sin(\omega\tau)}{\omega\tau}\right] \tag{4.83}$$

By inspection the part of the equation in square brackets has its minimum at $\omega = 0$. The

derivative is positive for all values of ω if it is positive as ω tends to 0 i.e:

$$\frac{d|(den.)|^2}{d\omega}\bigg|_{\omega \to 0} \geq 0 \tag{4.84}$$

When peaking occurs in the closed loop magnitude response (i.e |T(s)|) for a single pole system with delay, the response will always rise as the frequency is increased from zero i.e there will never be a dip between DC and the crest of the peak.

By setting equation 4.82 to be greater than or equal to zero for small ω, the no peaking condition will be satisfied

$$\omega - \omega\tau Kp + (\tau Kp^2 + Kp)\omega\tau \geq 0$$
$$\Rightarrow \tau Kp(\tau p + 2) \leq 1 \tag{4.85}$$

Now since τp is usually much less than 2 then the no-peaking condition can be satisfied by:

$$2Kp\tau \leq 1 \tag{4.86}$$

For a system with a pole location of 126krad/sec (20kHz) and a delay of 50ns, the non-peaking condition would exist if the loop gain is kept below 80 (38dB) giving an open loop phase margin pm_G of 61.9° and a gain margin of 9.92dB. This is clearly a limitation on the maximum possible distortion reduction of a cartesian feedback system. A small degree of peaking can however, be tolerated in which case the frequency at which the peak occurs can be found by setting the derivative of the denominator, as given by equation 4.82, to zero. The approximation $\omega \approx 0$ is no longer valid so the Newton-Raphson numerical method for equation solving is applied giving:

$$\omega_{n+1} = \omega_n - \frac{\tau Kp^2 \sin\omega_n\tau + Kp\sin\omega_n\tau + \omega_n\tau Kp\cos\omega_n\tau - \omega_n}{\tau^2 Kp^2 \cos\omega_n\tau + 2\tau Kp\cos\omega_n\tau - \omega_n\tau^2 Kp\sin\omega_n\tau - 1} \tag{4.87}$$

To find the position of the peak the initial selection of ω_n must be in the vicinity of the peak. This is easily achieved since it is known that the peak will be somewhere between the frequency at which the phase margin of *G(s)* is calculated and the frequency at which the gain margin of *G(s)* is calculated (as shown in figure 4.26). The frequency at which

the phase margin of *G(s)* is calculated, ω_{0dB}, is given in equation 4.39 and is approximately equal to *Kp* (with *g* = 1). Substituting *Kp* for ω_n in equation 4.87 gives a good first approximation and following a few iterations the frequency at which the peak occurs, ω_{pk} is obtained.

Back substitution into equation 4.80 will give the magnitude of the closed loop response at the peaking frequency. The peaking with respect to the closed loop DC gain is given by

$$
\begin{aligned}
M_{pk} &= \frac{|T(\omega)|\big|_{\omega = \omega_{pk}}}{|T(\omega)|\big|_{\omega = 0}} \\[2mm]
&= \frac{p + Kp}{\sqrt{(p + Kp\cos\omega_{pk}\tau)^2 + (\omega_{pk} - Kp\sin\omega_{pk}\tau)^2}}
\end{aligned}
\tag{4.88}
$$

For the system illustrated by figure 4.26, the peak frequency occurs at ω_{pk} = 26.95Mrad/s (4.29MHz), giving a relative peaking of M_{pk} = 2.65 (8.46dB).

It is possible to avoid the above computational effort if a rough estimate of the degree of peaking is acceptable. By definition the phase margin, pm_G, is obtained when the magnitude of the open loop response is equal to one. From equation 4.80 the amount of peaking at the phase margin frequency when the loop is closed is then

$$
\begin{aligned}
M_{pm} &= \frac{1\angle(pm_G - \pi)}{1 + 1\angle(pm_G - \pi)} \\[2mm]
&= \frac{1}{2\sin\dfrac{pm_G}{2}}
\end{aligned}
\tag{4.89}
$$

At the gain margin frequency the phase of the open loop transfer function is $-\pi$. The amount of relative peaking at the gain margin frequency is then

$$
M_{gm} = \left| \frac{-1/(gm_G)}{1 - 1/(gm_G)} \right|
\tag{4.90}
$$

where gm_G (the gain margin) is not in dB but in linear form.

The peaking can thus be approximately determined for the system plotted in figure 4.26

($pm_G = 30°$) giving, $M_{pm} = 1.93$ (5.72dB) and $M_{gm} = 2.02$ (6.09dB). The peaking will be greater than these factors (in this case 2-3dB), but the method still provides a reasonable qualitative estimate. Since the margins are naturally small when peaking occurs, the degree of peaking can also be qualitatively assessed by how close the amplifier characteristics are operating to the stability boundaries given in figures 4.11 and 4.17.

It is interesting to note that if distortion is present at the peaking frequency then it too will be increased along with the noise.

From a stability point of view the positioning of the filtering function *G(s)* is irrelevant. From the noise point of view however, the position of the filter can have a significant effect. When the noise sources are referred to the input as in figure 4.25(*b*) it is easy to compare the relative contribution of each noise source. At low frequencies, noise from the demodulator chain n_3 dominates since $1/G(s) \approx 1$. At higher frequencies $1/G(s)$ rises and consequently n_2 becomes the dominant noise source. For low in-band noise K_3 must be kept small (and hence L_3 is small), and for low out-of band noise K_1 must be large (i.e the compensation must be applied as far up the amplifier chain as possible making K_2 small). There are practical limitations which govern how small K_3 and K_2 can be made. K_2 represents the gain of the RF sections of the cartesian feedback loop. There must be some gain in these circuits to enable RF power amplification. As K_2 is lowered the drive signal into the Up-converting quadrature modulator is increased leading to the increased generation of intermodulation distortion. K_2 is therefore constrained by distortion considerations. Similar constraints exist on K_3. If the demodulated signals are too large, the down-converting quadrature demodulator will generate unacceptable levels of intermodulation distortion. Therefore K_3 and hence L_3 are also constrained by distortion considerations.

The darker trace (bottom trace) of figure 4.27 shows the improvement which can be achieved by moving the filtering away from the summation point whilst under the practical constraints described above. The lighter trace of figure 4.27 was a measurement

```
ATTEN       10dB        VAVG      10          MKR      -66.00dB
RL    0dBm                      10dB/              -10.0kHz
```
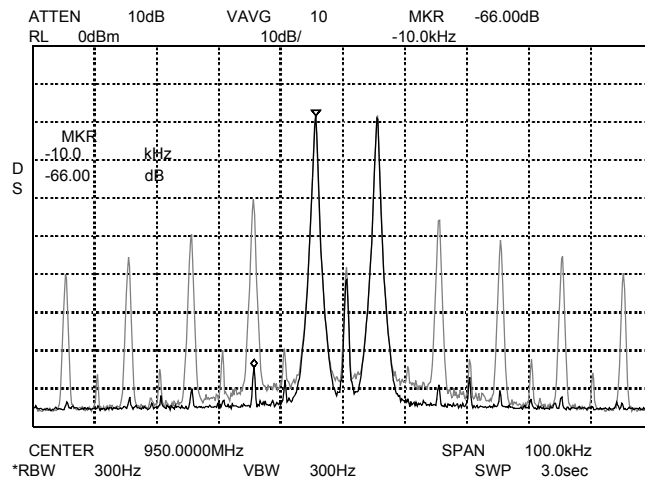
Figure 4.28

Figure 4.28: Measured narrowband spectrum of a cartesian feedback transmitter. Lighter trace indicates

unlinearized open-loop two-tone test. Darker trace shows linearized closed-loop response with worst case

taken with the filtering placed right after the summation point (the worst point for out of band noise). These experimental results demonstrate the advantage of placing the filter as far away as possible from the summation point. The darker trace of figure 4.28 is a zoomed-in plot of the darker trace of figure 4.27 showing the narrowband closed-loop performance of the linearized transmitter.

4.9 CONCLUSION

The piecewise MIMO analysis presented demonstrates how RF amplifier non-linearity, the RF phase adjuster setting, and loop gain effect the stability of the cartesian feedback loop. It was shown that when the amount of RF phase introduced by AM/PM distortion and by RF phase adjuster error equalled the original phase margin, instability resulted. The graphical technique developed from this fact, demonstrates the important mechanisms which influence stability and can be utilized at the design stage, or in the practical assessment of an experimental cartesian loop.

Non-linear amplifiers have complex gains which vary and hence cannot be represented by a series of fixed complex gains in a piecewise stability analysis. Instead an additional

parameter to the complex gain is needed to represent the effects of amplitude and phase non-linearities.

Placing the non-linear amplifier model developed into a MIMO model of a cartesian feedback loop, enabled a stability analysis to be made. The results from the analysis were presented in graphical form. The stability boundaries shown in this analysis gives an indication as to how stable a given RF amplifier will be when placed in a cartesian feedback loop. The curves derived from the simplified amplifier model (weak non-linearities) are shown to give a worst case stability boundary for the full comprehensive amplifier model. The simple graphical approach of section 4.3 is therefore a good design tool for cartesian feedback systems. The only amplifier parameters required by the model are the worst case gain (largest of the differential and absolute gain) and the amplifier phase rotation.

For the BLU98 low power amplifier used in the analysis suitable for non-linear amplifiers, it was found that: if the RF phase adjuster was adjusted above optimum, instability resulted just after the transistor turn-on region. When adjusted lower than optimum, the instability resulted at transistor saturation.

When placed in a feedback loop the perturbed behaviour of non-linear RF amplifiers display two forms of operation - Spiral mode and Stationary mode. When spiralling is in effect, the noise within the cartesian feedback loop will tend to cause the noise floor of the output spectrum to rise on one side depending on the direction of the spiralling. The direction of this spiralling is in turn dependent on the setting of the RF phase adjuster of the cartesian feedback loop. When the phase adjuster is in the forward path, phase adjustments lower than optimum, will cause the noise to rise on the right side of the output spectrum (anti-clockwise spiralling) and vice-versa. With the phase adjuster in the feedback path the reverse is true.

Loops with low stability margins were demonstrated to exhibit closed-loop peaking

which can effect the out of band noise performance of a cartesian feedback transmitter. The condition of no-peaking was derived (with $\delta = 0$) along with the degree of peaking resulting from a closed loop system with a single pole and a delay. In order to achieve a non-peaking condition the phase margin of the loop needs to be around 60°. This is a rather high margin since a first order system already forces the phase margin to be less 90°. This leaves less than 30° of phase shift, which can be easily consumed by RF amplifier AM/PM distortion and misadjustment of the RF phase adjuster. This highlights again that the RF amplifier needs to be rather linear for well behaved practical cartesian feedback loops. And such loops should have a means of adjusting the RF phase adjuster accurately and automatically. Alternatively a filtering at the output of the loop could be used but this would be impractical since it would need to have a tunable center frequency that could follow the carrier frequency.

It was also shown how the degree of peaking could be approximately obtained from the gain and phase margins. And finally it was also concluded and demonstrated that the loop compensation should be placed as far up the forward chain as possible in order to minimize the out-of-band noise floor.

5 DYNAMICALLY BIASED CARTESIAN FEEDBACK

The previous chapters have largely examined conventional cartesian feedback. In the last chapter two important system requirements for any linearization scheme were examined. These were stability and noise performance.

Another important issue concerning linearization system is power efficiency. In this chapter novel methods of improving the efficiency of cartesian feedback are presented and investigated.

First, linearization schemes are grouped into classes based on efficiency. Section 5.1 discusses linearization schemes which modify the power supply of the RF power amplifier being linearized and hence typically have high efficiency. Section 5.2 discusses linearization schemes which modify the drive to the RF power amplifier being linearized and which typically have good linearization performance. Cartesian feedback belongs to this class of linearization schemes.

Section 5.3 shows how using the techniques discussed in section 5.1, the efficiency of cartesian feedback can be improved whilst still maintaining good linearization performance. A new linearization scheme is presented which utilizes an RF power amplifier whose bias is varied to obtain good efficiency within a cartesian feedback loop.

This scheme is called Dynamically Biased Cartesian Feedback.

In order to modify the bias in line with higher efficiency, the RF amplifier must be extensively characterized. This too is given in section 5.3. These measurements were used first to determine the correct bias for a given output and also as a basis for a multidimensional amplifier model used in the simulations of section 5.4. The simulations provide both the ideal and more realistic assessments of the performance of dynamically biased cartesian feedback.

To efficiently alter the operating bias of a power amplifier, a switchmode power supply (SMPS) is required. The implementation of this supply is given in section 5.5. And once implemented, the dynamic bias concept was applied to the cartesian feedback loop described in the previous chapters. The results from this system are given in section 5.6

5.1 HIGH LEVEL MODULATION LINEARIZATION TECHNIQUES

The use of high level collector, drain or anode power supply modulation is widely used in AM transmitters. When combined with reasonably efficient high level power supply modulators, this technique can achieve good linearity and efficiency.

Kahn [48-49] extended high level modulation to linear modulation schemes by utilizing envelope elimination and restoration with SSB transmitters. Splitting the linear modulation into the polar components of amplitude and phase enables the phase component to be conventionally amplified by a high efficiency non-linear amplifier. The amplitude component is then applied to the power supply of this amplifier which high level modulates the RF output signal. The resultant linear amplifier retains the efficiency and linearity attributes associated with high-level modulation.

Feedback can be incorporated into the polar concept to provide an improvement in

linearity. The feedback can be applied to the amplitude only [50-53] or to both amplitude and phase. Amplitude only feedback is applicable to systems where the AM/PM distortion is low and generally is not suitable for amplifiers using BJT's. Full polar feedback can control AM/PM distortion and often uses a PLL (Phase-Locked-Loop) to facilitate phase feedback.

Although the polar loop has the potential for high efficiency, the amplitude and phase components of many linear modulations (in contrast with AM-only systems) have wide bandwidths as a result of the non-linear relationship between these components and the actual modulation (in I,Q form). This is demonstrated for a two-tone test in figure 5.1, where the amplitude and phase components are shown in both the time and frequency domains.

The polar loop components processing these polar signals must consequently be capable of accommodating the larger bandwidths. Failing to do so minimizes the linearization efficacy. The weakest link in regards to bandwidth is the high level power supply modulator. If it is to accommodate high bandwidth signals effectively and utilize
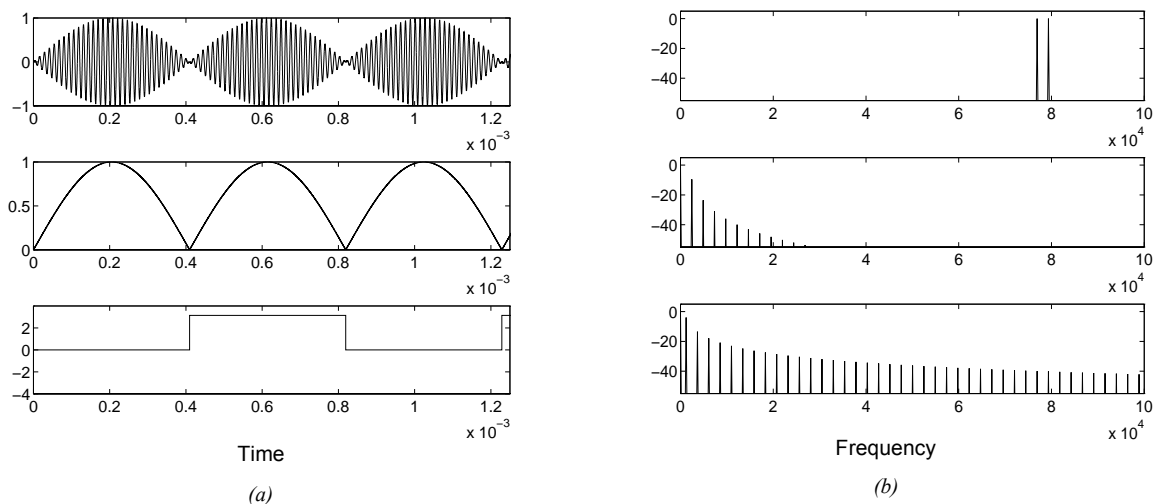

Figure 5.1: Demonstration of polar components for a two-tone test in (a) time domain and (b) frequency domain. RF signal given by top traces, amplitude component given by middle traces, and phase component given by bottom traces.

switched-mode techniques, the switching frequency must be made high. A high switching frequency however, results in greater switching losses and this in-turn imposes a limit on the bandwidth of the modulating signal. As will be shown, the dynamically biased linearization technique discussed here relaxes the need for the high level modulator to track the envelope exactly hence reducing switching frequency requirements.

5.2 RF DRIVE MODULATION LINEARIZATION TECHNIQUES

The source of excess power consumption in cartesian feedback[55-62] stems from the manner by which the desired RF envelope output level is achieved. This class of linearization scheme can only control the RF input of the power amplifier, it follows then that the desired RF output envelope is achieved by a change in the amplifier RF input drive level. Since in general, RF amplifiers operate more efficiently in saturation mode, any reduction in amplifier RF input drive level results in the amplifier not operating at its peak efficiency. This is especially true at low output levels in a given power control range. It is therefore advantageous to maintain the amplifier RF input drive at a level which achieves the highest power added or collector efficiency. With this constraint however, the necessary envelope level modulation must be obtained by other means. The means adopted here is by high level collector bias modulation used in addition to a cartesian linearization system. This combination gives the excellent spectral control and intermodulation distortion reduction of the cartesian linearization scheme coupled with the high efficiency of the high level collector bias modulation.

5.3 DYNAMICALLY BIASED LINEARIZATION

Dynamic bias defined in the context of this thesis, is a term used to indicate a dynamic variation in the RF amplifier bias operating point other than that caused by a change in the RF input drive. High level collector bias modulation is one way this bias operating point

can be varied dynamically (as in section 5.1). The bias operating point can also be dynamically modulated by varying the DC base bias. This is not to be confused with changing the RF input drive level discussed in section 5.2. Intuitively, one expects that a certain combination of collector and base bias will give higher efficiency if chosen correctly, for a desired output level.

Figure 5.2 (reproduced from figure 2.28) is a drawing of the dynamic bias concept applied with cartesian feedback linearization. The circuits below the dashed box represents a standard cartesian feedback loop as described in the previous chapters.

The dashed box shows the dynamic bias components which select the desired high efficiency operating point. First the quadrature input signals are applied to an envelope determining circuit. This circuit essentially determines the envelope R from the I and Q inputs (i.e. $R = \sqrt{I_{in}^2 + Q_{in}^2}$). The way by which R can be obtained may range from a DSP circuit where R is determined via calculation or look-up table, to an analog computing circuit or even detection of the RF envelope.
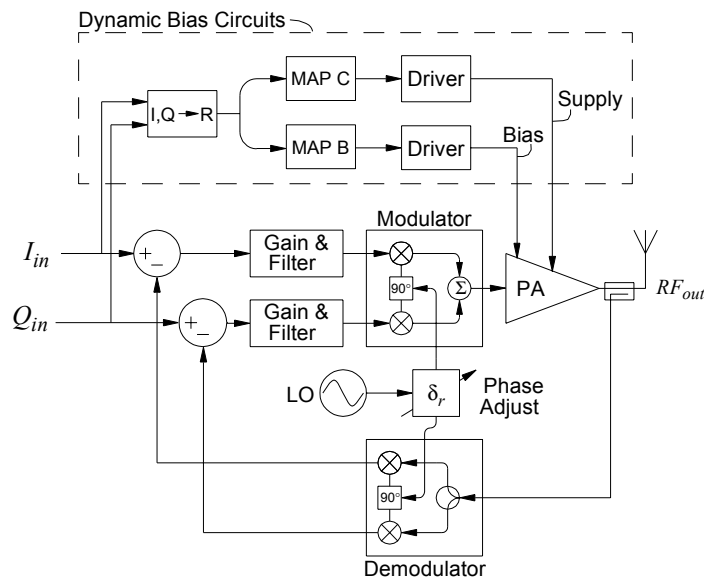

Figure 5.2: Dynamically biased cartesian feedback transmitter.

Once the *R* signal is obtained it is modified by the two functions shown as MAP C (for collector) and MAP B (for base) in figure 5.2. These functions select the optimum RF amplifier power supply voltage and DC base bias voltage for the desired RF envelope output level.

These mapping functions were obtained by the following means: The RF power amplifier was connected to the measurement apparatus which measured RF input level, RF output (amplitude and phase) and power supply current consumption as shown in figure 3.3. Since the power supply voltage was known, in addition to the RF parameters, power added and collector efficiency could be determined. To obtain comprehensive characteristics of the RF amplifier for use in the simulations of section 5.4, the following parameters were swept: RF input drive level, DC power supply voltage (*Vcc*) and DC bias voltage (*Vbe*).

The results of one sweep with *Vbe* = 0V is shown in figure 5.3 Note the results taken actually consist of a number of these curves with different *Vbe* voltages. The mesh giving the amplitude characteristics (figure 5.3*(a)*) shows how high level modulation on the collector, with a fixed drive, can alter the desired output. This relationship is essentially linear provided the drive level is sufficient (e.g V_{in} = 2.5Vrms). Figure 5.3*(a)* also shows how RF drive modulation can effect the output whilst the collector bias is fixed but requires some means of precorrected drive to achieve a linear output (such as those given by the predistorted drive voltages shown in chapter 3). This is the characteristic conventional cartesian feedback attempts to linearize. Figure 5.3*(b)* is the corresponding phase characteristic of the amplifier. Some phase distortion is still present, whenever high level collector bias modulation is applied.

A computer program was utilized to process the data such that optimum collector and base voltages (for maximum efficiency) were generated as a function of the desired output. The use of the desired output is necessary since the cartesian feedback loop alters the RF amplifier drive input to keep the amplifier output equivalent to the system input.
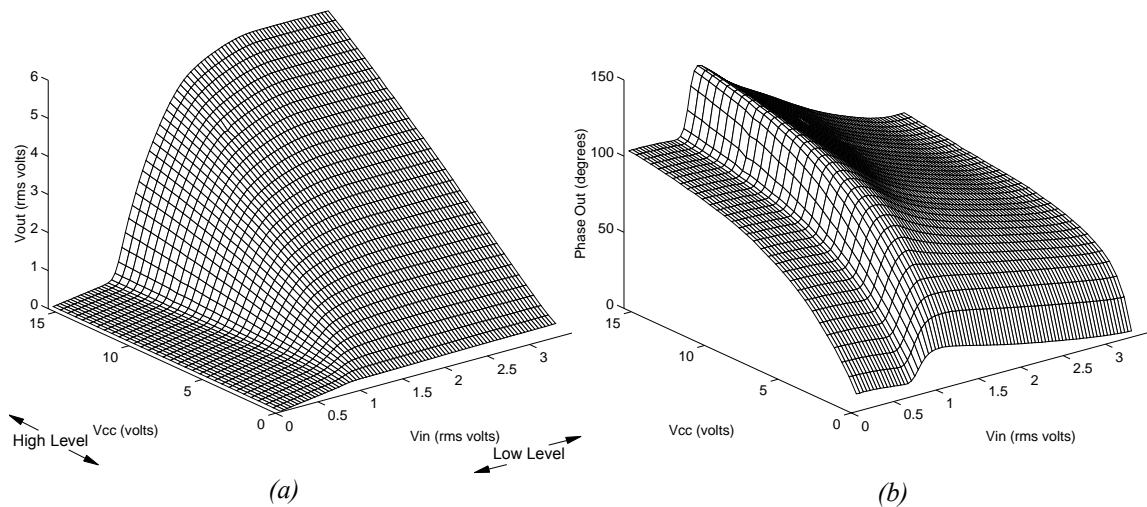
Figure 5.3: Amplifier characteristics with vbe = 0 volts. (a) amplitude response, (b) phase response.

Making the assumption that the system input is approximately equal to the amplifier output, allows the maps to be driven from the magnitude of the system input (R) even though they were determined from the output

The result of the data processing is shown in figures 5.4-5.5. Figure 5.4 shows the optimum (for the best collector efficiency, η_{coll}) collector bias voltage of the BLU98 low power RF amplifier with the base voltage fixed to zero volts. Figure 5.5 gives the optimum collector (figure 5.5*(a)*) and base bias voltages (figure 5.5*(b)*) when both are dynamically varied. The straight-line approximation given by these graphs form the basis

Figure 5.4: Optimum collector voltage for maximum collector efficiency (Vbe=0V).
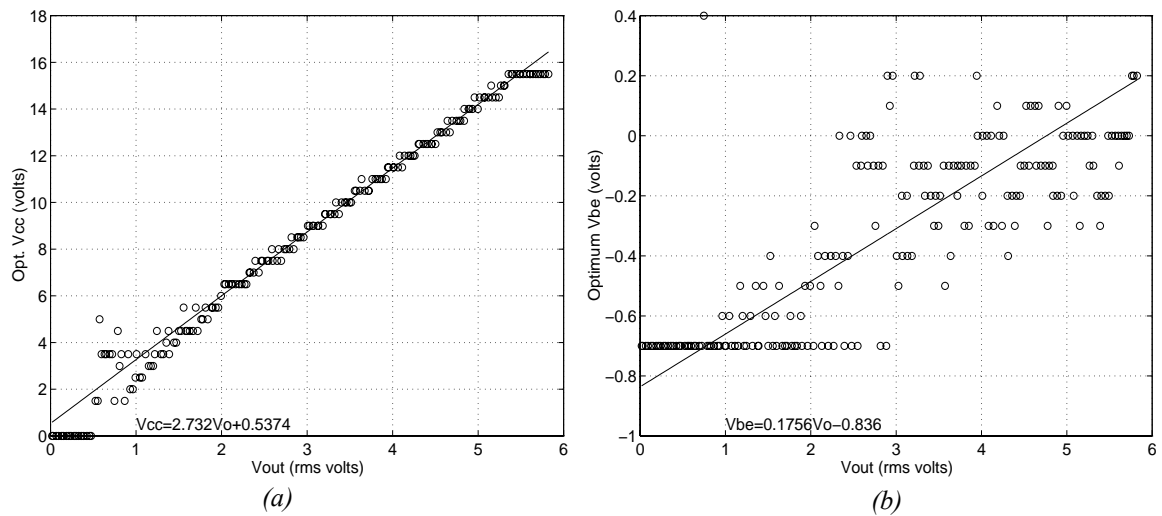
Figure 5.5: (a) Optimum collector and (b) base (i.e Vbe = variable) voltages for maximum collector efficiency.

of the maps C and B. The actual straight line approximation equation is given in each of the figures.These equations will be used in subsequent sections to compare performance when collector or power added efficiency is maximized. The circular dots are the actual measurement data showing the measurement uncertainty and "bin" nature of the data/function reversing process. Similar additional functions could be generated for maximum power added efficiency (η_{add})[73] (figures 5.6-5.7). This would be applicable if the driver stage to the amplifier being linearized was not operated in class A.

Some interesting amplifier features are demonstrated from the mapping functions. Figure 5.4 clearly shows that optimum collector efficiency is obtained when the collector voltage is proportional to the desired output voltage. This is a somewhat expected result since the RF output load impedance is constant. The combination of dynamically biasing the collector voltage with *Vbe* = 0 was also implemented and measured, and is presented in section 5.6.

Figure 5.5(*a*) also shows the same relationship for the collector voltage as described above. Figure 5.5(*b*) shows that *Vbe* should be reduced as the desired output is reduced.

This is because low desired RF outputs can be obtained with very little transistor gain when the RF drive power is sufficient (as provided by a fixed power consuming class A driver for example). And since collector efficiency does not consider the RF input power, the data reversing functions naturally ignore RF input power and allow this low gain - high drive operation. At higher desired RF output levels however, the drive power is not sufficient and some gain is required to achieve the output objective. The extra gain is provided by extra base bias.

Figure 5.6 also shows the increasing collector voltage for increasing outputs to some extent. Except at low RF outputs the relationship is weak as indicated by the spread in the points. This is caused by leakage through the RF transistor at low RF levels and is almost independent of the collector voltage as the transistor is not biased on ($Vbe = 0$).

Figure 5.7(a) again also shows the increasing collector voltage for increasing output. Compared to figure 5.6, the relationship is stronger at low level due to appropriate application of base bias voltages (figure 5.7(b)). As the desired RF output is increased, less base bias is introduced. This has the effect of effectively gradually swapping the DC power injected into the transistor for RF power injected into the amplifier input. In combination with increasing collector voltage, this swapping tends to linearize the transistor transfer function and stabilize its gain over the desired RF output range (see
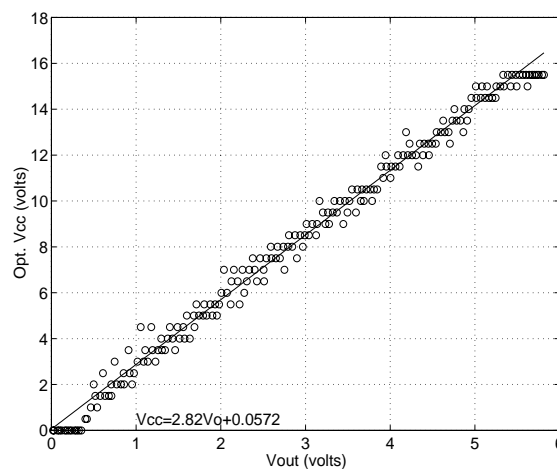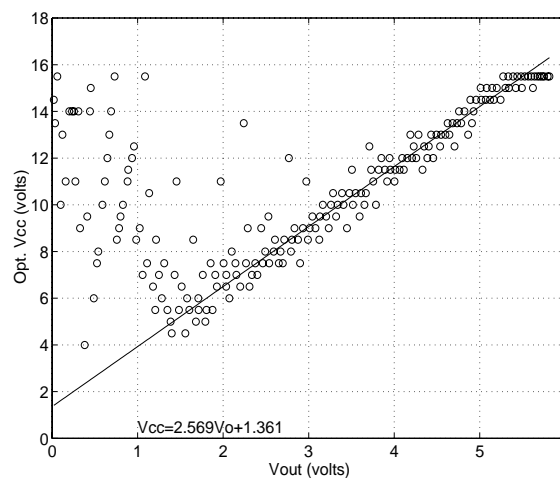

Figure 5.6: Optimum collector voltage for maximum power added efficiency (Vbe=0V).
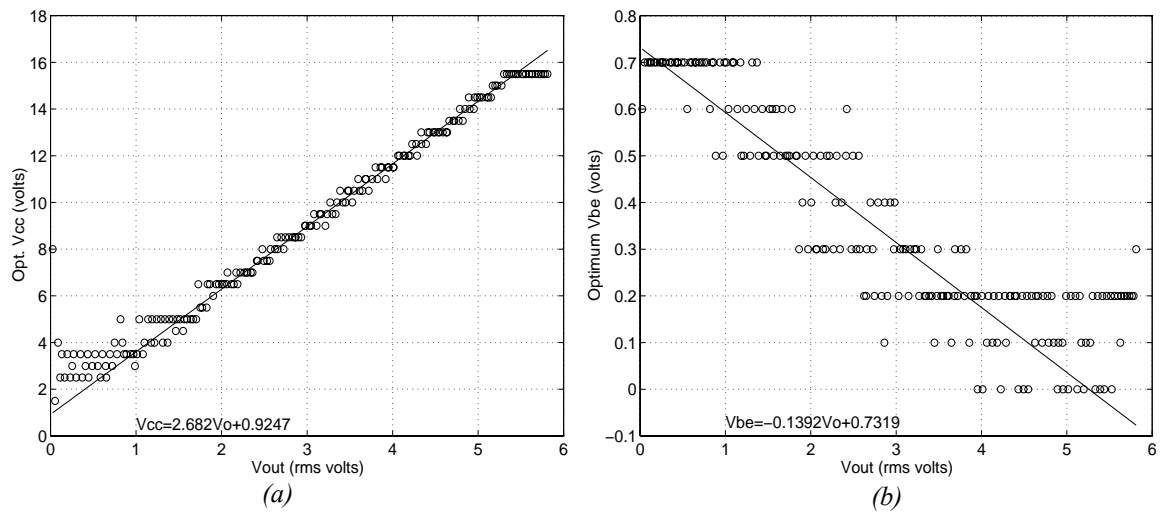
Figure 5.7: (a) Optimum collector and (b) base (i.e Vbe = variable) voltages for maximum power added efficiency.

figure 5.10(*b*)).

In section 5.4, simulations will be presented based on the function provided by figure 5.4. This is performed to compare with an experimental system utilizing the same function (presented in section 5.6), and to determine the efficiency improvement possible using 2-tone test signals. The functions provided by figure 5.7 will also be presented in simulation to further examine the linearization and efficiency improvements driving the base can provide.

Referring back to figure 5.2, the resultant signals from the MAP B and MAP C functions are applied to the RF power amplifier by power supply drivers. The driver discussed in this thesis which was used for the high level collector bias modulation utilized a switched mode power supply in a "buck" configuration (see figure 5.11 & appendix B). Other power supply techniques such as resonant, semi-resonant, or multi-resonant supply converters, or Class D modulators could also have been suitable.

It will be shown in the next sections that improvements in efficiency are achieved as a result of the novel combination of high level collector bias modulation and cartesian feedback. Additional improvements to linearization efficacy will also be shown when the

base bias is also dynamically varied resulting in a system which has high efficiency and high linearity.

The improvements in efficiency obtained with this system result from the dynamic bias circuitry selecting the best operating bias for a given output signal and the cartesian feedback adjusting the RF drive predistortion to the amplifier to achieve exact linearization. This is in contrast to conventional polar feedback techniques which utilize high level amplitude modulation in an effort to achieve both high efficiency and some degree of linearization performance. To achieve reasonable linearization performance, the SMPS in polar feedback must switch at a high frequency to enable it to accurately track the desired high level collector bias modulation function.

With dynamically biased cartesian feedback however, the SMPS does not have to be perfectly accurate and hence some error is allowed on the high level collector bias modulation. This implies the SMPS can be allowed to switch at lower frequencies hence reducing switching losses. The inband switching artifacts are removed by the action of cartesian feedback, provided the collector voltage is higher than the minimum collector voltage required for a given output level. The cartesian feedback loop can hence pull back the RF drive level slightly to achieve the exact desired output.

5.3.1 Transistor Amplifier Gain Variations with Dynamic Bias

The main disadvantage with changing the bias of a BJT based power amplifier is the gain reduction when the collector and base voltages are lowered. Figure 5.8 shows a block diagram used to calculate the differential and absolute gain of the RF power amplifier whilst it is operated within a dynamically biased cartesian feedback loop. The absolute and differential gain of the low power amplifier is given in figure 5.9 when the bias generating functions for maximum efficiency are used (from figures 5.4-5.5). Amplifier gain is important to assess. At low levels for example, the cartesian feedback loop is
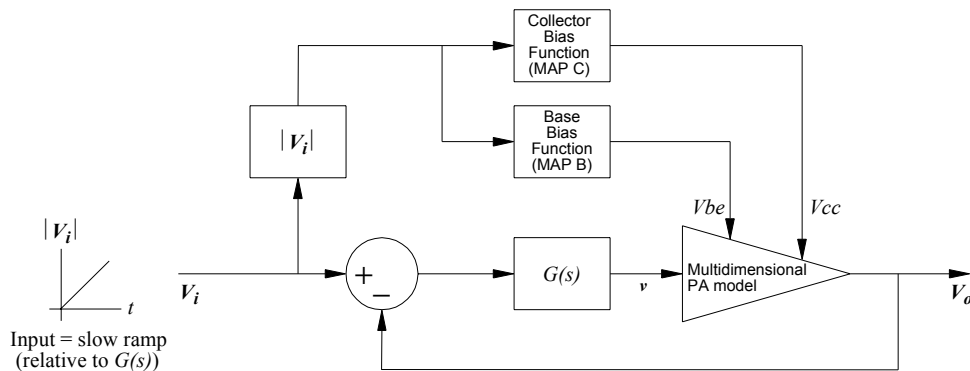
Figure 5.8: Model used to determine RF amplifier gain within a dynamically biased cartesian feedback loop.

shown to operate with a smaller gain and hence will not be able to linearize as effectively. While at high levels instability may result. One mitigating factor however is that generally speaking IM distortion reduces at lower output levels. The dynamically biased cartesian feedback loop should therefore be designed for stability at high levels.

If the power added efficiency is maximized when generating the bias driving functions, the gain of the amplifier is more constant as shown in figure 5.10. The flattening of the two gains as a function of output level hence indicates an improvement in linearity.

(a)   *(b)*
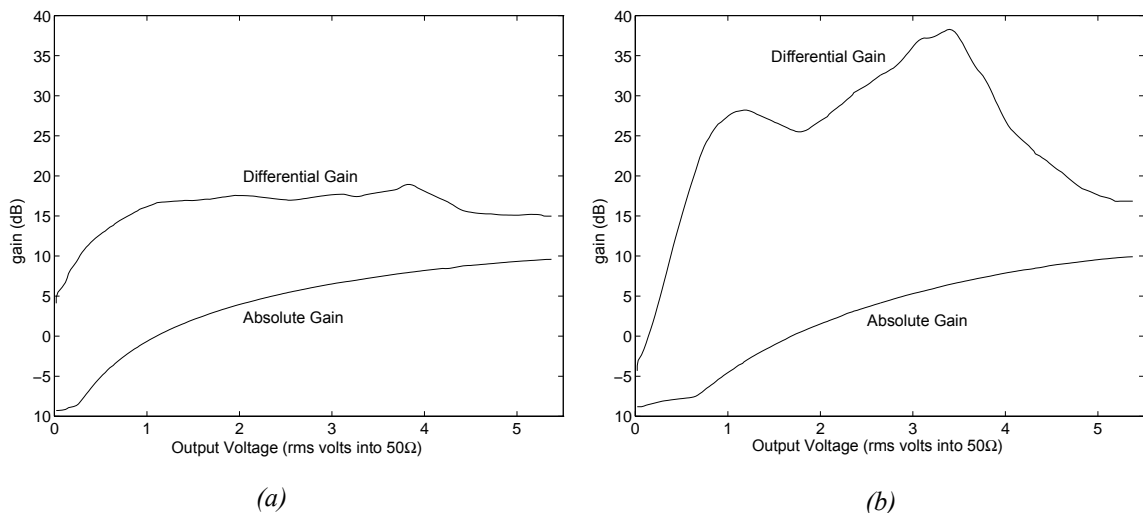
Figure 5.9: Differential and absolute gain as output is varied with (a) vbe=0 (b) vbe=variable, for maximum collector efficiency.

(a)   *(b)*
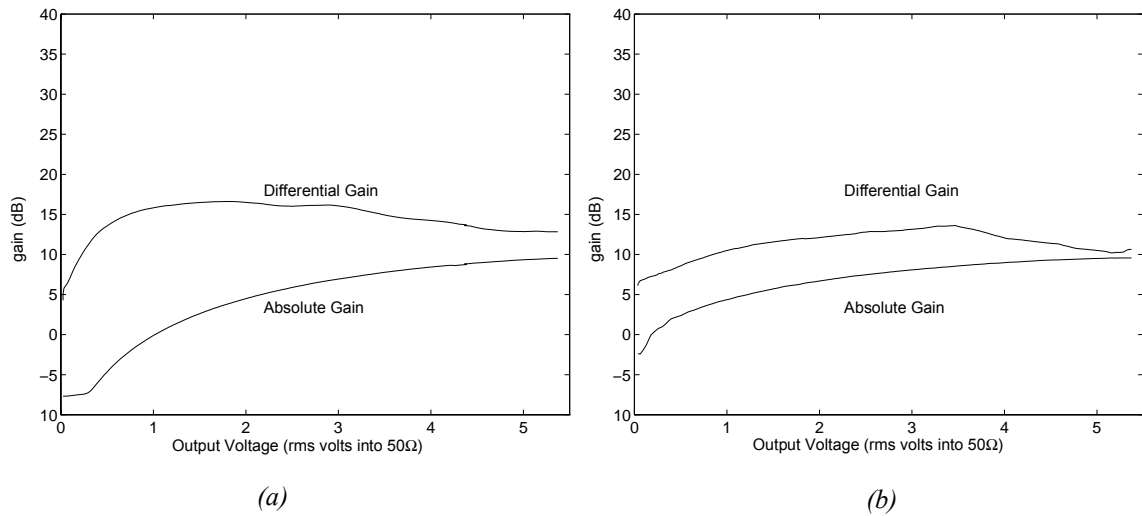
Figure 5.10: Differential and absolute gain as output is varied with (a) vbe=0 (b) vbe=variable, for maximum power added efficiency.

5.3.2 Stability and Dynamic Bias

The stability analysis presented in the previous chapter considered only fixed *Vbe* and *Vcc* bias. Under these conditions only one amplifier curve is generated for the graphical stability analysis.

Under dynamic bias conditions however a number of amplifier curves are generated. This is due to the fact that the RF input drive into the amplifier (provided by the cartesian feedback loop) is independent of the dynamically applied bias voltages (provided as a function of the input signal). Furthermore the application of the dynamic bias is not instantaneous but time dependent. To analyze stability therefore requires that the curves (which have to be determined) be all placed on the graphically stability analysis approach.

If one assumes however that the dynamic bias is applied instantaneously and accurately, then the input drive to the amplifier can be predicted and will also be unique. This would therefore yield one amplifier curve and hence the stability analysis can be performed as presented in the previous chapter.
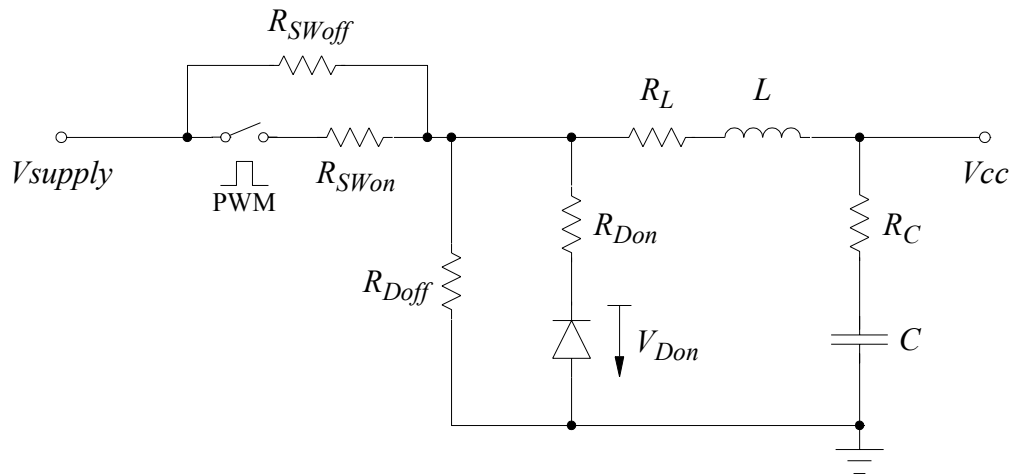
Figure 5.11: Buck convertor circuit used in simulations.

5.4 SIMULATION RESULTS

Simulation of the dynamically biased cartesian feedback loop (figure 5.2) required the addition of a SMPS to the earlier cartesian feedback loop simulations. This was performed in a brute force time domain fashion using appropriate difference equations for a given SMPS state. A linear driver was used to drive the base voltage of the BJT amplifier and was assumed to be lossless.

The simulation of the switched-mode driver was performed in accordance with the diagram shown in figure 5.11. This circuit is commonly referred to as a "buck" converter and enables step-down conversion. Regulation is achieved by controlling the switch with a Pulse Width Modulated (PWM) waveform. This simulation utilizes a conventional free-wheeling diode to maintain inductor current flow when the active switch is off. The diode voltage drop and various resistive losses are also shown in the diagram. The values used for the SMPS simulation are given below:

Switch:	R_{SWon}	0.5Ω	R_{SWoff}	400kΩ	T_{on}/T_{off}	60ns
Diode:	R_{Don}	0.2Ω	R_{Doff}	100kΩ	V_{Don}	0.5V
Ind.:	R_L	0.046Ω	L	100μH		
Cap.:	R_C	0.003Ω	C	220nF		

The simulation model of the switched-mode driver is designed to model the dynamic nature of the circuit as it tracks a desired output voltage. Most of the losses associated with the SMPS are included except for the quiescent DC power of the drive and feedback circuits. The results therefore provide an indication of real performance especially since a well characterized power amplifier is used as the SMPS load.

The control of the switch was by way of free-running feedback and hysteresis. The dynamic components were simulated by difference equations. The difference equations used to model the reactive components of the buck circuit were arranged to be functions of demanded output current (see Appendix A). With the components shown the highest switching frequency was 150kHz.

Using the functions developed from figures 5.4-5.7 it is possible to generate numerous simulations each examining different dynamic bias functions. The number of simulations is further increased if the ideal situation of applying dynamic bias is compared with the real application of the high level collector bias modulation by a SMPS. Some of the simulated advantages of dynamically biased cartesian linearization are demonstrated in figures 5.13 and 5.14 for a two-tone test with an average output power in dBm. The intention with all of these curves is to compare the performance of two different dynamic bias systems with conventional cartesian feedback under static power supply conditions. Note the term "static" refers to the fact that the supply is fixed for a certain output power (as is often used in conventional power control). With dynamic bias some attempt to track the RF envelope dynamically is made. As expected this generally results in an improvement in efficiency.

Figure 5.12 defines schematically the various simulations performed and presented in figures 5.13 and 5.14. The solid line of figure 5.13(*a*) shows the collector efficiency of conventional cartesian feedback with a fixed collector supply (figure 5.12(*a*)) and is useful as a control trace for the comparison. Since the supply voltage is fixed at 13V, efficiency falls as the output power is reduced (backed-off). Efficiency falls at the top end

when saturation is reached and the loop tries to maintain an unsaturated output.

The dot dashed trace of figure 5.13(*a*) gives the collector efficiency with *Vbe* = 0 when the best static collector bias is applied to the amplifier ideally without SMPS dynamics (filtering and switching effects) or losses (figure 5.12(*b*)). This is the ideal version of the conventional power control technique described earlier. Since this curve does not include any power supply losses it represents the best possible performance static collector bias can achieve. As shown, collector efficiency improves as the power is reduced since the power amplifier no-longer has to drop the entire supply voltage at these low power levels.

(a) Conventional fixed supply cartesian feedback.

(b) Ideal best static bias as used in conventional power control optimized for maximum collector efficiency (upper equations from figure 5.4), and maximum power added efficiency (lower equations from figure 5.7).

(c) Real best static bias which includes the dynamics (filtering and switching effects) and losses of the SMPS. Equation for maximum collector efficiency given.

(d) Ideal dynamic bias with dynamics of SMPS modeled, and real dynamic bias with losses of the SMPS also modeled. Dynamic bias functions optimized for maximum collector efficiency (upper equations from figure 5.4), and maximum power added efficiency (lower equations from figure
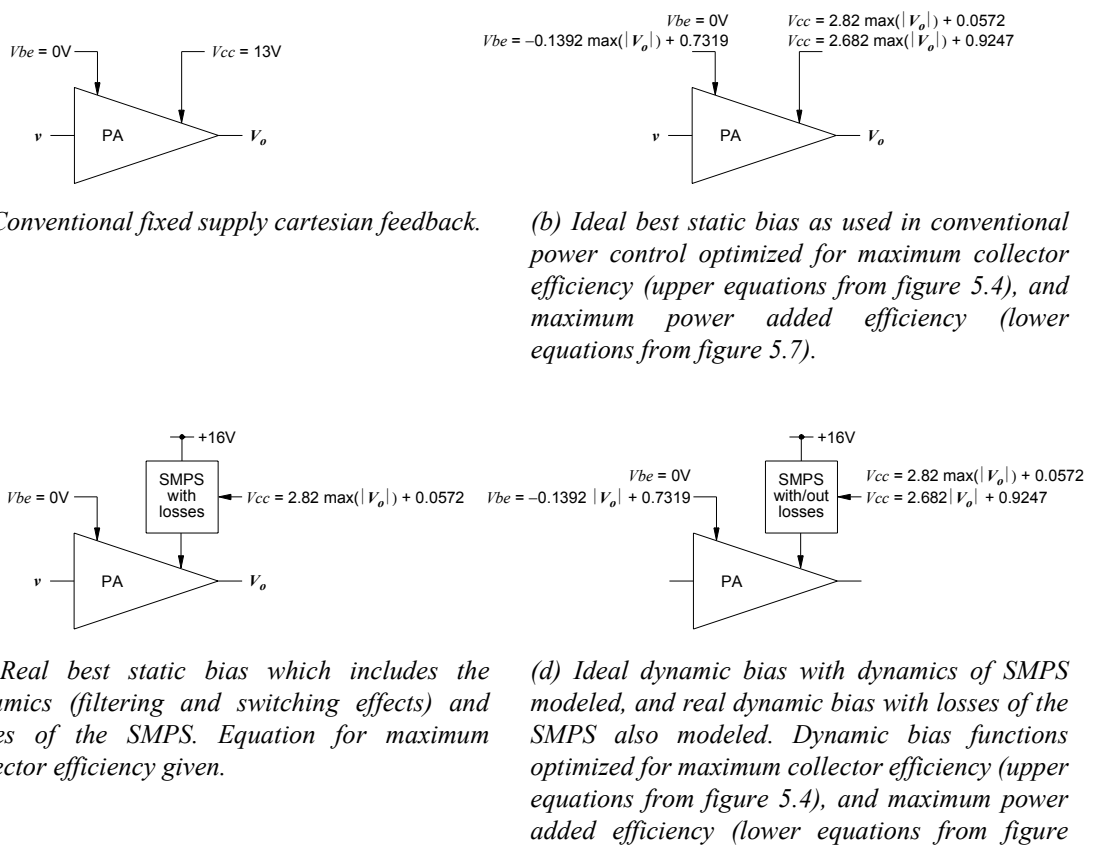
Figure 5.12: Simulation conditions for: (a) Conventional cartesian feedback, (b) Ideal best static bias, (c) Real best static bias, and (d) Real dynamic bias. v is the RF drive, V_o is the amplifier output, $|V_o|$ is the signal envelope, and $\mathrm{max}(|V_o|)$ gives the peak signal envelope.

(a) *(b)*
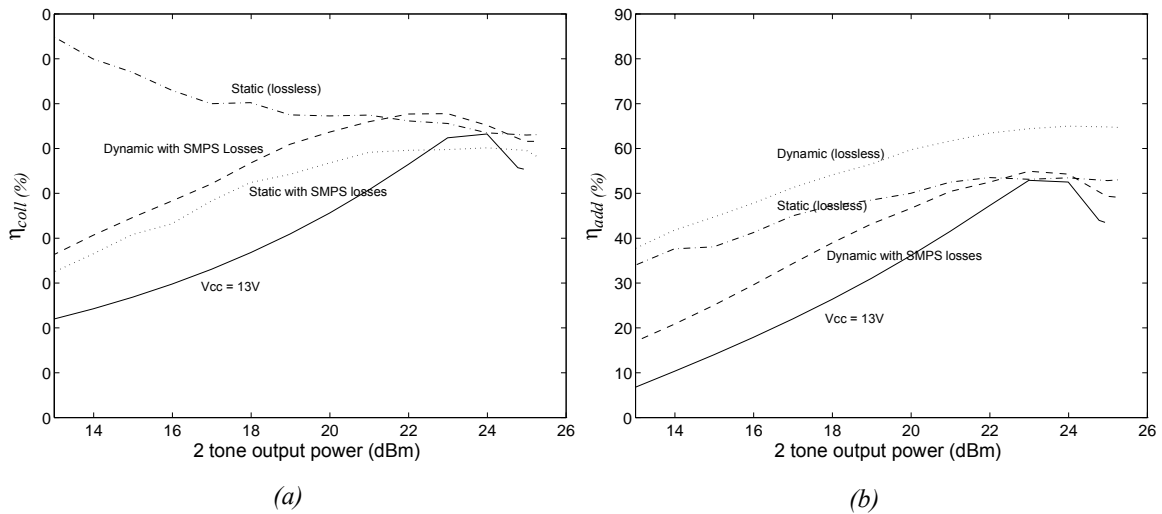
Figure 5.13: Improvement in efficiency with dynamic bias for (a) maximum collector efficiency with Vbe=0 and (b) maximum power added efficiency. Simulation conditions are defined in figure 5.12.

Adding the simulated SMPS dynamics and losses gives the dotted trace of figure 5.13(*a*), i.e. real best static bias (figure 5.12(*c*)). Here the simulation gives an expected degradation in collector efficiency at higher power levels (compared with conventional fixed supply) but improves as the output power is reduced. This is expected since at low outputs the gains in collector efficiency are higher and hence offset the SMPS losses to a greater extent.

Adding the dynamic collector bias function optimized for maximum collector efficiency with *Vbe* = 0V (figure 5.12(*d*)) gives the dashed trace of figure 5.13(*a*) (i.e real dynamic bias). Since tracking the envelope gives a greater improvement in the collector efficiency than conventional power control, the SMPS losses experienced by conventional power control are offset at all power levels. The simulations predict an improvement in collector efficiency at the power levels shown when high level dynamic collector bias modulation is applied to cartesian feedback.

Figure 5.13(*b*) gives the similar results for power added efficiency except *Vbe* is now variable as obtained from figure 5.7. As in figure 5.13(*a*) the standard cartesian feedback

loop (figure 5.12(*a*)) results are given by the solid trace as a comparison reference.

The dot-dash trace of figure 5.13(*b*), ideal best static bias (figure 5.12(*b*)), gives the results of ideally applying (i.e no SMPS) the optimum fixed bias voltage for a particular output power. This approach shows again a potential for a marked improvement in efficiency especially at low output levels for this type of power control. With SMPS losses however this improvement is expected to degrade at higher output powers.

The dotted trace of figure 5.13(*b*), ideal dynamic bias (figure 5.12(*d*), without SMPS losses), gives the results of tracking the envelope of the desired output and applying the appropriate bias dynamically under the restriction of the buck convertor filtering function. This result shows again dynamic bias has the potential to improve the power added efficiency above that given by static bias control.

The dashed trace of figure 5.13(*b*), real dynamic bias (figure 5.12(d) with SMPS losses), shows the result of introducing the SMPS losses into the simulation. With the losses simulated, an improvement in efficiency is predicted across all power levels. The SMPS losses reduces efficiency by 12%-20% and indicates there is a potential for even higher efficiencies with better SMPS techniques.

Figure 5.14 gives the linearization effectiveness of dynamic bias by plotting worst-case intermodulation distortion product (IMW) versus two-tone output power. The linearization effectiveness with different bias conditions are compared with the unlinearized open loop performance of the power amplifier (dotted trace). The open loop intermodulation performance actually improves relative to the carrier level as the output power is raised. If the amplifier was driven even harder, then saturation would have eventually occurred resulting in an increase in distortion. This intermodulation distortion behaviour is characteristic of bipolar transistor power amplifiers not operating in class A.

The other curves give the performance of cartesian feedback with different biasing schemes presented in figure 5.13. The solid trace again provides a reference back to conventional one supply cartesian feedback (figure 5.12(*a*)).

In figure 5.4(*a*) the best static power supply selection for maximum collector efficiency with *Vbe*=0 with the simulated SMPS supply is shown by the dot-dashed line (conditions as per figure 5.12(*b*)), and dynamic bias is shown by the dashed line (conditions as per figure 5.12(*d*)). The curves of figure 5.14(*b*) are the same except the functions chosen for best static bias selection (conditions as per figure 5.12(*b*)) and dynamic bias (conditions as per figure 5.12(*d*)) are those which maximize power added efficiency as opposed to maximizing collector efficiency.

From figure 5.14(*a*) it is evident that when favouring collector efficiency the linearization effectiveness does not change significantly, in fact a slight degradation results when dynamic bias (dashed trace) is introduced. This is because the SMPS introduces switching remnants into the output spectrum.

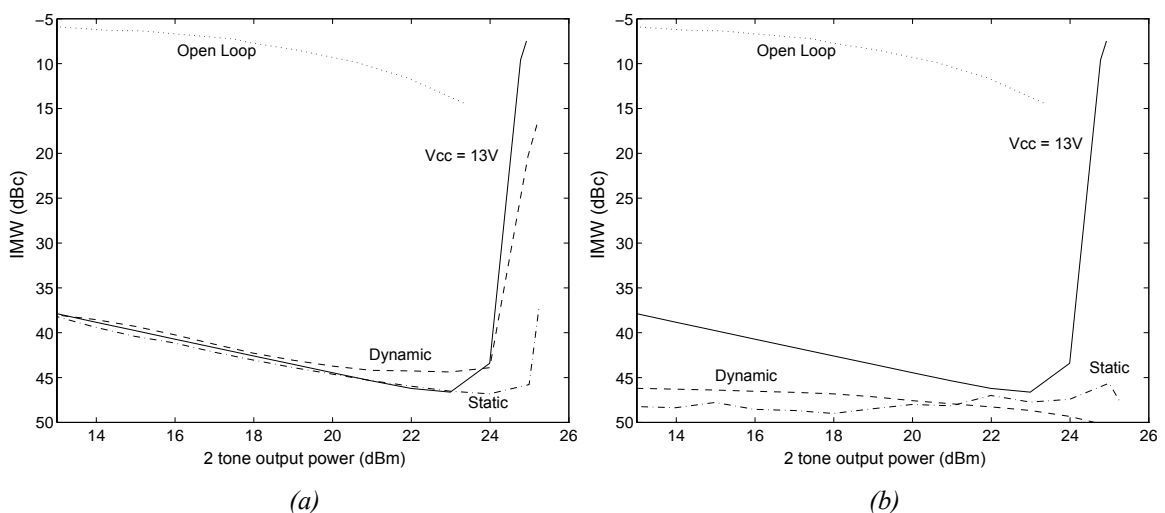*(a)*   *(b)*

Figure 5.14: Linearization effectiveness of dynamic bias for (a) Dynamic and static supply chosen for maximum collector efficiency, (b) dynamic and static bias chosen for maximum power added efficiency.

Favouring power added efficiency does however yield improvements in linearization performance, this improvement indicates that dynamic bias and best power supply selection have a linearization effect by themselves. In fact, the relative flatness of the gain curves presented in figure 5.10(*b*) tends to support the expected linearization improvement given by dynamic bias. Also in the case of dynamic bias the improvement in linearization is sufficient to overcome the switching remnants.

As an added benefit, the improvement in intermodulation performance delivered by the base and collector modulation can be exchanged for extra bandwidth or stability in the cartesian feedback loop. The useable power control range is also improved.

Since the power supply modulation is not used entirely for linearization purposes as in polar feedback linearization systems, the modulation circuits do not have to be exact. This is because the cartesian linearization scheme is able to modify the input drive signals slightly to achieve the exact desired output. The feedback sees the switching ripple as an undesired disturbance and attempts to control it out. The dynamically biased cartesian feedback system can therefore tolerate ripple in a switch-mode driver which can also have in-band frequency components. This allows the use of a simple free-running switched mode supply which only occasionally switches at high rates.

5.5 IMPLEMENTATION OF SWITCH MODE POWER SUPPLY

A relatively simple switched mode buck convertor was constructed to experimentally verify the improvement in efficiency and linearization performance. Dynamically biased cartesian feedback was tested with the low power amplifier. Because the output power was low, great care was taken in shaving off as many microamps as possible in the SMPS control circuits. A schematic of the SMPS is given in appendix B.

The experimental buck type SMPS was similar to that presented in the previous section.
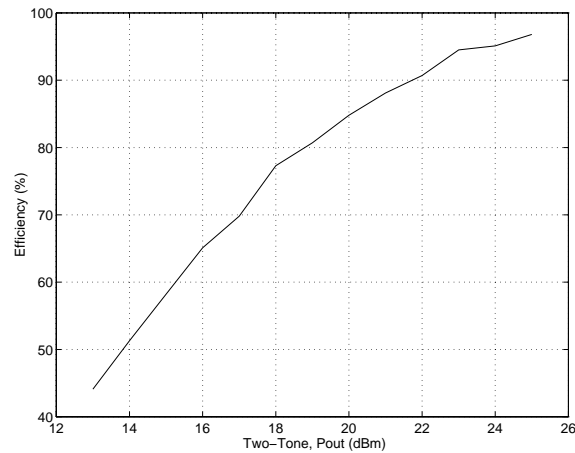
Figure 5.15: Measured efficiency of SMPS operating in static conditions with the amplifier as the load.

A pnp transistor was used as the main switching element and a differential comparator made up of discrete transistors was used to control it, using free running feedback from the output.

Figure 5.15 shows the measured performance of the SMPS when operated from a 16 volt power supply with the low power amplifier as the load. The efficiencies obtained were deemed reasonable for use with the dynamically biased cartesian feedback loop. As is common for this type of convertor the efficiency drops at low output powers because of the relative increase in overhead current consumption of the control circuits and greater relative losses in the flywheel diode when the output voltages are reduced.

5.6 MEASURED PERFORMANCE

A dynamically biased cartesian feedback loop was assembled using the low power amplifier and the SMPS described in the previous section. An arbitrary waveform generator was used to provide one baseband input into the cartesian feedback loop (I_{in}) and a full-wave rectified reference voltage for the SMPS to apply to the collector of the BJT RF power amplifier. There was no dynamic control of the base bias voltage *Vbe*. It was set to 0V.

A series of two-tone tests was performed. Figure 5.16 shows the results of one such test. Figure 5.16(*a*) shows time domain voltages similar to those of chapter 3 except an additional waveform is shown at the top. This waveform is the collector voltage presented to the RF power amplifier by the SMPS.

With a tone separation frequency of 10kHz and an average output power of 20dBm, the worst case IM product is −44dBc. This compares with −46dBc for the conventional cartesian feedback loop (a degradation of 2dB, see figure 5.17(*b*)). The collector efficiencies for the dynamically biased case is however 67% compared to 47% (using the same power meter/dc power measurement apparatus in both cases). This represents an improvement of 20% inclusive of all of the SMPS losses.

When the separation frequency is low the free running SMPS will tend to switch at a high rate on the upward swing of the collector voltage envelope. This means some switching remnants will fall outside the cartesian loop bandwidth. Figure 5.16 shows these remnants roughly centred around 140kHz. The worst of these components is −44dBc which is comparable to the worst case close in-band product.

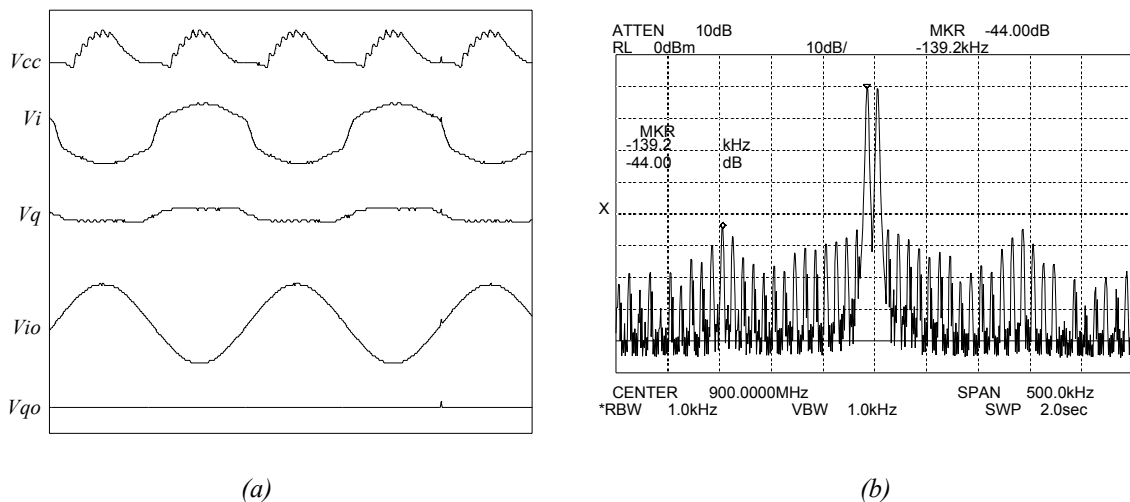|	
(a)	*(b)*

Figure 5.16: Measured time domain and frequency domain results while under dynamic bias. Traces in (a) from top to bottom: collector voltage (Vcc), I &Q predistorted drive signals (Vi & Vq), and I & Q output signals (Vio & Vqo). Input to system was a single sinewave in the I channel.

A series of two-tone tests were preformed to yield the graphs of figure 5.17. The figure concisely shows the performance of dynamic bias of the collector with different operating conditions whilst under power control and is similar to some of the results presented in section 5.4.

The solid traces are again used as the comparison reference. Adjusting the power supply staticly as a function of output power yields a significant improvement in collector efficiency (dotted lines). This improvement is degraded once the SMPS losses are included in the measurement (dot-dashed trace). No improvement is achieved at high output levels. With dynamic bias however (dashed traces), the collector efficiency is improved over the power control range measured. The improvement is good enough to justify the added SMPS circuitry for systems that are expected to require output power control. If however the amplifier is to be operated at maximum efficiency only (no power control), then the 2% improved efficiency does not justify the extra circuitry involved.

Figure 5.17(*b*) shows the equivalent linearization performance. The dotted trace represents the unlinearized open loop worst case intermodulation distortion products relative to the desired carrier tones. Applying cartesian feedback results in a significant
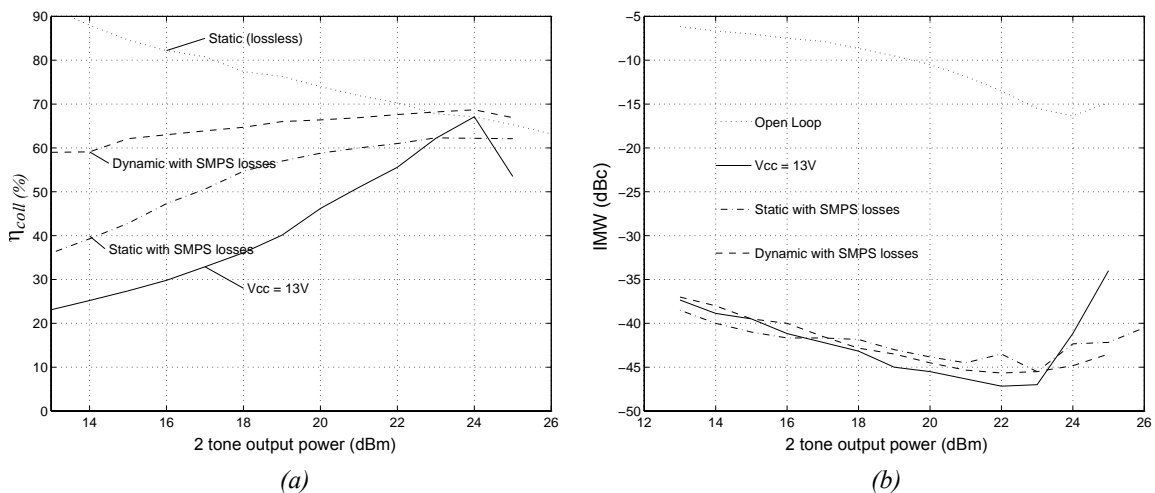

Figure 5.17: Measured performance of dynamic and static supply chosen for maximum collector efficiency, (a) Efficiency performance and (b) linearization performance.

improvement (around 35dB) as shown by the solid trace.

With the SMPS providing the power supply voltage to the RF power amplifier, the worst case intermodulation distortion products are slightly improved at lower powers and slightly degraded for most of the rest of the output levels. This degradation was predicted in the simulations when collector only dynamic bias was applied (see figure 5.4(*a*)).

Closer inspection of figure 5.16(*b*) shows that the third order IM product on the right side of the spectrum is slightly higher than that of the left (see figure 5.18(*a*) for greater detail). The cause of this is the result of applying collector modulation via the dynamic bias circuits which is delayed relative to the main drive modulation.

Figure 5.18(*a*) shows a zoomed-in version of the output spectrum given in figure 5.16(*b*). In figure 5.18(*b*), the baseband input has been delayed by 4 degrees to equalize the IM3 products either side of the centre frequency. This delay marginally improved the efficiency by 0.3% to 67.3% whilst the worst case IM product improved by 0.8dB to −44.8dBc.

The conclusion is then that some minor improvements can be obtained by equalizing the delays through the high level path and low-level path.
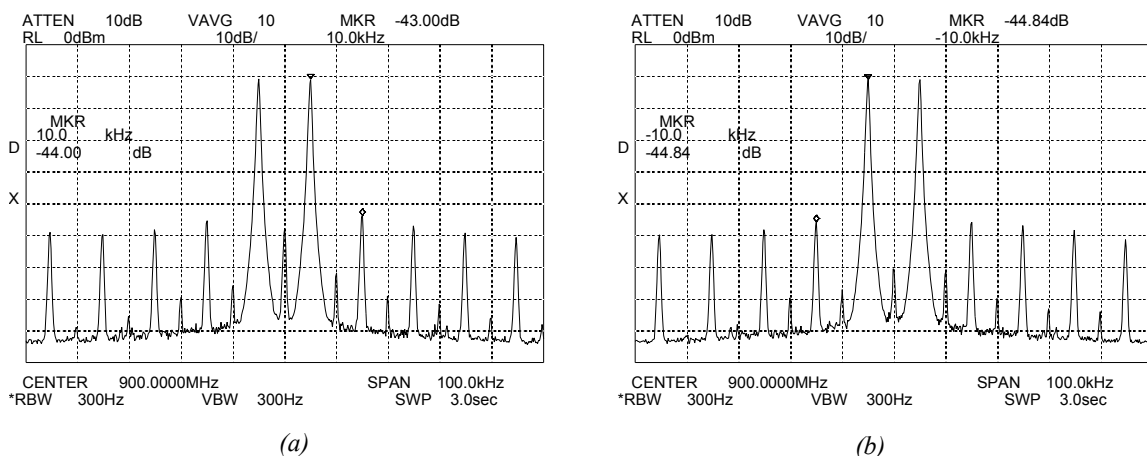

(a)   *(b)*

Figure 5.18: Equalization of Switched-mode delay.(a) No delay equalization, (b) with delay equalization.

5.7 CONCLUSION

It has been shown that dynamic bias applied to an RF amplifier's bias and supply lines can enhance the efficiency of the cartesian feedback linearization process. The efficiency improvement is higher at lower output powers. The improvement is reduced when a switched-mode driver is included in the dynamic bias circuitry. The reduction is caused by dynamic tracking errors and by losses inherent in switched-mode power supplies. In cases where the amplifier is operated at maximum output power this degradation will be unacceptable and conventional cartesian feedback will be more cost effective. However when power control is necessary and operation at reduced outputs permitted, dynamic bias can lead to more than a halving of the DC power required for a given output power.

Since the cartesian feedback automatically adopts the necessary state to maintain exact linearization, the problem of having to generate wideband and accurate high level modulation found in polar feedback techniques is avoided. This enables the use of relatively simple SMPS drivers with lower switching frequencies and greater output ripple. In-band switching residues caused by ripple are reduced by loop gain. The largest switching residue spectral component was of the same magnitude of the third order intermodulation product.

Substantially characterizing the BLU98 low power amplifier enabled base bias and collector bias functions to be determined that enhance the performance of conventional cartesian feedback. This was shown by comparing the differential and absolute gains whilst base and collector bias voltages were varied in accordance with these functions. The benefits of dynamic bias were also directly simulated. Some of these simulations included a simulated SMPS and gave good agreement with measured results for the intermodulation performance of the various schemes (figures 5.14(*a*) and 5.17(*b*)). The curves were within about 2dB of each other over most of the power output range. The large deviation at the end was due to the simulated amplifier reaching saturation approximately 1dB before the measured amplifier. The efficiency curves (fig. 5.13(*a*) and 5.17(*a*)) were also in good agreement, being within about 5% of each other. A notable

exception was the dynamic bias curve which had much better efficiency at low power levels than predicted from the simulations. The most probable reason for this is that dynamic behaviour of the SMPS was difficult to reproduce, particularly when it was tracking a changing signal, since the control circuit was heavily modified to reduce the quiescent overhead current taken by this part of the circuit. Some of the modifications affected the switching operation (threshold and hysteresis levels) and so changed the dynamic behaviour. Apart from this, the agreement was surprisingly good, considering the combined difficulties of RF measurements and SMPS design.

Design of the SMPS was not easy. At the time (and even now) an acceptable IC did not exist - most having too high a quiescent current for the control circuits. This overhead current killed any potential for efficiency improvements of dynamic bias. A discrete solution was adopted since this allowed small quiescent currents, and other power saving ideas such as returning control currents to internal voltage lines other than to ground (see collector of Q3, appendix B) as would be done in conventional designs. The SMPS would not perform as well in mass production since the transistors were individually selected from a small batch for high gain! Future work should include a more robust SMPS design, hopefully with even higher efficiency as well as being capable of accommodating a wider tolerance spread in components.

Still, the SMPS was constructed and achieved an efficiency of 95% at high output levels. When applied to a cartesian feedback loop efficiency was markedly improved and at an output power of 20dBm average, the efficiency improved by 20%, leading to a reduction in power amplifier current consumption of 33%. The worst case intermodulation distortion product degraded however by 2dB as a result of switching remnants.

The efficiency improvement was greater at lower output powers and less at higher output powers (2% at 24dBm). The use of power control in radio systems is now common practice and as the density of basestations increases the need for high transmitter powers reduces, which makes dynamic bias schemes such as this more effective.

Delay in the dynamic bias circuitry was also examined. It was found that equalizing this delay marginally improved both efficiency and the worst case intermodulation product.

All performance measurements were based on a two-tone test. More practical signals have less dynamic range (i.e $\pi/4$ shift QPSK) and this should improve the tracking of the SMPS, leading to an expected improved performance, both in terms of efficiency and spectrum output.

6 CONCLUSION

The motivation for the research presented in this thesis is derived from the move towards spectrally efficient modulation schemes with varying envelopes. These signals require linear processing in modern transceiver architectures and this includes the RF power amplifier in the transmitter. In addition to linearity, the RF power amplifier must also be power efficient, small and of low cost. The first three requirements are met by taking an efficient yet non-linear amplifier and applying a linearization means to reduce distortion. Whilst the cost requirement is met by selecting relatively simple hardware, such as that used in a typical cartesian feedback loop.

The background material of chapter 2 presented the effects of amplifier distortion on communications systems particularly on adjacent channels. Feedforward, vector summation, predistortion and feedback were examined and compared, each as possible means by which efficient non-linear powers amplifiers can be linearized.

Various aspects of cartesian feedback were investigated in chapters 3, 4, and 5. In chapter 3, two RF power amplifiers were carefully measured and characterized. The characterization process presented eliminated the erroneous effects of network analyzer power levelling uncertainty by the addition of an external power meter. Amplifier current consumption was also characterized giving accurate amplifier models that could also predict efficiency performance. Care was also taken with modelling the frequency

dependent components in the cartesian feedback loop. Since most of the loop components were wideband compared to the modulation bandwidth, the system was modelled with a single pole filter and a delay. The delay was designed to model the effects of high frequency poles and zeros along with through transmissive delay. Since stability is an important issue in all feedback systems, the digital domain simulation of the frequency dependence was performed by bilinear transformation. This enabled bode responses to be accurately simulated and could hence be used as a platform for bode stability analysis. These models enabled simulations to be performed which predicted performance to within 2dB (IMD) and 4% (for efficiency calculations) of the practical measurements.

The simulations were backed up with experimental hardware that demonstrated cartesian feedback as a means of obtaining linear amplification with good efficiency. The best results showed that the low power amplifier (Vbe = 0V) is capable of achieving −62dBc with a collector efficiency of 42% when transmitting π/4 QPSK. Cartesian feedback improves the intermodulation distortion by 36dB for a two-tone test and 44dB for π/4 QPSK modulation, no doubt because π/4 QPSK modulation avoids the zero crossing region of the amplifier characteristics (unlike the two-tone test). The effect of changing base bias was also examined in chapter 3. It was shown that with a two-tone test, adding base bias could reduce closed loop intermodulation distortion by 18dB, however efficiency was reduced by 14% as a result.

Chapter 4 presented the piecewise MIMO analysis which demonstrated how RF amplifier non-linearity, the RF phase adjuster setting, loop gain, bandwidth and delay affect the stability of the cartesian feedback loop. It was shown that instability resulted when the amount of RF phase introduced by AM/PM distortion and by RF phase adjuster error equalled the original phase margin. The graphical technique developed from this fact, demonstrates the important mechanisms which influence stability and can be utilized at the design stage, or in the practical assessment of an experimental cartesian loop.

Non-linear amplifiers cannot be represented by a series of fixed complex gains in a

piecewise stability analysis. Instead an additional parameter to the complex gain is needed to represent the effects of amplitude and phase non-linearities. This is because the complex gain changes with the phase of the input perturbation.

Placing the developed non-linear amplifier model into a MIMO model of a cartesian feedback loop, enabled a stability analysis to be made. The results from the analysis was presented in graphical form. The stability boundaries shown in this analysis gives an indication as to how stable a given RF amplifier will be when placed in a cartesian feedback loop. For the very non-linear BLU98 low power amplifier used in the analysis, it was found that instability resulted just after the transistor turn-on region when the RF phase adjuster was adjusted above optimum, and instability resulted at transistor saturation when adjusted lower than optimum. This was also shown with experimental hardware.

The perturbed behaviour of non-linear RF amplifiers display two forms of operation when placed in a feedback loop - Spiral mode and Stationary mode. Spiralling will tend to cause the noise floor of the output spectrum to rise on one side depending on the direction of the spiral. The direction is in turn dependent on the setting of the RF phase adjuster of the cartesian feedback loop. When the phase adjuster is in the forward path, phase adjustments lower than optimum, will cause the noise to rise on the right side of the output spectrum (anti-clockwise spiralling) and vice-versa. With the phase adjuster in the feedback path the reverse is true.

The amplifier model (and hence the analysis) can be simplified if the amplifier only has weak non-linearities (class A or AB). Here, there is only one stability boundary corresponding to the worst case of all the stability boundaries of the general case. The important amplifier parameters are the worst case gain (differential or absolute) and the amplifier phase rotation. This analysis is much simpler and could be used as a practical engineering design tool.

Loops with low stability margins were demonstrated to exhibit closed-loop peaking which can effect the out of band noise performance of a cartesian feedback transmitter. The condition of no-peaking was derived (with $\delta = 0$) along with the degree of peaking resulting from a closed loop system with a single pole and a delay. In order to achieve a non-peaking condition the phase margin of the loop needs to be around 60° for the first order case described. It was also shown how the degree of peaking could be approximately obtained from the gain and phase margins. Finally it was concluded and demonstrated that the loop compensation should be placed as far up the forward chain as possible in order to minimize the out-of-band noise floor.

In chapter 5 the concept of dynamic bias modulation was introduced. The method shown works by setting up optimum bias conditions for the power amplifier and then having the cartesian feedback loop make fine adjustments to the RF drive to achieve the required output. This way the bias conditions do not have to be applied perfectly implying simple (i.e low switching frequency) SMPS can be used.

Substantially characterizing the BLU98 low power amplifier enabled base bias and collector bias functions to be determined that enhance the performance of conventional cartesian feedback. This was shown by comparing the differential and absolute gains (which tended to equalize) whilst base and collector bias voltages were varied in accordance these functions. The benefits of dynamic bias were also directly simulated. Some of these simulations included a simulated SMPS.

A simple buck SMPS was constructed. It achieved an efficiency of 95% at high output levels. When applied to a cartesian feedback loop efficiency was markedly improved and at an output power of 20dBm average the amplifier's efficiency was lifted from 45% to 67%, an improvement of over 20%. This would reduce current consumption by 33%. The worst case intermodulation distortion product degraded however by 2dB as a result of switching remnants.

Delay in the dynamic bias circuitry was also examined. It was found that equalizing this delay marginally improved both efficiency and the worst case intermodulation product.

6.1 CRITIQUE AND FUTURE WORK

It was shown in chapter 4 that delay, gain and bandwidth are essentially interchangeable. Delay hence consumes distortion reducing gain and valuable bandwidth. The only seeming exception (section 2.6.2) does broaden the bandwidth for a given delay but involves placing independent loops resulting in a discontinuous linearization spectrum. Nature does not yield so easily however, and delay is delay. When feedback is involved delay has detrimental consequences and ultimately places the fundamental limitation as to what continuous spectrum gain bandwidth can be achieved.

The so called delay in the constructed cartesian loop is mainly comprised of pole/zero induced phase shifts and some true transmissive delay. Reducing the physical size of the loop (say by chip integration) would yield some transmissive delay reduction but the largest reductions in so called delay can be achieved by careful wideband design. This has implications for all of the circuits which comprise the loop. The RF power amplifier must be made as wideband as possible whilst still ensuring carrier harmonics are not radiated at the output or applied to the feedback quadrature demodulator. The baseband processing circuits must also be wideband indicating the use of high FT transistors/op-amps. The essential loop itself should also be as simple as possible and involve as few filtering inducing components as possible whilst maintaining the large FT.

The delay not only influences the amount of loop gain that can be applied but also has a big impact on the closed loop transfer function (i.e high frequency peaking) and hence the out of band noise performance. Whilst moving the loop filter as far up the driving chain mitigates this problem, it may not be sufficient for all applications. And hence it all comes back to reducing loop delay by applying the techniques described above.

The stability analysis presented in this thesis assumed that the amplifier was relatively wideband and hence memoryless. The effects of memory on stability is therefore an area worthy of investigation especially when evidence of asymmetrical IMD is present. Further work on the stability analysis could also include examination of the influences of dynamic bias.

Automatic setting of the phase adjuster is another area worthy of further investigation although some solutions have been presented in the literature. In chapter 3 the relationship of current consumption with optimum phase adjuster setting was presented. This relationship could be used in an alternative automatic phase adjuster approach. Automatic phase adjustment may also be a way of adjusting out phase changes caused by RF amplifier load variations.

Although efficiency and linearity issues under power control were examined in Chapter 5, the noise and DC offset performance was not examined. The problems of DC offset could be accommodated through the use of CRISIS like circuits applied to the input of the cartesian feedback loop and could also have the additional benefit of providing corrections for all quadrature demodulator errors. Noise performance under power control is another matter and would require careful examination of signal levels around the loop and perhaps the introduction of variable gain devices to maintain optimum signal levels.

BIBLIOGRAPHY

[1]   Yoshihiko Akaiwa and Yoshinori Nagata, "Highly Efficient Digital Mobile Communications with a Linear Modulation Method", *IEEE Journal on Selected Areas in Communications*, vol. SAC-5, No. 5, June 1987, pp. 890-895.

[2]   Toshitake Noguchi, Yoshimasa Daido, and Josef A. Nossek, "Modulation techniques for microwave digital radio", in *Microwave Digital Radio* (edited by Larry J. Greenstein and Shafti Mansoor), IEEE Press, New York, 1988, pp. 21-30.

[3]   Rohde & Schwarz, "IQSIM Manual", 1992, pp. 6-10.

[4]   Michel C. Jeruchim, Philip Balaban, K. Sam Shanmugan, *Simulation of Communications Systems*, Plenum Press, New York, 1992, Chapter 2.

[5]   Dennis A. Jiraud, "Proper design yields efficient digital transmitters", *Microwaves & RF*, August 1991, pp. 91-101.

[6]   Herbert L. Krauss, Charles W. Bostian and Frederick H. Raab, *Solid State Radio Engineering,* John Wiley & Sons, New York, 1980.

[7]   T. A. H. Wilkinson and P. A. Matthews, "Assessment of UHF power amplifier linearization by measurement and simulation", *Proceedings of the 5th international Conference on Mobile Radio and Personal Communication*, Warwick, UK, December 1989, pp. 60-64.

[8]   Wolfgang Bösch and Giuliano Gatti, "Measurement and Simulation of Memory effects in Predistortion Linearizers", *IEEE Transactions on Microwave Theory and Techniques*, vol. 37, December 1989, pp. 1885-1890.

[9]   Sirikiat Ariyavisitakul and Ting-Ping Liu, "Characterizing the effects of Non-linear Amplifiers on Linear Modulation for Digital Portable Radio

Communications", *IEEE Transactions on Microwave Theory and Techniques*, vol. 31, December 1989, pp. 1885-1890.

[10] Adel A. M. Saleh and Donald C. Cox, "Improving the Power-Added Efficiency of FET Amplifiers Operating with Varying-Envelope Signals", *IEEE Transactions on Microwave Theory and Techniques*, vol. 31, January 1989, pp. 51-56.

[11] Harold S. Black, "Translating System", *U.S Patent No. 1 686 792*, October 1928.

[12] James K. Cavers, "Convergence Behaviour of an Adaptive Feedforward Linearizer", in *Proceedings of the 44th IEEE Vehicular Technology Conference*, Stockholm, Sweden, VTC-94, June 1994, pp. 499-503.

[13] Peter Blakeborough Kenington, Mark Anthony Beach, Andrew Bateman and Joseph Peter McGeehan, "Apparatus and Method for Reducing Distortion in Amplification", *PCT Patent No. WO 91/16760*, April 1991.

[14] P. B. Kenington, "Power Amplification Techniques for Linear TDMA Basestations", in *Proceedings of GLOBECOM '92*, Orlando, USA, December 1992, pp. 74-78.

[15] R. D. Stewart and F. F. Tusubira, "Feedforward Linearisation of 950MHz Amplifiers", *IEE Proceedings*, vol. 135, Pt. H, No. 5, October 1988, pp. 347-350.

[16] Kenneth A. Walsh, Jr., "Very Wide Bandwidth Linear Amplitude Modulation of RF Signals by Vector Summation", *U.S Patent No. 4 835 493*, May 1989.

[17] Donald C. Cox, "Linear Amplification with Non-linear Components", *IEEE Transactions on Communications*, vol. COM-22, December 1974, pp. 1942-1945.

[18] S. Tomisato, K. Chiba and K. Murota, "Phase Error Free LINC Modulator", *IEE Electronic Letters*, vol. 25, No. 9, April 1989, pp. 576-577.

[19] Fernando Casadevall and Juan J. Olmos, "On the behaviour of the LINC Transmitter", in *Proceedings of the 40th IEEE Vehicular Technology Conference*, Orlando, USA, VTC-90, May1990, pp. 29-34.

[20] S. A. Hetzel, A. Bateman and J. P. McGeehan, "A LINC Transmitter", *IEE Electronic Letters*, vol. 25, No. 10, 1991, pp. 844-845.

[21] A. Bateman, "The Combined Analogue Locked Loop Universal Modulator", in *Proceedings of the 42nd IEEE Vehicular Technology Conference*, Denver, USA, VTC-92, May 1992, pp. 759-763.

[22] K. Y. Chan, A. Bateman and M. Li, "Analysis and Realisation of the LINC

Transmitter using the Combined Analogue Locked Loop Universal Modulator (CALLUM)", in *Proceedings of the 44th IEEE Vehicular Technology Conference*, Stockholm, Sweden, VTC-94, June 1994, pp. 484-488.

[23] Donald C. Cox, "Linear Amplification by Sampling Techniques: A New Application for Delta Coders", *IEEE Transactions on Communications*, vol. COM-23, August 1975, pp. 793-798.

[24] Junji Namiki, "An Automatically Controlled Predistorter for Multilevel Quadrature Amplitude Modulation", *IEEE Transactions on Communications*, vol. COM-31, No. 5, May 1983, pp. 707-712.

[25] Toshio Nojima and Tohru Konno, "Cuber Predistortion Linearizer for Relay Equipment in 800MHz Band Land Mobile Telephone System", *IEEE Transactions on Vehicular Technology*, vol. VT-34, No. 4, November 1985, pp. 169-177.

[26] Yoshinori Fujiki, Masatoshi Ishida, Nobuaki Imai and Toshio Nojima, "Non-linear signal generating circuit and nonlinear compensating device using the same", *European Patent No. EP 0 277 636*, February 1988.

[27] Nobuaki Imai, Toshio Nojima and Takehiro Murase, "Novel Linearizer Using Balanced Circulators and Its Application to Multilevel Digital Radio Systems", *IEEE Transactions on Microwave Theory and Techniques*, vol.37, No. 8, August 1989, pp. 1237-1243.

[28] Toshio Nojima, Takehiro Murase and Nobuaki Imai, "The Design of a Predistortion Linearization Circuit for High-Level Modulation Radio Systems", in *Proceedings of GLOBECOM '85*, December 1985, pp. 47.4.1-47.4.5.

[29] P. Bura, D. Gelerman and P. Ntake, "Power Amplifier for Microwave Digital Radios with Inherent Phase Compensation", *IEE Proceedings*, vol. 135, Pt. H No. 5, October 1988, pp. 344-346.

[30] Herbet J. Wolkstein, "Method and Apparatus for Compensating Phase Shift through an RF Power Amplifier", *U.S Patent No. 4 488 122*, December 1984.

[31] Klaus Peterknecht, Ulrich Simon and Hermann Ens, "Analog Predistorter", *Australian Patent No. AU-A-52538/90*, October 1990.

[32] M. Ghaderi, S. Kumar and D.E Dodds, "Fast Adaptive Predistortion Lineariser using Polynomial Functions", *IEE Electronic Letters*, vol. 29, No. 17, August 1993, pp. 1526-1528.

[33] D. Hilborn, S.P Stapleton and J.K. Cavers, "An Adaptive Direct Conversion Transmitter", in *Proceedings of the 42nd IEEE Vehicular Technology Conference*, USA, VTC-92, May1992, pp. 764-767.

[34] Michael Faulkner and Mats Johansson, "Adaptive Linearisation using Predistortion - Experimental Results", *IEEE Transactions on Vehicular Technology*, vol.43, No. 2, May 1994, pp. 323-332.

[35] Anit Lohtia, Paul A. Goud and Colin G. Englrfield, "Power Amplifier Linearization using Cubic Spline Inerpolation", in *Proceedings of the 43rd IEEE Vehicular Technology Conference*, Secaucus, USA, VTC-93, May1993, pp. 676-679.

[36] M. Faulkner, T. Mattsson, and W. Yates, "Automatic Adjustment of Quadrature Modulators", *IEE Electronic Letters*, vol. 27, No. 3, 1991, pp. 214-216.

[37] Yoshinori Nagata, "Linear Amplification Technique for Digital Mobile Communications", in *Proceedings of the 39th IEEE Vehicular Technology Conference*, USA, VTC-89, May1989 pp. 159-164.

[38] M. Minowa, M. Onoda, E. Fukuda, and Y. Daido, "Back-off Improvement of an 800MHz GaAs FET Amplifier for a QPSK Transmitter using an Adaptive Non-linear Distortion Canceller", in *Proceedings of the 40th IEEE Vehicular Technology Conference*, Orlando, USA, VTC-90, May1990, pp. 542-546.

[39] James K. Cavers, "Amplifier Linearization Using a Digital Predistorter with Fast Adaptation and Low Memory Requirements", *IEEE Transactions on Vehicular Technology*, vol.39, No. 4, November 1990, pp. 374-382.

[40] L. Sundström, "RF Amplifier Linearisation using Digital Adaptive Predistortion", *Tecknisk Licentuat Thesis*, LUTEDX/(TETE-7076)/1-98(1993), Department of Applied Electronics, Lund University, June 1993.

[41] L. Sundström and M. Johansson, "Chip for Linearisation of RF Power Amplifiers using predistortion", *IEE Electronic Letters*, vol. 30, No. 14, July 1994, pp. 1123-1124.

[42] Harold S. Black, "Wave Translation System", *U.S Patent No. 2 102 671*, December 1937.

[43] H. A. Rosen and A. T. Owens, "Power Amplifier Linearity Studies for SSB Transmissions", *IEEE Transactions on Communications Systems*, June 1964, pp.

150-159.

[44] Amin K. Ezzeddine, Hing-Loi A. Hung and Ho C. Huang, "An MMAC *C*-Band FET Feedback Power Amplifier", *IEEE Transactions on Microwave Theory and Techniques,* vol.38, No. 4, April 1990, pp. 350-357.

[45] Eduardo Balleteros, Félix Pérez and Jorge Pérez, "Analysis and Design of Microwave Linearized Amplifiers Using Active Feedback", *IEEE Transactions on Microwave Theory and Techniques,* vol.36, No. 3, March 1988, pp. 499-504.

[46] Yongcai Hu, Jean Claude Mollier and Juan Obregon, "A New Method of Third-Order Intermodulation Reduction in Nonlinear Microwave Systems", *IEEE Transactions on Microwave Theory and Techniques,* vol. MTT-34, No. 2, February 1986, pp. 245-250.

[47] Kenneth G. Voyce and Jay H. McCandless, "Power Amplifier Linearization Using IF Feedback", in *Proceedings of 1989 IEEE Microwave Theory and Techniques Symposium,* 1989, pp. 863-866.

[48] Leonard R. Kahn, "Single-Sideband Transmission by Enevlope Elimination and Restoration", in *Proceedings of the IRE,* July 1952, pp. 803-806.

[49] Leonard R. Kahn, "Comparison of Linear Single-Sideband Transmitters with Enevlope Elimination and Restoration Transmitters", in *Proceedings of the IRE,* December 1956, pp. 1706-1712.

[50] V. Petrovic and W. Gosling, "Polar-Loop Transmitter", *IEE Electronic Letters*, vol. 15, No. 10, May 1979, pp. 286-287.

[51] V. Petrovic and C. N. Smith, "The Design of VHF SSB Polar-Loop Transmitters", in *Proceedings of IEE Conference on Communications Equipment and Systems*, April 1982, pp. 148-155.

[52] M. J. Koch and R. E. Fisher, "A High Efficiency 835MHz Linear Power Amplifier for Digital Cellular Telephony", in *Proceedings of the 39th IEEE Vehicular Technology Conference*, USA, VTC-89, May1989 pp. 17-18.

[53] Kohji Chiba, Toshio Nojima, and Shigeru Tomisato, "Linearized Saturation Amplifier with Bidirectional Control (LSA-BC) for Digital Mobile Radio", in *Proceedings of GLOBECOM '90*, December 1990, pp. 906.2.1-906.2.5.

[54] V. Petrovic, "Reduction of Spurious Emission from Radio Transmitters by means of Modulation Feedback", in *Proceedings of IEE Conference on Radio Spectrum*

Conservation Techniques, September 1983, pp. 44-49.

[55]   V. Petrovic and A. N. Brown, "Application of Cartesian Feedback to HF SSB Transmitters", in *Proceedings of IEE Conference on HF Communications Systems and Techniques"*, February 1985, pp. 81-85.

[56]   V. Petrovic, "VHF SSB Transmitter employing Cartesian Feedback", in *Proceedings of IEE Conference on Radio and Information Theory*, May 1984, pp. 161-165.

[57]   Mats Johansson and Thomas Mattsson, "Transmitter Linearization using Cartesian Feedback for TDMA Modulation", in *Proceedings of the 41st IEEE Vehicular Technology Conference*, New Orleans, USA, VTC-91, May1991, pp. 439-444.

[58]   Mats Johansson and Thomas Mattsson, "Linearised High-Efficiency Power Amplifier for PCN", *IEE Electronic Letters*, vol. 27, No. 9, April 1991, pp. 762-764.

[59]   Ross Wilkinson, John MacLeod, Mark Beach and Andrew Bateman, "Linear Transmitter Design for MSAT Terminals", in *Proceedings of the International Mobile Satellite Conference*, Ottawa, Canada, 1990, pp. 297-301.

[60]   A. N. Brown and V. Petrovic, "Phase Delay Compensation in HF Cartesian-Loop Transmitters", in *Proceedings of IEE 4th Conference on HF Communications Systems and Techniques"*, 1988, pp. 200-204.

[61]   Y. Ohishi, M. Minowa, E. Fukuda, and T. Takano, "Cartesian Feedback Amplifier with Soft Landing", in *Proceedings of the 3rd IEEE International Symposium on Personal, Indoor and Mobile Radio Communications*, Boston, USA, PIMRC '92, October 1992, pp. 12.7.1-12.7.5.

[62]   T. Kubo, Y. Ohishi, E. Fukuda, and Y. Daido, "Simulated Performance of Loop Parameters of Cartesian Feedback Amplifier for p/4 Shifted QPSK Transmitter", in *Proceedings of the 1st IEEE International Conference on Universal Personal Communications*, Dallas, USA, ICUPC '92, September 1992, pp. 12.7.1-12.7.5.

[63]   A. Bateman, D. Haines and R. Wilkinson, "Direct Conversion Linear Transceiver Design", in *Proceedings of the 5th International Conference on Mobile Radio and Personal Communications*, Warwick, UK, December 1989 pp. 53-56.

[64]   A. J. Wray and D.M. Boscovic, "Overcoming the Implementation Issues of Linear Transmitter Technology - Motorola's Experience", in *Proceedings of IEE*

Colloquim on Linear RF Amplifiers and Transmitters, April 1994 pp. 1/1-1/6.

[65]   Mats Johansson, Thomas Mattsson, Lars Sundström and Michael Faulkner, "Linearization of Multi-Carrier Power Amplifiers", in *Proceedings of the 43rd IEEE Vehicular Technology Conference*, Secaucus, USA, VTC-93, May1993, pp. 684-687.

[66]   M. Johansson and L. Sundström, "Linearisation of RF Multi-Carrier Amplifiers using Cartesian Feedback", *IEE Electronic Letters*, vol. 30, No. 14, July 1994, pp. 1110-1111.

[67]   Colin R. Smithers, "Bipolar Transistor RF Power Amplifier", *U.S Patent No. 4 631 491*, December 1986.

[68]   Frigyes Csaki, *Modern Control Theories: Non-linear, Optimal and Adaptive Systems*, Akademiai Kiado, Budapest, 1972, Chapter 2.

[69]   Mats Johansson, "Linearisation of RF Power Amplifiers using Cartesian Feedback", *Thesis for the degree of Teknisk Licentiat*, Department of Applied Electronics, Lund University, Sweden, November 1991.

[70]   M. Faulkner, T. Mattson, and W. Yates, "Automatic adjustment of quadrature modulators", *IEE Electronic Letters*, vol. 27, No. 3, July 1994, pp. 214-216.

[71]   J. Cavers, and M. Liao, "Adaptive compensation for imbalance and offset losses in direct conversion transceivers", in *Proceedings of the 41st IEEE Vehicular Technology Conference*, New Orleans, USA, VTC-91, May1991.

[72]   R. F. V. Anderson, *Introduction to linear algebra*, Holt Rinehart and Winston of Canada Ltd., 1986, pp. 221-226 & pp. 243-258.

[73]   Mark A. Briffa and Michael Faulkner, "Dynamically Biased Cartesian Feedback Linearization", in *Proceedings of the 43rd IEEE Vehicular Technology Conference*, Secaucus, USA, VTC-93, May1993, pp. 672-675.

[74]   Mark A. Briffa and Michael Faulkner, "Stability analysis of cartesian feedback linearisation with weak non-linearities", *IEE Proceedings - Communications*, Vol. 143, No. 4, August 1996.

[75]   M. Johansson, M. A. Briffa and L. Sundström, "Dynamic Range Optimization of the Cartesian Feedback Transmitter", *IEEE Transactions on Vehicular Technology,* Accepted for publication.

APPENDIX A
SMPS DIFFERENCE EQUATIONS

The simulations presented in chapter 5 utilized a difference equation representation of the SMPS circuit given in figure 5.11. This enabled the SMPS to be simulated in the digital time domain along with the cartesian feedback loop and other components.

The output circuit in the SMPS which is modelled as a series lossy L with a shunt lossy C can be considered as a two-port network with the node voltages and currents as shown in figure A.1.

Since the amplifier models used throughout this thesis provide the demanded current consumption for a given amplifier input power and voltage bias conditions, the SMPS
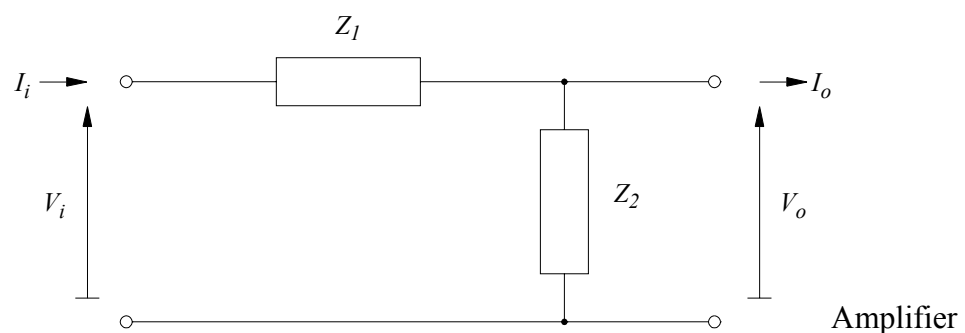

Figure A.1: Two-port representation of output section of SMPS convertor.

model needs to be described as a function of demanded SMPS output current (I_o) for a given input voltage (V_i) i.e

$$V_o = \text{f}(I_o, V_i)$$
$$I_i = \text{f}(I_o, V_i) \tag{A.1}$$

For network of figure A.1 this gives

$$V_o = -I_o \frac{Z_1 Z_2}{Z_1 + Z_2} + V_i \frac{Z_2}{Z_1 + Z_2} \tag{A.2}$$

$$I_i = V_i \frac{1}{Z_1 + Z_2} + I_o \frac{Z_2}{Z_1 + Z_2} \tag{A.3}$$

For the L and C output circuit of the SMPS, assigning $Z_1 = R_L + sL$ and $Z_2 = R_C + 1/sC$ gives (respectively)

$$V_o = -V_o s C (R_L + R_C) - V_o s^2 CL + V_i s CR_C + V_i - I_o s (CR_L R_c + L)$$
$$- I_o R_L - I_o s^2 CLR_C \tag{A.4}$$

$$I_i = -I_i s C (R_L + R_C) - I_i s^2 LC + V_i sC + I_o s CR_C + I_o \tag{A.5}$$

In differential form equations A.4 and A.5 are

$$V_o = -\frac{dV_o}{dt} C (R_L + R_C) - \frac{d^2 V_o}{dt^2} CL + \frac{dV_i}{dt} CR_C + V_i - \frac{dI_o}{dt}(CR_L R_c + L)$$
$$- I_o R_L - \frac{d^2 I_o}{dt^2} CLR_C \tag{A.6}$$

$$I_i = -\frac{dI_i}{dt} C (R_L + R_C) - \frac{d^2 I_i}{dt^2} LC + \frac{dV_i}{dt} C + \frac{dI_o}{dt} CR_C + I_o \tag{A.7}$$

Backward difference differentiation over time T (where T is one over the sample rate), transforms equations A.6 and A.7 to corresponding difference equations

$$V_o = -\frac{[V_o(n) - V_o(n-1)]}{T}C(R_L + R_C) - \frac{[V_o(n) - 2V_o(n-1) + V_o(n-2)]}{T^2}CL$$

$$+ \frac{[V_i(n) - V_i(n-1)]}{T}CR_C + V_i - \frac{[I_o(n) - I_o(n-1)]}{T}(CR_L R_c + L) - I_o R_L \quad \text{(A.8)}$$

$$-\frac{[I_o(n) - 2I_o(n-1) + I_o(n-2)]}{T^2}CLR_C$$

$$I_i = -\frac{[I_i(n) - I_i(n-1)]}{T}C(R_L + R_C) - \frac{[I_i(n) - 2I_i(n-1) + I_i(n-2)]}{T^2}LC$$

$$+ \frac{[V_i(n) - V_i(n-1)]}{T}C + \frac{[I_o(n) - I_o(n-1)]}{T}CR_C + I_o \quad \text{(A.9)}$$

Introducing the z^{-d} operator which signifies performing a delay operation of d times T and rearranging finally gives

$$V_o = \frac{\dfrac{C(R_L + R_C)}{T}\{V_o z^{-1}\} + \dfrac{LC}{T^2}[2\{V_o z^{-1}\} + \{V_o z^{-2}\}] + \dfrac{CR_C}{T}[V_i - \{V_i z^{-1}\}] + }{}$$

$$\frac{V_i - \dfrac{(CR_L R_c + L)}{T}[I_o - \{I_o z^{-1}\}] - I_o R_L - \dfrac{LCR_C}{T^2}[I_o - 2\{I_o z^{-1}\} + \{I_o z^{-2}\}]}{\left[1 + \dfrac{C(R_L + R_C)}{T} + \dfrac{CL}{T^2}\right]} \quad \text{(A.10)}$$

$$I_i = \frac{\dfrac{C(R_L + R_C)}{T}\{I_i z^{-1}\} + \dfrac{LC}{T^2}[2\{I_i z^{-1}\} - \{I_i z^{-2}\}] + \dfrac{C}{T}[V_i - \{V_i z^{-1}\}]}{}$$

$$\frac{+ \dfrac{CR_C}{T}[I_o - \{I_o z^{-1}\}] + I_o}{\left[1 + \dfrac{C(R_L + R_C)}{T} + \dfrac{CL}{T^2}\right]} \quad \text{(A.11)}$$

Equations A.10 and A.11 can be directly used in a digital time domain simulation to model the L and C part of the SMPS. The switching parts can be modelled by considering the rest of the SMPS circuit as given in figure A.2.

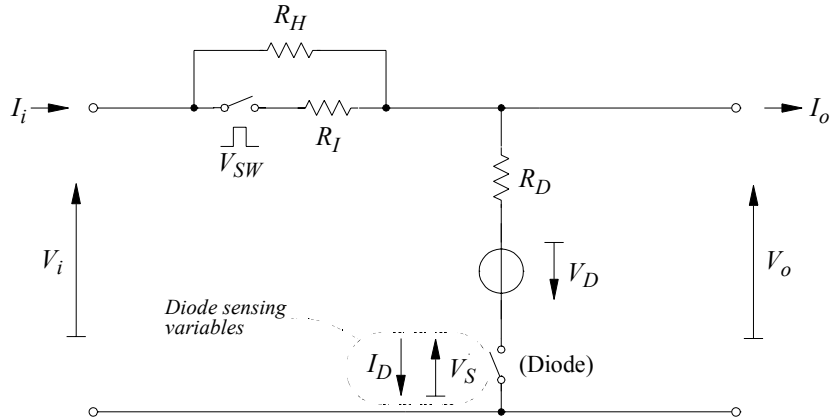The equations have to again be arranged as in equation A.1 to accommodate the use of the

Figure A.2: Switching part of SMPS.

amplifier models

$$V_o = f(I_o, V_i, V_{SW})$$
$$I_i = f(I_o, V_i, V_{SW})$$
$$(A.12)$$

There are four states this circuit can exist in depending on whether if the switch is open or closed in combination with whether the diode is conducting or not.

With the switch closed and the diode open

$$V_o = V_i - I_o R_I \tag{A.13}$$

$$I_i = I_o \tag{A.14}$$

With the switch closed and the diode conducting

$$V_o = \frac{V_i R_D - V_D R_I - I_o R_I R_D}{R_I + R_D} \tag{A.15}$$

$$I_i = \frac{V_i + V_D + I_o R_D}{R_I + R_D} \tag{A.16}$$

With the switch open and the diode open

$$V_o = V_i - I_o R_H \tag{A.17}$$

$$I_i = I_o \tag{A.18}$$

And finally with the switch open and the diode conducting

$$V_o = \frac{V_I R_D - V_D R_H - I_o R_H R_D}{R_H + R_D} \tag{A.19}$$

$$I_i = \frac{V_i + V_D + I_o R_D}{R_H + R_D} \tag{A.20}$$

Since the diode is modelled as being either conducting or not (much like a resistive switch with a dropping offset voltage), a sensing method is required to determine what state the diode is in. The state of the diode must again be determined as a function of I_o, V_i and the state of the switch (equation A.12) but it is also dependent on the previous state of the diode itself with the sensing method described below.

If the diode is previously not conducting then the voltage across the open diode can be sensed (V_S) to determine what the next diode state should. With the switch closed then

$$V_S = V_I - V_D - I_o R_I \tag{A.21}$$

And with the switch is open

$$V_S = V_I - V_D - I_o R_H \tag{A.22}$$

The next diode state is hence given by

$$\text{IF } V_S < 0 \text{ THEN CLOSE DIODE}$$
$$\text{ELSE KEEP DIODE OPEN} \tag{A.23}$$

If the diode is previously conducting then the current through the closed diode can be sensed (I_D) to determine what the next diode state should. With the switch closed then

$$I_D = \frac{V_i + V_D - I_o R_H}{R_H + R_D} \tag{A.24}$$

And with the switch is open

$$I_D = \frac{V_i + V_D - I_o R_H}{R_H + R_D} \tag{A.25}$$

The next diode state is hence given by

$$\text{IF } I_D > 0 \text{ THEN OPEN DIODE}$$
$$\text{ELSE KEEP DIODE CLOSED} \tag{A.26}$$

The models of both the reactive components and switching components as described above were cascaded to form the complete model of the SMPS in the simulations presented in chapter 5.

APPENDIX B
SMPS SCHEMATIC

SMPS for Dynamically Biased Cartesian Feedback